

Tectonics

RESEARCH ARTICLE

10.1029/2020TC006231

Special Section:

Tethyan Dynamics: From Rifting to Collision

Key Points:

- The northern Indo-Burma Ranges expose a Cenozoic southwest to west directed thrust belt that is bounded by two active right-slip faults
- Thrusting since ~36 Ma accommodated >280 km (86%) shortening during clockwise crustal flow around the eastern Himalayan syntaxis
- Our findings support an increase in Cenozoic shortening and/or continental underthrusting along the easternmost India-Asia plate boundary

Supporting Information:

- Supporting Information S1

Correspondence to:

P. J. Haproff,
haproffp@uncw.edu

Citation:

Haproff, P. J., Odlum, M. L., Zuza, A. V., Yin, A., & Stockli, D. F. (2020). Structural and thermochronologic constraints on the Cenozoic tectonic development of the northern Indo-Burma Ranges. *Tectonics*, 39, e2020TC006231. <https://doi.org/10.1029/2020TC006231>

Received 6 APR 2020

Accepted 28 JUL 2020

Accepted article online 7 AUG 2020

Structural and Thermochronologic Constraints on the Cenozoic Tectonic Development of the Northern Indo-Burma Ranges

Peter J. Haproff¹ , Margaret L. Odlum^{2,3} , Andrew V. Zuza⁴ , An Yin⁵ , and Daniel F. Stockli³ 

¹Department of Earth and Ocean Sciences, University of North Carolina Wilmington, Wilmington, NC, USA,

²Department of Geosciences, Utah State University, Logan, UT, USA, ³Department of Geological Sciences, University of Texas at Austin, Austin, TX, USA, ⁴Nevada Bureau of Mines and Geology, University of Nevada, Reno, Reno, NV, USA,

⁵Department of Earth, Planetary, and Space Sciences, University of California, Los Angeles, Los Angeles, CA, USA

Abstract The ~1,500-km-long, north trending Eastern Flanking Belt of the Himalayan-Tibetan orogenic system is located along the eastern margin of the Indian subcontinent. Although the belt is a key element of the Cenozoic India-Asia collisional zone, its tectonic evolution remains poorly understood. This lack of knowledge has impacted our ability to differentiate between competing hypotheses for the evolution of the India-Asia collision. To address this problem, we integrate constraints on the structural framework and magnitude of Cenozoic shortening strain with thermochronology of the northernmost segment of the belt located directly southeast of the eastern Himalayan syntaxis (i.e., the northern Indo-Burma Ranges). The study area exposes a southwest directed thrust belt that is bounded by the Indian craton in the west and the right-slip Jiali fault zone in the east. New and existing (U-Th)/He and ⁴⁰Ar/³⁹Ar thermochronologic data indicate that thrust-related cooling occurred from ~36 Ma in the northeast to ~5.6 Ma in the southwest. Episodes of out-of-sequence thrusting occurred at ~30–20, ~14–12, and ~11–6 Ma within the thrust belt. Restoration of the thrust belt yields a minimum horizontal shortening of ~280 km (~86%). These results combined with (1) the recorded local absence of several major Himalayan-Tibetan lithologic units (i.e., Tethyan Himalayan Sequence, Greater Himalayan Sequence, and southern Gangdese batholith) and (2) the southward decrease in the thrust-belt width (33–5 km) suggest a complex history of thrusting in the northern Indo-Burma Ranges and an spatial increase in Cenozoic crustal shortening and/or continental underthrusting from west to east across the eastern Himalayan syntaxis.

1. Introduction

The Himalayan-Tibetan orogen has served as a testing ground for competing models of mountain building and collisional deformation since the advent of the plate tectonics theory (e.g., Allégre et al., 1984; Dewey et al., 1988; Dewey & Burke, 1973; England & Houseman, 1986; Hodges, 2000; Le Fort, 1975; Molnar & Tapponnier, 1975; Royden et al., 2008; Tapponnier et al., 2001; Yin, 2010; Yin & Harrison, 2000; Zuza et al., 2016). In addition to generating the east trending Himalayan orogen and the vast Tibetan Plateau in its hinterland, the Cenozoic indentation of India into Asia has also resulted in the formation of the >1,500-km-long, north trending Eastern and Western Flanking Belts that bound the margins of the Indian subcontinent (Gansser, 1964; Haproff et al., 2018; Tapponnier et al., 2001; Yin, 2006) (Figure 1). Despite the large areal extent of the Flanking Belts (Figure 2), past efforts have centered mostly on the Himalayan orogen between the eastern and western syntaxes (e.g., Avouac, 2003; Carosi et al., 2018; DeCelles et al., 2001; Gansser, 1964; Hodges, 2000; Kapp & DeCelles, 2019; Le Fort, 1975; Murphy et al., 1997; Nelson et al., 1996; Webb et al., 2017; Yin, 2006) and the Tibetan Plateau (e.g., Armijo et al., 1986; Armijo et al., 1989; Kapp & DeCelles, 2019; Wang et al., 2001; Laskowski et al., 2016; Leary et al., 2016; Murphy & Yin, 2003; Yin & Taylor, 2011). The lack of knowledge regarding the evolution of the Eastern Flanking Belt has hampered a more complete understanding of the India-Asia collision.

The structural framework and kinematics of the Eastern Flanking Belt have been predicted in tectonic models based on analog experiments and numerical simulations of the India-Asia collision (e.g., Cobbold & Davy, 1988; Davy & Cobbold, 1988; England & Houseman, 1986; Royden et al., 1997; Tapponnier

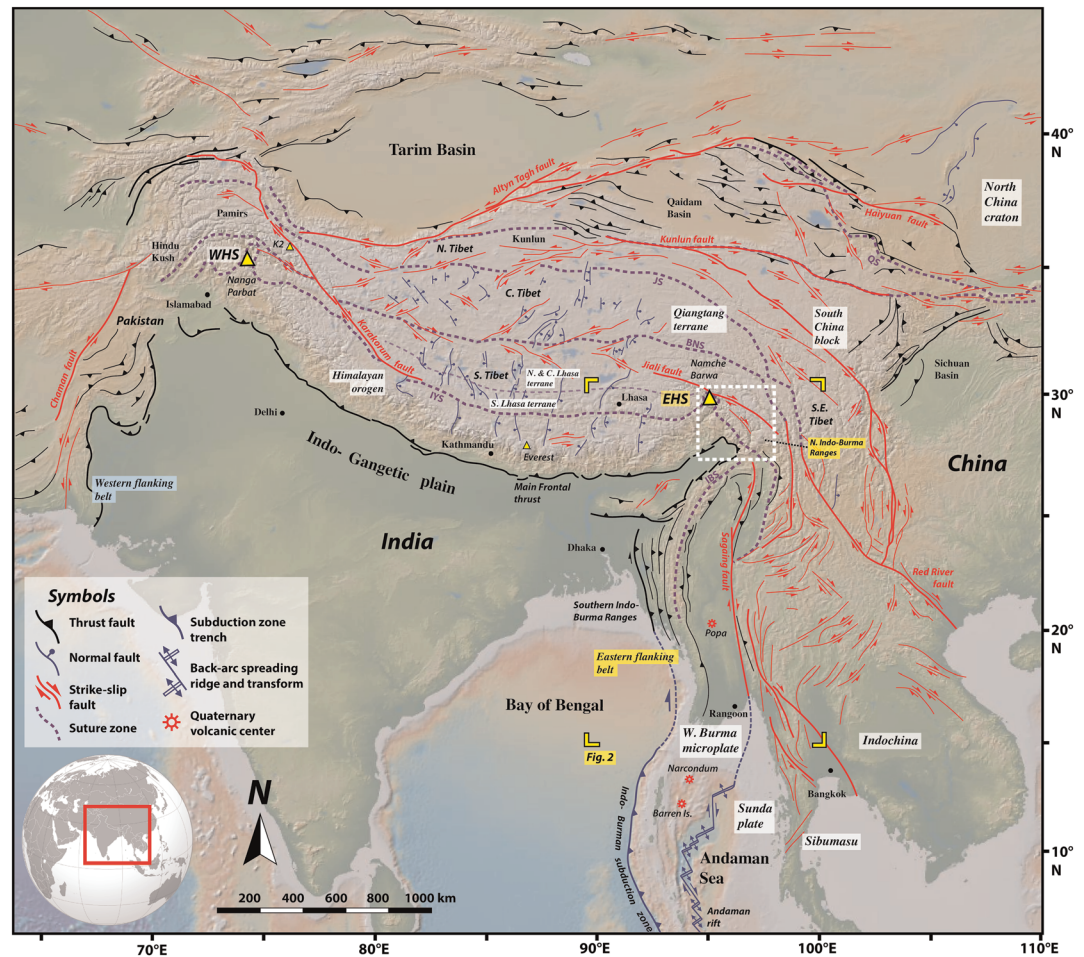


Figure 1. Tectonic map of the India-Asia collisional system showing major faults and suture zones, modified from Taylor and Yin (2009) and Haproff et al. (2018). The northern Indo-Burma Ranges are located within the white dashed box. The digital elevation map was acquired using geomapp.org (Ryan et al., 2009). The Earth index map was acquired through Generic Mapping Tools (gmt.soest.hawaii.edu). Abbreviations: BNS: Bangong-Nujiang suture, EHS: eastern Himalayan syntaxis, IYS: Indus-Yarlung suture, JS: Jinsha suture, QS: Qilian suture, WHS: western Himalayan syntaxis.

et al., 1982). The lateral extrusion model of Tapponnier et al. (1986) and Peltzer and Tapponnier (1988) (Figure 3a) and the bookshelf faulting model of England and Molnar (1990) (Figure 3b) require the Eastern Flanking Belt to be dominated by discrete strike-slip faults that accommodate progressive north-south India-Asia convergence. In contrast, the continuum-flow models (England & Houseman, 1986; Li et al., 2013; Royden et al., 1997) and the analog experiments of Cobbold and Davy (1988) all predict clockwise crustal flow around the eastern Himalayan syntaxis (Figure 3c). Specifically, this class of models requires the Eastern Flanking Belt to have formed as an east to southeast striking thrust system that subsequently rotated clockwise to the current north striking orientation. The predicted clockwise rotation around the eastern Himalayan syntaxis, which is supported by paleomagnetic studies (e.g., Li et al., 2020; Pellegrino et al., 2018), implies the development of a strain gradient such that Cenozoic crustal shortening increases across the syntaxis from the east trending Himalayan orogen to the Eastern Flanking Belt, as outlined in Haproff et al. (2018). Shortening estimates across the Eastern Flanking Belt can also be used to test models of orogen-parallel variations of Cenozoic strain, specifically (1) shortening increases west to east due to spatial variations in India-Asia convergence (Dewey et al., 1989; Guillot et al., 1999; Patriat & Achache, 1984), (2) shortening variations are controlled by the precollisional stratigraphic and structural configurations of Greater India and/or the Lhasa terrane (Long et al., 2011), or (3) maximum shortening occurs at the orogen center (Elliott, 1976). However, few Cenozoic crustal

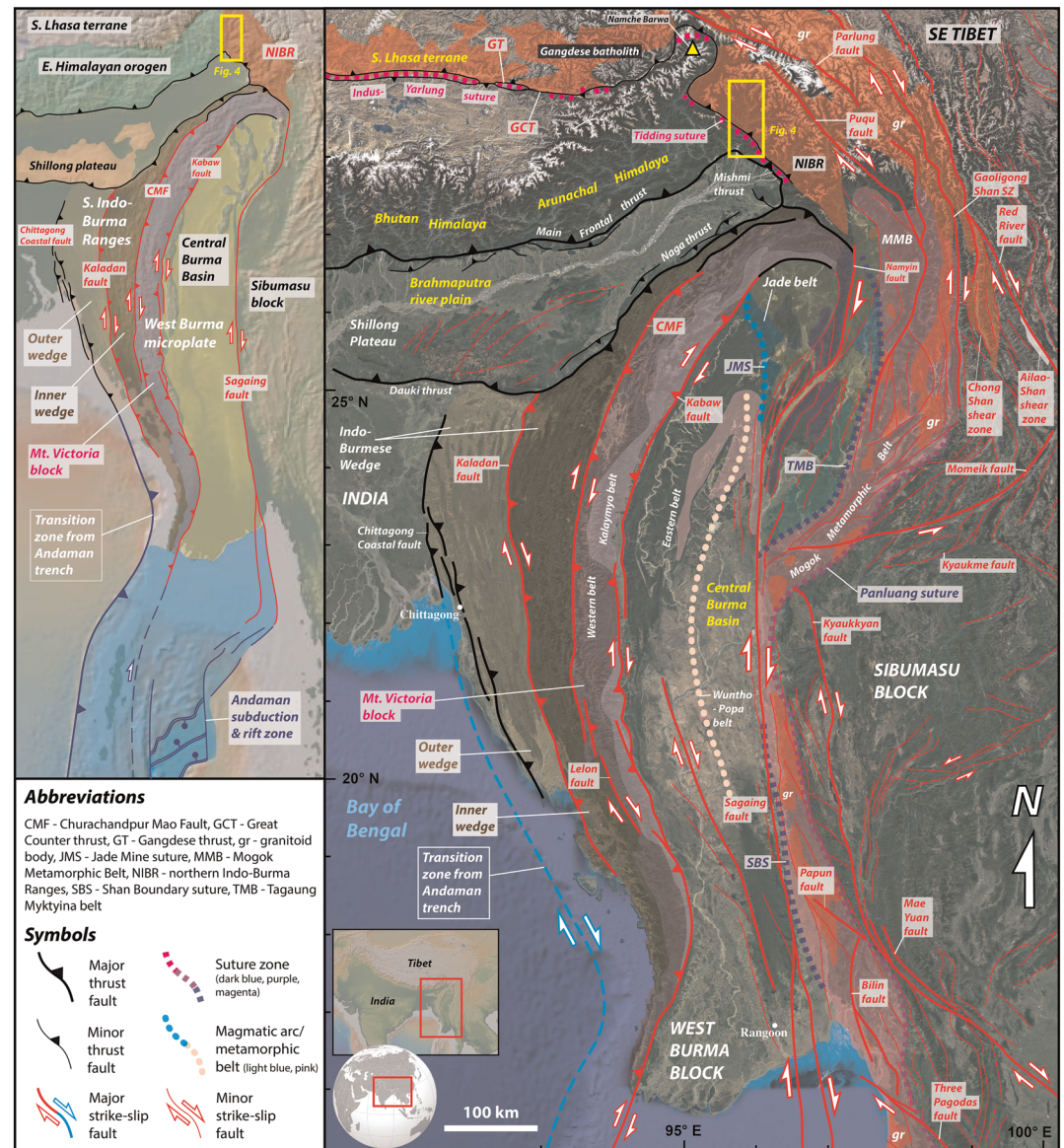


Figure 2. Tectonostratigraphic map of the Eastern Flanking Belt showing major faults, suture zones, and magmatic and metamorphic belts (compiled from Acharyya, 1987; Ding et al., 2001; Mitchell et al., 2007; Morley, 2004; Morley et al., 2020; Morley & Searle, 2017; Ridd & Watkinson, 2013; Searle & Morley, 2011; Searle et al., 2007; Tun et al., 2014; Watkinson, 2011; Watkinson et al., 2011).

shortening estimates have been available for the Eastern Flanking Belt based on systematic geologic mapping, rigorous palinspastic reconstruction, and high-resolution age constraints (Ningthoujam et al., 2015; Salvi et al., 2020).

In this paper, we present the results of new geological mapping and combine new and existing zircon (U-Th)/He and $^{40}\text{Ar}/^{39}\text{Ar}$ thermochronology across the northern Indo-Burma Ranges, the northernmost segment of the Eastern Flanking Belt (Figures 1 and 2). We include an estimate of minimum Cenozoic horizontal shortening based on the restoration of one balanced cross section and present active fault maps to show the mode of strain partitioning around the eastern Himalayan syntaxis. Our findings are integrated with existing constraints on the geological framework of the northern Indo-Burma Ranges (e.g., Haproff et al., 2018, 2019) and the paleogeography of southern Asia (e.g., Hall, 2012; Lee & Lawver, 1995; Metcalfe, 2013; Morley & Searle, 2017; van Hinsbergen et al., 2011; van Hinsbergen et al., 2019;

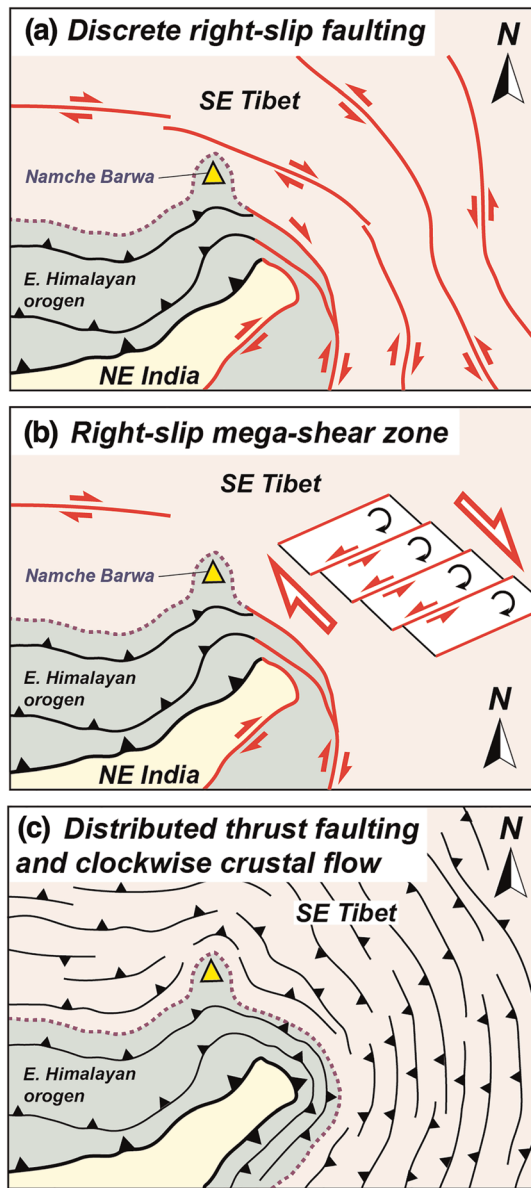


Figure 3. Models of deformation in the Eastern Flanking Belt near the eastern Himalayan syntaxis during the Cenozoic India-Asia collision including tect21384(a) discrete right-slip faulting, (b) series of left-slip bookshelf faults accommodating southeast-northwest oriented right-slip shear, and (c) distributed thrust faulting during clockwise crustal flow (modified from Haproff et al., 2018).

et al., 2008; Montomoli et al., 2015; Yin et al., 2006; Yin, Dubey, Webb, et al., 2010), the Main Boundary thrust (MBT) at the base of the LHS (Acharyya, 1994; Acharyya & Ray, 1977; DeCelles et al., 2016; Gansser, 1964, 1983; Kumar, 1997; Le Fort, 1975; Long et al., 2011; Long, McQuarrie, Tobgay, & Grujic, 2011; Long, McQuarrie, Tobgay, Rose, et al., 2011; McQuarrie et al., 2008; Yin, Dubey, Webb, et al., 2010), and the MFT at the base of the SHS (Acharyya, 1994; Burgess et al., 2012; DeCelles et al., 2016; Yin, Dubey, Webb, et al., 2010). Each of these faults is expressed as kilometer-scale zones of brittle faulting (e.g., MFT) and/or ductile shear (e.g., MCT and STD) (Hodges, 2000; Yin, 2006).

The eastern Himalayan orogen is bounded by the southern Lhasa terrane to the north (Figures 1 and 2), which in turn is bounded by a zone of ultramafic rocks interpreted as a possible Permian suture zone to the north (e.g., Dong et al., 2011; Hsü et al., 1995; Zhang et al., 2014; Zhu et al., 2012) or telescoped

Westerweel et al., 2019) to produce a comprehensive model for the tectonomagmatic evolution of the easternmost India-Asia collisional system since the latest Jurassic.

2. Geological Setting

The major tectonic domains relevant to this study include the eastern Himalayan orogen, the southern Lhasa terrane, and the Eastern Flanking Belt. The Eastern Flanking Belt is further divided into the southern Indo-Burma Ranges, the West Burma block, and the northern Indo-Burma Ranges (Figure 2). We briefly outline the geological framework of these domains below.

2.1. Eastern Himalayan Orogen and Southern Lhasa Terrane

The eastern segment of the Himalayan orogen extends from longitude 89°E in the west to the eastern Himalayan syntaxis at longitude 95°E. This segment of the orogen is bounded by the Indus-Yarlung suture zone and southern Lhasa terrane to the north and the Main Frontal thrust (MFT) to the south (Yin, 2006) (Figures 1 and 2). From north to south, the eastern Himalayan orogen exposes Proterozoic-Eocene siliciclastic and carbonate sedimentary rocks interbedded with Paleozoic and Mesozoic volcanic rocks of the Tethyan Himalayan Sequence (THS) (Aikman et al., 2008; Harrison et al., 2000; Yin et al., 1994, 1999), Paleoproterozoic-Ordovician high-grade metamorphic rocks and ~500-Ma granitoids of the Greater Himalayan Sequence (GHS) (e.g., Gansser, 1983; Webb et al., 2013; Yin et al., 2010), Proterozoic-Cambrian medium- to low-grade metasedimentary rocks of the Lesser Himalayan Sequence (LHS) (Gansser, 1983; Long et al., 2011; McQuarrie et al., 2008; Yin, Dubey, Webb, et al., 2010), and late Cenozoic siliciclastic strata of the Sub-Himalayan Sequence (SHS) (Acharyya, 1994; Gansser, 1983; Kumar, 1997; McQuarrie et al., 2008; Yin et al., 2006; Yin, Dubey, Webb, et al., 2010). These major Himalayan lithologic units are bounded by the following faults: the South Tibetan detachment (STD) at the base of the THS (Burchfiel et al., 1992; Burg et al., 1984; Caby et al., 1983; Carosi et al., 1998; Edwards et al., 1996, 1999; Edwards & Harrison, 1997; Law et al., 2004; Webb et al., 2013; Wu et al., 1998), the Main Central thrust (MCT) at the base of the GHS (Acharyya & Ray, 1977; DeCelles et al., 2016; Gansser, 1964, 1983; Heim & Gansser, 1939; Kumar, 1997; Le Fort, 1975; Searle et al., 2008; Yin, Dubey, Webb, et al., 2010), thrusts within the GHS (e.g., the Zimithang thrust, the Kakhtang thrust, and the Higher Himalayan Discontinuity) (Carosi et al., 2018, 2019; Gansser, 1983; Grujic et al., 2002; Long, McQuarrie, Tobgay, & Grujic, 2011; Long, McQuarrie, Tobgay, Rose, et al., 2011; McQuarrie

fragments of the Late Jurassic-Early Cretaceous Bangong-Nujiang suture zone to the north (Coward et al., 1988; Girardeau et al., 1984; Kapp et al., 2003; Yin & Harrison, 2000). The >2,000-km-long Gangdese batholith is the most prominent feature of the southern Lhasa terrane (Figure 2), which is divided into a northern belt of late Triassic-Cretaceous plutonic rocks (Wang et al., 2016; Wen et al., 2008; Zhu et al., 2009) and a southern belt of Cretaceous-Eocene plutonic rocks and Paleocene-Eocene volcanic rocks and dikes (Copeland et al., 1995; Coulon et al., 1986; Ding et al., 2003; Guan et al., 2012; Guo et al., 2012; Guo et al., 2013; Ji et al., 2009; Lee et al., 2009; Schärer et al., 1984; Wen et al., 2008; Yin et al., 1994; Zhu et al., 2008; Zhu et al., 2009; Zhu et al., 2009; Zhu et al., 2013). The southern Lhasa terrane is bounded to the south by the south directed Gangdese thrust (Harrison et al., 1992; Yin et al., 1994) and the north directed Great Counter thrust (Heim & Gansser, 1939) (Figure 2).

2.2. Eastern Flanking Belt

The ~1,000-km-long, north trending Eastern Flanking Belt extends southward from the eastern Himalayan syntaxis to the Andaman subduction zone. The belt is bounded by the Indian subcontinent and Bengal basin to the west and north striking Sagaing fault and Sibumasu block to the east (longitude 90–97°E) (Figure 2). From south to north, the Eastern Flanking belt consists of three domains: (1) the Andaman subduction zone and backarc rift system (N6° to N17°), (2) a central domain that includes the southern Indo-Burma Ranges (N17° to N27°), and (3) the northern Indo-Burma Ranges (N27° to N28°) (Figure 2).

2.2.1. Southern Indo-Burma Ranges

The southern Indo-Burma Ranges expose a westward tapering, thin-skinned fold and thrust belt that is divided into two salients: (a) an outer belt to the west involving lower Miocene submarine deposits, upper Miocene continental shelf deposits, and Pliocene-Pleistocene fluvial deposits; and (b) an onshore inner belt to the east involving Eocene flysch deposits (Maurin & Rangin, 2009a; Rangin et al., 2013; Yang et al., 2020) (Figure 2). The inner belt is considered part of the early Cenozoic accretionary prism of the India-Burma subduction zone and includes the Naga Hills thrust belt (or Assam-Arakan thrust belt) (Maurin & Rangin, 2009a; Rangin et al., 2013) (Figure 2). The outer belt includes the Chin-Chittagong Hills-Tipura thrust belt, which is bounded by the leading Chittagong Coastal fault (Figure 2). Thrust faults of both belts exhibit subhorizontal fault striations and right-lateral thrust sense of shear (Maurin & Rangin, 2009a). The outer and inner belts of the southern Indo-Burma Ranges are divided by the right-lateral thrust Kaladan fault, which terminates to the north near the merger of the Naga and Dauki thrusts (Figure 2). The Dauki thrust along with the south dipping Oldham fault are thought to be responsible for uplift of the Shillong plateau, located south of the Himalayan orogen (Bilham & England, 2001; Clark & Bilham, 2008).

2.2.2. West Burma Block

East of the southern Indo-Burma Ranges, the West Burma block, or Burma terrane, is divided into the Mount Victoria block to the west and the Central Burma basin to the east, separated by the right-lateral thrust Kabaw fault (Figure 2). The core of the Mount Victoria block consists of Jurassic-Cretaceous ophiolitic fragments of the Western Belt Ophiolites (Acharyya et al., 1990; Ao & Bhowmik, 2014; Maurin & Rangin, 2009a, 2009b; Morley & Searle, 2017; Rangin et al., 2013) (Figure 2), which are considered the southern continuation of the Indus-Yarlung suture zone (e.g., Maurin & Rangin, 2009a, 2009b; Rangin et al., 2013). The Western Belt Ophiolites are thrust atop Late Triassic-Late Cretaceous carbonate and shale and the Paleozoic Kanpetlet schist (Socquet et al., 2002). In the Chin Hills of Myanmar, the Western Belt Ophiolites are overlain by fossiliferous flysch and conglomerate of the Late Cretaceous-Early Paleogene Kabaw Formation (Socquet et al., 2002). In the Naga Hills of northeastern India, limestone and metasedimentary rocks of the early Paleozoic-Mesozoic Naga Metamorphics are thrust to the northwest atop the Early Cretaceous-Eocene Nagaland Ophiolitic Complex and late Eocene-Oligocene Jopi-Phokphur Formation (Aitchison et al., 2019; Brunnschweiler, 1966; Chatterjee & Ghose, 2010). The Nagaland Ophiolitic Complex is notable for containing blueschist and eclogite blocks with Early Jurassic peak metamorphic ages, which have been interpreted to reflect the earliest phase of Neo-Tethys subduction beneath the West Burma block (Rajkakati et al., 2019). The Naga Ophiolitic Complex and Jopi-Phokphur Formation are thrust to the northwest atop the Late Cretaceous-Eocene Disang Flysch (Chatterjee & Ghose, 2010).

East of the Mount Victoria block, the north trending Central Burma basin—which includes the Chindwin, Minbu, and Patheingyi subbasins—is composed of Cenozoic terrestrial and marine strata (Rangin et al., 1999;

Rangin et al., 2013) (Figure 2). The Central Burma basin is considered either a series of forearc and back-arc basins related to subduction of Indian oceanic lithosphere beneath Burma (e.g., Mitchell, 1993) or Cenozoic right-slip pull-apart basins related to slip along the Sagaing fault (Bertrand & Rangin, 2003; Rangin et al., 1999). The Central Burma basin is bisected by intermittent exposures of Cretaceous igneous rocks of the Mawgyi Andesites, metasedimentary roof pendants, Permian limestone, dismembered ophiolites, and the Wuntho-Popa magmatic belt (Figure 2), the latter of which consists of Cretaceous (~106–91 Ma) and Eocene-Oligocene I-type granitoids (~52–37 Ma) (Barley et al., 2003; Barley & Zaw, 2009; Mitchell, 1993; Mitchell et al., 2012). Detrital zircon U-Pb ages from the surrounding Central Burma basin further constrain magmatism in the Wuntho-Popa belt to ~110–80 and ~70–40 Ma (Wang et al., 2014). The youngest exposed igneous rocks are Eocene-Oligocene granitoids and Miocene-Quaternary volcanic flows (Lee et al., 2016).

Bounding the Central Burma basin to the east is the ~1,000-km-long, right-slip Sagaing fault that extends from the southeast striking restraining bend in northern Myanmar to the Andaman Sea where the fault transitions into series of right-stepping transform faults and spreading centers of the Andaman backarc rift system (Figure 2). The Global Positioning System (GPS)-derived slip rates along the northern and central segments of the Sagaing fault are 18–20 mm/yr, which is less than the India-Sibumasu relative velocity of ~35 mm/yr (Maurin et al., 2010; Vigny et al., 2003). One paleoseismic study by Wang et al. (2011) determined a Holocene slip rate of 14 mm/yr along the southernmost segment of the Sagaing fault. The initiation age of the Sagaing fault has been bracketed to middle Miocene to early Pliocene based on the onset of seafloor spreading in the Andaman rift (Raju et al., 2004). Estimates of the total right-slip displacement since the Miocene range from ~400–460 km (Curry et al., 1979; Maung, 1987) to ~600 km (Morley & Searle, 2017).

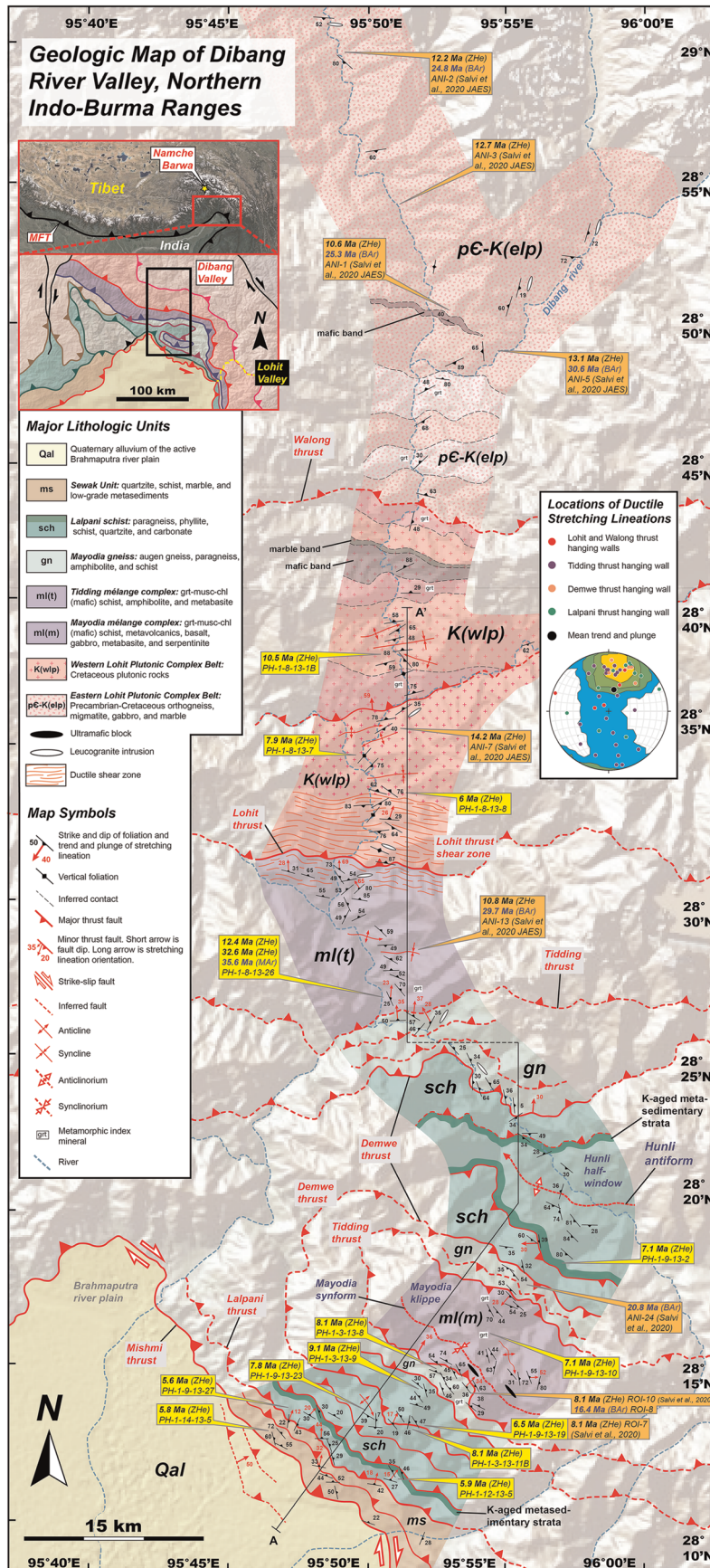
The Sagaing fault separates the West Burma block in the west from the Mogok-Mandalay-Mergui Belt of the Sibumasu block, or the Shan plateau, in the east (Figure 2). The Mogok-Mandalay-Mergui Belt consists of high-grade metamorphic rocks including Cenozoic biotite granite and leucogranite dikes, orthogneisses and granodiorites with Jurassic-Cretaceous crystallization ages, and ophiolitic rocks of the Jade Mines Belt Ophiolite and Eastern Belt Ophiolites (Barley et al., 2003; Searle et al., 2007; Searle et al., 2017).

2.2.3. Northern Indo-Burma Ranges

Our study is focused on the northern Indo-Burma Ranges, the northernmost segment of the Eastern Flanking Belt (Figure 2). Several previous field-based studies established the basic lithostructural framework of the area (e.g., Acharyya, 1980, 1987; Goswami, 2008, 2011; Goswami, 2013a, 2013b; Gururajan & Choudhuri, 2003; Misra, 2009; Misra & Singh, 2002; Nandy, 1973; Sarma et al., 2009; Sarma et al., 2012; Sharma et al., 1991; Sharma & Sarma, 2013; Thakur & Jain, 1975; Wadia, 1931). Haproff et al. (2019) recently divided the exposed rocks into six major lithologic units based on different lithologies, U-Pb zircon ages, and geochemical compositions. Lithologic units are bounded by <1- to 5-km-wide, southwest to west directed thrust shear zones (Figure 4). Detailed descriptions of structural observations across the area as part of this study are presented in section 4.

The northernmost unit is the Lohit Plutonic Complex (Gururajan & Choudhuri, 2003; Misra, 2009; Misra & Singh, 2002; Thakur & Jain, 1975), which consists of a western belt of latest Jurassic-Cretaceous, southern Gangdese-equivalent granitoids, and an eastern belt of Mesoproterozoic migmatite and Cretaceous plutonic rocks, separated by the Walong thrust (Bikramaditya et al., 2019; Gururajan & Choudhuri, 2003; Haproff et al., 2019; Misra, 2009; Pebam & Kamalakannan, 2019) (Figure 4). The eastern Lohit Plutonic Complex belt is cut in the northeast by two northwest striking strands of the right-slip Jiali fault zone: the Puqu fault, or the Pu-Chu fault, in the south and the Parlung fault in the north (Figure 2) (e.g., Armijo et al., 1989; Molnar & Tapponnier, 1975). Both the Puqu fault and the Parlung fault are interpreted to be active based on local seismicity and their geomorphic expression including ~10-km-long, linear scarps and beheaded and right-laterally deflected stream channels (Figure 5) (Mukhopadhyay & Dasgupta, 2015; Ni & York, 1978; Thingbaijam et al., 2008). Lee et al. (2003) documented right-slip mylonitic shear zones parallel to the brittle traces of the Puqu fault and the Parlung fault and suggested shearing initiated at ~18–12 Ma based on $^{40}\text{Ar}/^{39}\text{Ar}$ thermochronology.

The Lohit thrust places the western belt of the Lohit Plutonic Complex atop the Tidding mélangé complex (Figure 4), also called the Tuting-Tidding suture zone (Gururajan & Choudhuri, 2003; Kundu et al., 2020;



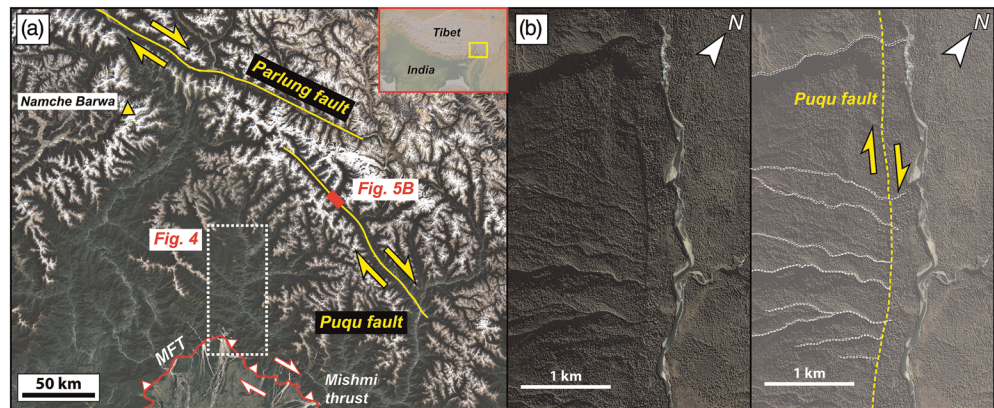


Figure 5. Google Earth-based maps of (a) the northern Indo-Burma Ranges and easternmost Himalaya showing the locations of the Main Frontal thrust, the Mishmi thrust, the Puqu fault, and the Parlung fault and (b) linear scarps and beheaded and right-laterally deflected river channels along the Puqu fault.

Nandy, 1980; Nandy et al., 1975; Singh & Singh, 2011, 2013). The mélangé complex is exposed in two locations along Dibang Valley: (1) the Tidding mélangé complex at the root zone of the Tidding thrust in the hinterland of the thrust belt and (2) the Mayodia mélangé complex bounding an isolated klippe in the foreland of the thrust belt (Figure 4). The Tidding mélangé complex in the north consists of interlayered garnet-biotite-muscovite-hornblende schist, chlorite schist, chert, quartzite, and marble intruded by mafic and leucogranite dikes (Goswami, 2013a; Haproff et al., 2018, 2019; Misra, 2009; Salvi et al., 2020). The Mayodia mélangé complex in the south contains dismembered blocks of serpentized ultramafic rocks, pyroxenite, dunite, paragneiss, amphibolite, hornblendite dikes, metabasite, and gabbro surrounded by a deformed matrix of chert, carbonate, and garnet-actinolite-chlorite-albite-epidote schist (Haproff et al., 2018, 2019; Misra, 2009; Salvi et al., 2020; Sarma et al., 2012; Singh & Singh, 2011, 2013; Sinha Roy & Singh, 2002; Thakur & Jain, 1974).

We interpret that the Tidding and Mayodia mélangé complexes originate from the same tectonic mélangé in the hanging wall of the Tidding thrust (see section 6). The Tidding-Mayodia mélangé complex is considered the easternmost continuation of the Indus-Yarlung suture zone that wraps around the eastern Himalayan syntaxis (Gururajan & Choudhuri, 2003; Haproff et al., 2019; Kundu et al., 2020; Misra, 2009; Nandy, 1980; Nandy et al., 1975; Singh & Singh, 2011, 2013).

The Tidding thrust places the Tidding-Mayodia mélangé complex atop metasedimentary rocks correlative with the LHS, which are divided into the Mayodia gneiss and structurally lower Lalpani schist (Figure 4). The Mayodia gneiss contains amphibolite-facies paragneiss, quartzo-feldspathic schist, quartzite, amphibolite, and augen gneiss with youngest Mesoproterozoic-Cambrian-aged detrital zircons and ϵ_{Nd} values of -17 to -10 (Gururajan & Choudhuri, 2003; Haproff et al., 2019; Misra, 2009; Salvi et al., 2020). The uppermost Mayodia gneiss reaches garnet grade along the southern margin of the Mayodia klippe (Figure 4). Salvi et al. (2020) report that the uppermost Mayodia gneiss contains epidote zoisite garnet schist with a mineral assemblage indicative of peak metamorphism in amphibolite facies conditions and subsequent greenschist facies retrogression.

In the footwall of the Demwe thrust, the Lalpani schist contains hornblende schist, garnet-biotite schist, carbonaceous calcite schist, paragneiss, quartzite, and carbonate (Misra, 2009; Misra & Singh, 2002; Salvi et al., 2020) with youngest Mesoproterozoic-Cretaceous-aged detrital zircons and ϵ_{Nd} values of -27 to -16 (Haproff et al., 2019). Gururajan and Choudhuri (2003) and Misra (2009) report that metasedimentary rocks

Figure 4. Geological map of the Dibang Valley traverse, modified from Haproff et al. (2018, 2019). Thermochronologic ages from this study and Salvi et al., (2020) are shown in yellow and orange, respectively. The stereogram depicting stretching lineation orientations was generated using Stereonet Version 10.0 (Allmendinger et al., 2012; Cardozo & Allmendinger, 2013). The digital elevation map was acquired using geomapapp.org (Ryan et al., 2009). Abbreviations: EHS: eastern Himalayan syntaxis, MAR: muscovite $^{40}\text{Ar}/^{39}\text{Ar}$ age, MBr: biotite $^{40}\text{Ar}/^{39}\text{Ar}$ age, MFT: Main Frontal thrust, ZHe: zircon (U-Th)/He age.

of the Lalpani schist experienced peak amphibolite facies metamorphism. The timing of peak metamorphism in the region remains unconstrained through absolute dating methods.

The Lalpani thrust places the Lalpani schist atop the southernmost-exposed Sewak unit (Figure 4), which contains unmetamorphosed to low-grade metasedimentary rocks including quartz arenite, chert, quartzite, marble, slate, phyllite, and quartzo-feldspathic schist (Misra, 2009; Misra & Singh, 2002) with youngest Oligocene-aged detrital zircons (Haproff et al., 2019).

The southernmost Tezu unit is intermittently exposed along the southeastern margin of the northern Indo-Burma Ranges and contains sandstone and conglomerate, comparable to the Miocene-Pliocene Siwalik Group of the Himalayan orogen. The Sewak unit and Tezu unit are in the hanging wall of the brittle Mishmi thrust (Figure 4), which is the southernmost exposed fault in the study area and the easternmost extension of the MFT (Coudurier-Curveur et al., 2020).

Major tectonostratigraphic units of the Himalayan-Tibetan orogen including the THS, GHS, Mesozoic-Cenozoic igneous rocks of the southern Gangdese batholith, Linzizong volcanic sequence, and Xigaze forearc sequence are not exposed in the northern Indo-Burma Ranges (Haproff et al., 2019). However, Gangdese-equivalent Mesozoic-Cenozoic igneous rocks and adjacent forearc basin sediments are present throughout the Eastern Flanking Belt to the south of the study area (e.g., Mitchell, 1993; Mitchell et al., 2012; Wang et al., 2014). The existence of these rocks to the northeast and south of the study area suggests Mesozoic-Cenozoic arc magmatism and forearc sedimentation occurred as a laterally continuous belt along the southern margin of the Asian continent (Bikramaditya et al., 2019; Lin et al., 2013).

Despite extensive work in the northern Indo-Burma Ranges since Wadia (1931), researchers have disagreed over the structural architecture and lateral continuity of major Himalayan thrust faults such as the MBT and MCT across the eastern Himalayan syntaxis (e.g., Gururajan & Choudhuri, 2003; Misra, 2009; Salvi et al., 2020). Furthermore, only relatively few studies have applied modern geochronologic, thermochronologic, and geochemical techniques to further understand the geological evolution of the northern Indo-Burma thrust belt (e.g., Bikramaditya et al., 2019; Haproff et al., 2019; Li et al., 2013; Salvi et al., 2020).

3. Methods

The findings of this paper are based on geological mapping and zircon (U-Th)/He (ZHe) and muscovite $^{40}\text{Ar}/^{39}\text{Ar}$ thermochronology along the northeast trending Dibang Valley across the northern Indo-Burma Ranges (Figures 4 and 6a). Our thermochronology data were combined with recently published ZHe and $^{40}\text{Ar}/^{39}\text{Ar}$ ages by Salvi et al. (2020) in the area (Table S1 in the supporting information). We also conducted petrographic analysis of key bedrock samples, mapped active faults of the region based on their geomorphic expression on Google Earth imagery, and constructed and restored a balanced cross section parallel to the Dibang Valley traverse (Figure 6b). The integrated thermochronology data sets allows for a palinspastic reconstruction of the Dibang Valley cross section.

3.1. Zircon (U-Th)/He Thermochronology

Fourteen samples were collected for ZHe thermochronology from each major lithologic unit exposed along the Dibang Valley traverse to constrain cooling through $\sim 130\text{--}200^\circ\text{C}$ (Guenther et al., 2013; Reiners, 2005; Wolfe & Stockli, 2010) (Figures 4 and 6a). Quartzite Sample PH-1-14-13-5 was collected from the middle section of the southernmost-exposed Sewak unit in the foreland of the thrust belt. Six metasedimentary rock samples from the southernmost exposure of the Lalpani schist were collected from the structurally lowermost (PH-1-12-13-5 and PH-1-9-13-27), middle (PH-1-9-13-23 and PH-1-3-13-11B), and uppermost section (PH-1-9-13-19A and PH-1-3-13-9) of the unit. One augen gneiss sample (PH-1-3-13-8) from the southernmost exposure of the Mayodia gneiss was collected from the structurally uppermost section of the unit. Garnet schist sample PH-1-9-13-10 was collected from the Mayodia mélangé complex in the Mayodia klippe. Quartzo-feldspathic schist Sample PH-1-9-13-2 was collected from the Lalpani schist in the Hunli half-window within the core of the thrust belt. Garnet schist Sample PH-1-8-13-26 was collected from the Tidding mélangé complex in the hinterland of the thrust belt. The northeasternmost three granitoid samples (PH-1-8-13-8, PH-1-8-13-7, and PH-1-8-13-1B) were collected from the structurally lowermost and middle parts of the western belt of the Lohit Plutonic Complex.

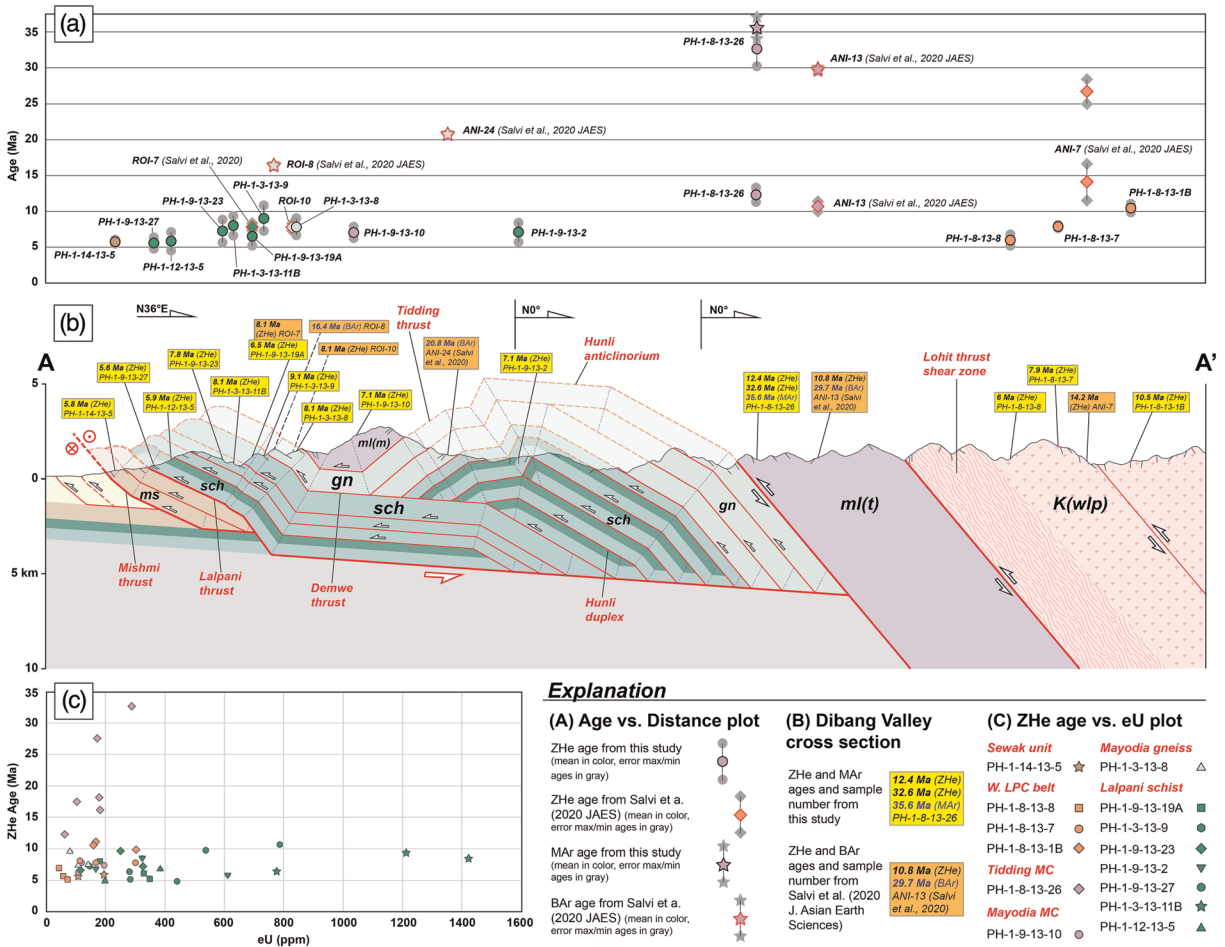


Figure 6. (a) Plot of zircon (U-Th)/He and $^{40}\text{Ar}/^{39}\text{Ar}$ thermochronologic ages versus distance, (b) balanced cross section along the Dibang Valley traverse (modified from Haproff et al., 2018), and (c) plot of zircon (U-Th)/He ages (ZHe) versus effective uranium (eU) for all analyses. Average ZHe ages from this study and Salvi et al. (2020) are shown as black-outlined circles and red-outlined diamonds, respectively. Black outlined circles for Sample PH-1-8-13-26 represent the maximum and minimum ZHe ages of the population. Weighted mean $^{40}\text{Ar}/^{39}\text{Ar}$ ages from this study and Salvi et al. (2020) are shown as black-outlined and red-outlined stars, respectively. Symbol colors correspond to the major lithologic unit of the sample. Maximum and minimum errors are shown in gray. Abbreviations: biotite (BAR) and muscovite (MAR).

Zircon (U-Th)/He analyses were conducted at the UTChron lab at the University of Texas at Austin following procedures described in Wolfe and Stockli (2010). Detailed descriptions of the sample preparation and ZHe analytical methodology are presented in the supporting information. Details of individual ZHe analyses including ages and 2-sigma errors are listed in Table S2. Plots of ZHe age versus effective uranium (eU) and ZHe age versus effective spherical radius (ESR) are shown on Figures 6c and S1, respectively. Reported sample ZHe ages and corresponding errors shown in Table 1 are the mean and standard deviation of all single zircon grain analyses, except Sample PH-1-8-13-26 that yields a range of ZHe ages of 32.6–12.4 Ma (see section 5).

3.2. Muscovite $^{40}\text{Ar}/^{39}\text{Ar}$ Thermochronology

Muscovite $^{40}\text{Ar}/^{39}\text{Ar}$ thermochronology was conducted on garnet schist Sample PH-1-8-13-26 to constrain cooling through an effective closure temperature range of ~350–425°C (Hames & Bowring, 1994; Harrison et al., 2009). Mineral separation and $^{40}\text{Ar}/^{39}\text{Ar}$ analyses were performed at the Nevada Isotope Geochronology Lab at University of Nevada, Las Vegas (e.g., Staudacher et al., 1978). Detailed description of the $^{40}\text{Ar}/^{39}\text{Ar}$ methodology is presented in the supporting information. $^{40}\text{Ar}/^{39}\text{Ar}$ analytical data and age spectra are shown in Table S3 and Figure S2, respectively.

Table 1
List of Mean Zircon (U-Th)/He (ZHe) Ages for All Bedrock Samples

Sample	Rock type	Location	Elevation (m)	Average ZHe age (Ma)	Standard deviation	Zircon U-Pb age (Ma) ($\pm 2\sigma$) ^a
<i>Sewak unit</i>						
PH-1-14-13-5	phyllite	N28° 12.686 E95° 46.841	417	5.8	0.2	27 ± 1
<i>Lalpani schist</i>						
PH-1-9-13-2	schist	N28° 18.625 E95° 57.287	1,196	7.1	1.4	150 ± 4
PH-1-3-13-11B	paragneiss	N28° 13.167 E95° 51.687	1,810	8.1	1.4	525 ± 3
PH-1-9-13-23	schist	N28° 13.098 E95° 50.312	1,483	7.8	1.6	1,054 ± 19
PH-1-12-13-5	paragneiss	N28° 11.415 E95° 50.882	542	5.9	1.3	913 ± 5
PH-1-9-13-27	paragneiss	N28° 13.131 E95° 47.572	1,064	5.6	0.8	974 ± 6
PH-1-3-13-9	paragneiss	N28° 14.484 E95° 53.241	2,062	9.1	1.8	499 ± 3
PH-1-9-13-19A	paragneiss	N28° 13.263 E95° 51.781	1,639	6.5	1.3	1,022 ± 16
<i>Mayodia gneiss</i>						
PH-1-3-13-8	paragneiss	N28° 14.745 E95° 53.110'E	2,061	8.1	1.2	1,069 ± 13
<i>Tidding mélangé complex</i>						
PH-1-8-13-26 ^b	schist	N28° 26.897 E95° 50.957	729	30.1 16.1	2.5 2.5	40 ± 1 ^c
<i>Mayodia mélangé complex</i>						
PH-1-9-13-10	schist	N28° 16.145 E95° 54.358	2,363	7.1	0.8	940 ± 9
<i>Western Lohit Plutonic Complex Belt</i>						
PH-1-8-13-1B	monzodiorite	N28° 37.975 E95° 51.138	798	10.5	0.6	96 ± 3
PH-1-8-13-7	quartz monzonite	N28° 34.809 E95° 50.009	688	7.9	0.1	94 ± 3
PH-1-8-13-8	diorite	N28° 33.579 E95° 50.865	736	6	0.8	115 ± 13

^aYoungest zircon U-Pb ages of each sample are taken from Haproff et al. (2019). Lohit Plutonic Complex samples are weighted mean U-Pb ages. All other sample ages are the youngest detrital zircon age populations. ^bSample PH-1-8-13-26 has a range of ZHe ages of 32.6–12.4 Ma that forms bimodal populations centered at 30.1 and 16.1 Ma. ^cThe 40 ± 1-Ma zircon U-Pb age for sample PH-1-8-13-26 from Haproff et al. (2019) is interpreted to be a metamorphic age. In the thermal history modeling, we used a protolith depositional age of ~100–80 Ma based on the next youngest cluster of detrital zircon ages.

3.3. Thermal History Modeling

ZHe and muscovite ⁴⁰Ar/³⁹Ar ages of one garnet schist sample (PH-1-8-13-26) from the Tidding mélangé complex were incorporated into a HeFTy inverse thermal history model (Ketchum, 2005) to explain the over-dispersion of ages for this sample, leverage the observed age-eU pattern and better constrain the thermal history, and test the viability of our palinspastic reconstruction of the Dibang Valley cross section. Thermochronologic ages, model parameters, and model results used in the thermal history simulations are presented in the supporting information following the reporting protocol of Flowers et al. (2015) (Figures S3–S6).

3.4. Balanced Cross Section

One northeast-southwest oriented balanced cross section was constructed along the Dibang Valley traverse (Figure 6b) to constrain the magnitude of shortening strain for comparison with shortening estimates for the Himalaya to the west and present a basic thermokinematic model for the development of the thrust belt that can be incorporated in the larger evolution of the India-Asia collision. The line of cross section is oriented perpendicular to the trend of the orogen and parallel to the principal shortening direction defined by the general trend of mineral stretching lineation (Figure 4). We utilized the kink-bend method of Suppe (1983) and adhered to typical thrust geometries including ramps and bedding-parallel flats (e.g., Boyer & Elliott, 1982; Butler, 1987; Dahlstrom, 1970). Measurements of true dip were converted to apparent dips and grouped into average dip domains. The orientations of kink lines are the angle bisector between average dip domains. Thrusts depicted in the cross section were observed in the field as <1- to 5-km-thick mylonitic shear zones that display more discrete ductile strain than adjacent thrust sheets. Thrust sheets involving the Lalpani schist and the Mayodia gneiss are shown with variable thicknesses, which were based on field observations (Figure 4). The thickest thrust sheets (~1 km) are composed of both Mesoproterozoic-Mesozoic metasedimentary strata, whereas thrust sheets of lesser thickness (<1 km) involve Mesoproterozoic-Cambrian metasedimentary strata (Haproff et al., 2019). In addition, we show the Mayodia gneiss not continuing to crustal depths of >6 km with the Tidding mélangé complex but

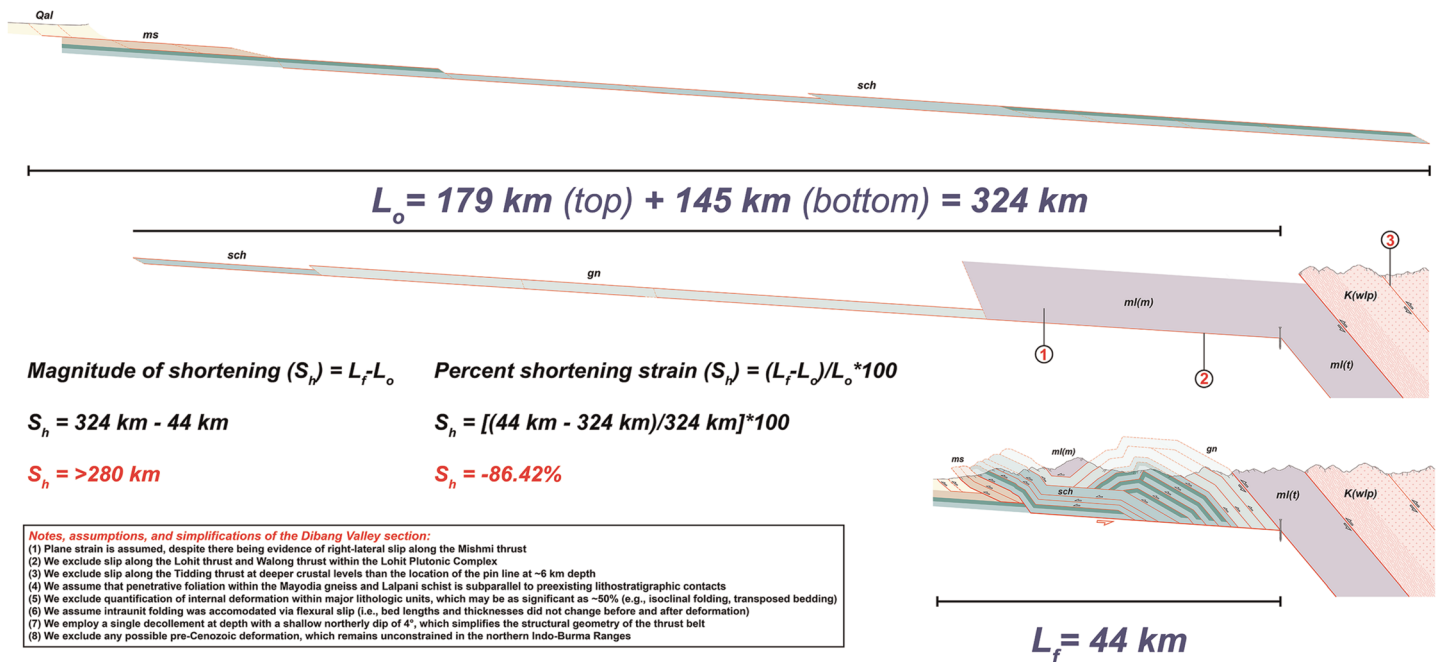


Figure 7. Restoration of the Dibang Valley balanced cross section. The original 324-km-long section was shortened to 44 km, yielding >280-km shortening (~86%). Notes, assumptions, and simplifications regarding the restoration are listed in the bottom left box.

instead forming series of stacks within the same thrust duplex system involving the Lalpani schist, which is a major departure from the previously published cross sections of Haproff et al. (2018) and Salvi et al. (2020) (Figure 6b). This new interpretation is based on the recent finding that the Mayodia gneiss and Lalpani schist are laterally continuous sections of the LHS based on similar youngest detrital zircon ages and negative ϵ_{Nd} values (Haproff et al., 2019).

The Dibang Valley cross section was restored using the line length measuring technique of Dahlstrom (1969) to produce a minimum horizontal shortening estimate (Figure 7). We note that our use of the kink-bend method and line length measuring technique involve several inherent uncertainties, assumptions, and simplifications that are discussed in the following sections.

3.4.1. Plane Strain Requirement

We assume that shortening strain is parallel to the plane of the cross section (i.e., plane strain), despite evidence of a possible right-slip component along the active, range-bounding Mishmi thrust (see section 4) (e.g., Coudurier-Curveur et al., 2020; Haproff et al., 2018). More studies are needed to test the possibility of oblique-slip kinematics along the Mishmi thrust. In this study, we assume that a right-slip component is negligible given the significant magnitude of crustal shortening oriented perpendicular to the orogen (Figure 7). The trends of mineral stretching lineation throughout the orogen are oriented down dip (Figure 4) and thus give no indication of oblique shearing during the development of the orogen.

3.4.2. Geometry of the Main Himalayan Detachment

We assume that thrusts located south of the Tidding mélange complex sole into a single décollement at depth (i.e., the Main Himalayan Detachment) that has a very shallow northerly dip of 4° (Figure 6b). This dip amount was constrained via geophysical studies by Mitra et al. (2005) for the western Arunachal Himalaya located ~200 km to the west and was used in the balanced cross sections of Yin et al. (2010). The décollement steepens significantly to 50° beneath the Tidding mélange complex, which is based on the general dip of surficial foliation measurements within the mélange complex. The steeper dip of the décollement in the hinterland also satisfies the interpretation of Coudurier-Curveur et al. (2020) that the average dip of the Main Himalayan Detachment may be as much as 28° across an orogen-perpendicular, map view distance of ~120 km measured between the Mishmi thrust and the Puqu fault. The steeper décollement may imply that more duplexing has occurred at depth. The depth of the Main Himalayan

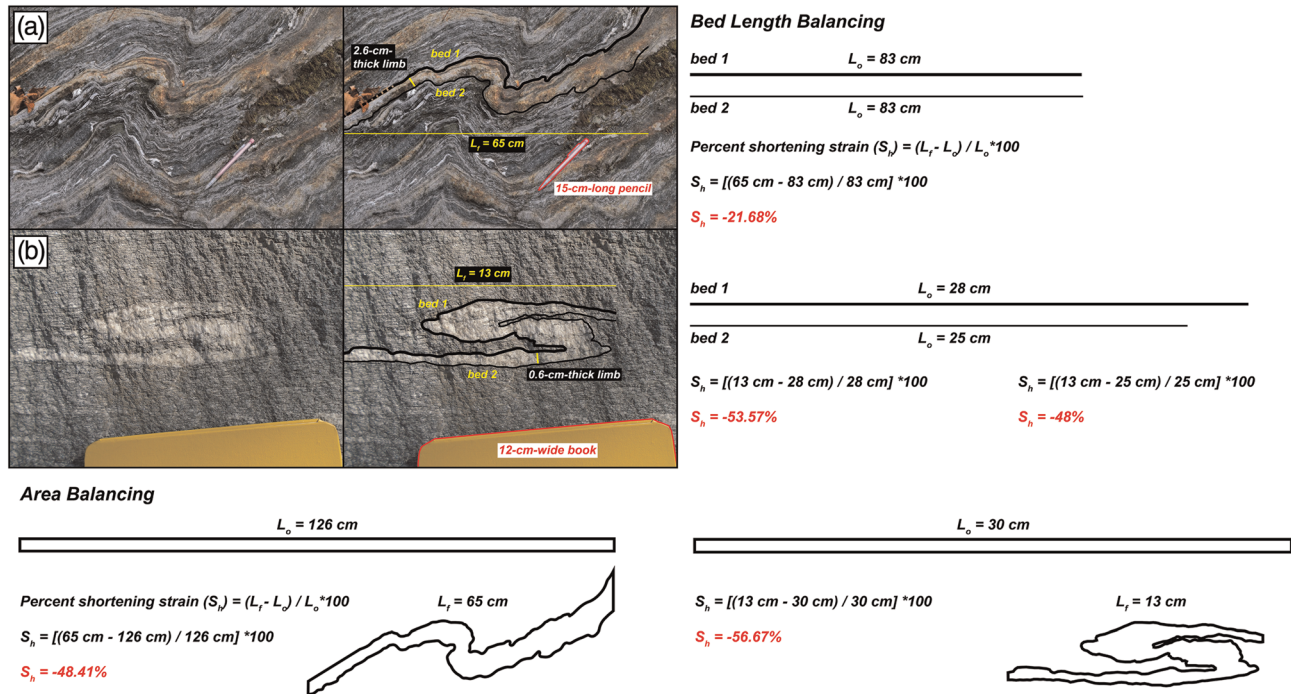


Figure 8. Field photographs of (a) an asymmetric fold within paragneiss of the Lalpani schist, located in the Lalpani thrust shear zone (modified from Haproff et al., 2018) and (b) a similar fold within paragneiss of the Mayodia gneiss, located in the Mayodia thrust shear zone. To the right of the original photographs are illustrations of the horizontal lengths of the deformed Beds 1 (upper) and 2 (lower) ($L_f = 65 \text{ cm}$ for a and 13 cm for b) and thicknesses between Beds 1 and 2 for each photograph (2.6 cm for a and 0.6 cm for b). On the far right, we show the results of bed length balancing of Beds 1 and 2. The use of this balancing method assumes folding via bedding-parallel flexural slip. This method results in percent shortening estimates of (a) ~22% and (b) ~48–54%. On the bottom, we show the results of area balancing for Folds A (bottom left) and B (bottom right). We used the most representative thicknesses of each fold limb as minimum values for the original bed thicknesses and used the areas between Beds 1 and 2 to determine the original bed lengths. This method results in percent shortening estimates of (a) ~48% and (b) ~57%.

Detachment was determined from the combined thickness of the Lalpani schist and overlying Sewak unit (Figure 6b).

3.4.3. Intraunit Shortening and Folding Mechanism

Major lithologic units exposed in the northern Indo-Burma Ranges including the Lalpani schist and Mayodia gneiss consist of metasedimentary strata that display extensive penetrative deformation including isoclinal folds and transposed original bedding (Figure 8). Exceptions to this include the low-grade to unmetamorphosed strata of the Sewak unit, which preserves original bedding at some stratigraphic levels, and unmetamorphosed conglomerate and sandstone of the Tezu unit exposed near Lohit Valley (Figure 4). Bedding measurements within the Sewak and Tezu units are subparallel to the geometry of the range-bounding Mishmi thrust at depth (Figures 4 and 6b). In the balanced cross section, we assume that penetrative foliation within the Sewak unit, the Lalpani schist, and the Mayodia gneiss is subparallel to pre-existing lithostratigraphic contacts and basal thrusts. This relationship has been observed in the LHS and GHS throughout the Himalaya as unmetamorphosed sedimentary rocks interlayered with schist and gneiss (Brunel et al., 1985; Kayastha, 1992; Sakai, 1983; Schelling, 1992; Yin, Dubey, Kelty, et al., 2010) and foliation containing relict sedimentary structures and fossils, both of which are subparallel to basal thrusts (Enos, 2017; Gansser, 1983; Long & McQuarrie, 2010). Given this assumption for the northern Indo-Burma thrust belt, we also minimized the projections of eroded hanging wall cutoffs above the surface exposure of thrusts (Figure 6b).

Our use of the balanced cross section assumes that folding of lithologic units was accommodated via flexural slip, where the original lengths and thicknesses of beds are preserved after deformation. As mentioned above, original bedding within metasedimentary strata of the Lalpani schist and the Mayodia gneiss is commonly transposed, which resulted in the development of slaty cleavage. In addition, meter- to kilometer-scale folds within lithologic units near major thrusts display thickened hinge zones and thinned

limbs (Figure 8). Area balancing is the preferred technique of mitigating this problem; however, this approach requires knowledge of the precollisional, undeformed thickness of the section involved. Given that the Himalayan orogen mostly consists of metamorphic and internally deformed rocks, the precollisional stratigraphic thicknesses remain largely unknown (Yin, Dubey, Kelty, et al., 2010; Yin, Dubey, Webb, et al., 2010). To demonstrate and quantify the influence of folding and internal deformation on these lithologic units, we calculated percent shortening strain of outcrop-scale folds within major shear zones using both the line length and area balancing techniques (Figure 8). Photograph A depicts an asymmetric fold within paragneiss of the Lalpani schist (modified from Haproff et al., 2018). Photograph B shows an isoclinal similar fold (i.e., thickened hinge and thinned limbs) within paragneiss of the Mayodia gneiss. We interpret that these folds were generated during progressive deformation where Cenozoic shear zone-parallel stretching is divided into a synkinematic pure shear component that generated the flattening fabric (i.e., foliation and isoclinal folds) and a simple shear component that generated the asymmetric folds (e.g., Fossen et al., 2019). Use of the line balancing technique (assuming bedding-parallel flexural slip) yields percent shortening estimates of ~22% for Outcrop A and ~48–54% for Outcrop B. Use of the area balancing technique results in percent shortening estimates of ~48% for Outcrop A and ~57% for Outcrop B. This exercise shows that (1) internal thickening of the Lalpani schist and the Mayodia gneiss can account for >50% strain and (2) the use of different restoration techniques can result in shortening estimates that vary from 3–9% (Outcrop B) to >25% (Outcrop A) depending on the mechanism of folding. Thus, our use of kink bend and line length measuring techniques to restore mesoscopic folds and calculate shortening strain is a simplification that yields a minimum estimate. Nonetheless, the methods provide constraints of the first-order structural architecture and minimum finite strain and allow for an admissible palinspastic reconstruction of the thrust belt based on field observations and thermochronology.

3.4.4. Pre-Cenozoic Deformation

Evidence of pre-Cenozoic deformation has been recorded in the LHS of the western Arunachal Himalaya, where the mylonitized Proterozoic Bomdila augen gneiss is conformably overlain by the undeformed Proterozoic Rupa Group (Yin, Dubey, Kelty, et al., 2010), and in the central Himalaya (e.g., Catlos et al., 2002; Gehrels et al., 2006). In our study area, we did not observe evidence of pre-Cenozoic deformation, although this does not preclude that such deformation exists. For the calculation of minimum crustal shortening calculation, we exclude intraunit strain (pre-Cenozoic and Cenozoic) and interpret that mylonitic deformation within thrust shear zones was generated during Cenozoic orogenesis. This interpretation is reasonable because hanging wall foliation and stretching lineations are subparallel to the geometry of thrust shear zones at their base and the kinematics of major thrusts matches those of hanging wall ductile fabrics.

3.4.5. Exclusion of Slip Along the Tidding Thrust, Lohit Thrust, and Walong Thrust

Propagation of thrust ramps and bedding-parallel flats is not viable within plutonic rocks, which precludes determination of slip along the Lohit thrust and Walong thrust within the Lohit Plutonic Complex (Figure 6b). For this reason, we calculated slip along major thrusts located between the Mishmi thrust and the pin line in the basal décollement located at ~6-km depth beneath the Tidding mélange complex. Slip along the Tidding thrust was measured from the southern boundary of the Mayodia klippe to the pin line in the basal décollement (Figure 7). The Tidding thrust certainly propagated from deeper crustal levels than the pin line, however, this magnitude of displacement remains unconstrained.

4. Structural Observations

Major north to northeast dipping thrust faults were observed as <1- to 5-km-wide, discrete zones of more significant ductile strain that bound less-deformed rock packages (Figure 4). In the following sections, we present detailed descriptions of major thrust shear zones and brittle faults from north to south, along with respective hanging wall structures.

4.1. Lohit Thrust and Its Hanging Wall Structures

The east striking, north dipping Lohit thrust of Nandy (1973) is the widest (~5 km) and best-expressed mylonitic shear zone along Dibang Valley based on the well-developed mylonitic fabrics and excellent exposure (Figure 4). Lithologies within the shear zone consist of a ~4-km-wide, northern section of predominantly dioritic orthogneiss and leucogneiss and a ~1-km-wide, southern section of alternating ~1- to 5-m-thick layers of amphibolite, quartzo-feldspathic schist, quartzite, and marble (Figures 4 and S7). Foliation

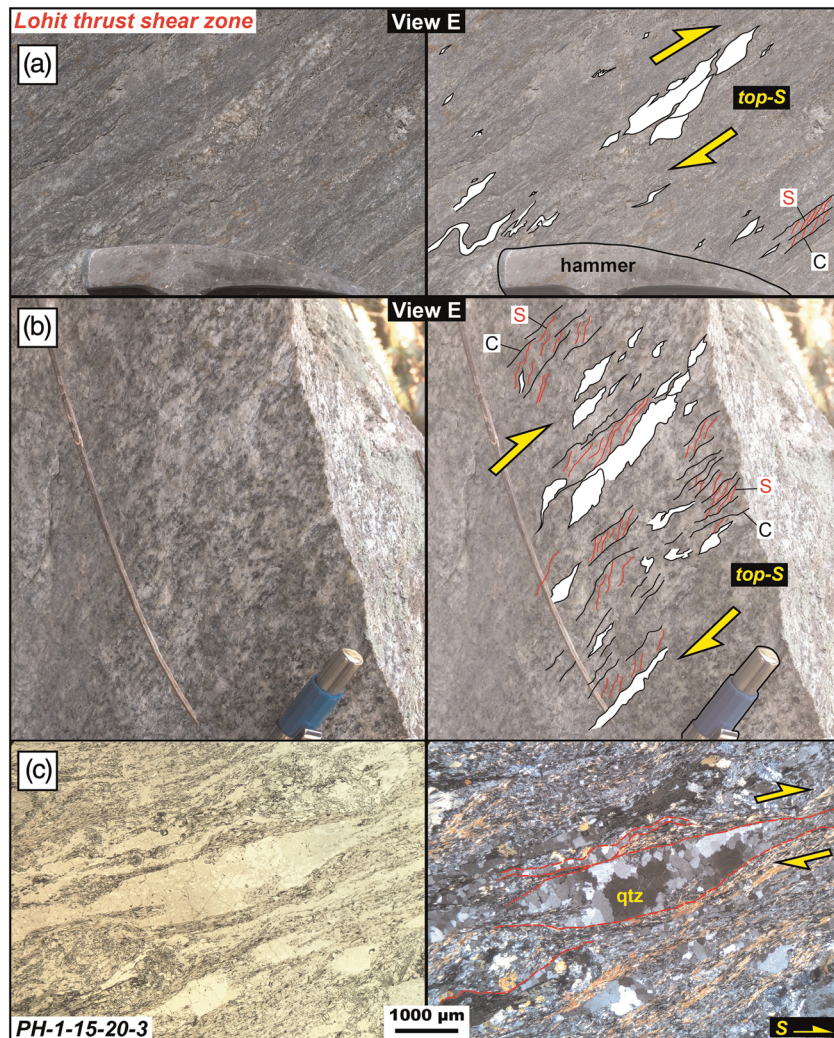


Figure 9. Field photographs of (a) schist and (b) orthogneiss within the Lohit thrust shear zone of Dibang Valley. Mylonitic fabrics including asymmetric clasts, S-C fabric, and asymmetric folds indicate top-south sense of shear. (c) Photomicrographs in plane-polarized light (left) and crossed-polarized light (right) of asymmetric quartz ribbons indicating top-south sense of shear.

throughout the shear zone dips 30° N to vertical (Figure 4) and commonly forms south vergent recumbent and isoclinal folds with wavelengths of ~ 1 to <1 m. Mineral stretching lineation within the shear zone is largely defined by quartz and feldspar and trend north-northeast (Haproff et al., 2018). Recent road construction along Dibang Valley within the shear zone revealed new exposures of a ~ 100 -m-wide deformed leucogranite body and several ~ 1 - to <1 -m-wide leucogranite dikes emanating from the body (Figure 4). The orientations of foliation and stretching lineation within the leucogranite body and dikes are less developed but oriented subparallel to the ductile fabrics of shear zone wall rocks. Outcrop-scale mylonitic fabrics observed throughout the shear zone include ~ 1 -m-long and <1 -m-wide quartz boudins, <1 m wide, north to northeast plunging sheath folds, and top-south rotated clasts, S-C fabrics, and asymmetric quartz ribbons (Figures 9a and 9b). In thin section, orthogneiss and leucogneiss samples show top-south σ and δ porphyroclasts and asymmetric ribbons and folds defined predominantly by quartz and feldspar (Figure 9c). Top-south S-C microfabrics formed by biotite, muscovite, and amphibole are common (Figure S8).

We interpret the location of the structural discontinuity between the overlying Lohit Plutonic Complex and the underlying Tidding mélangé complex within the Lohit thrust shear zone to be the boundary between the

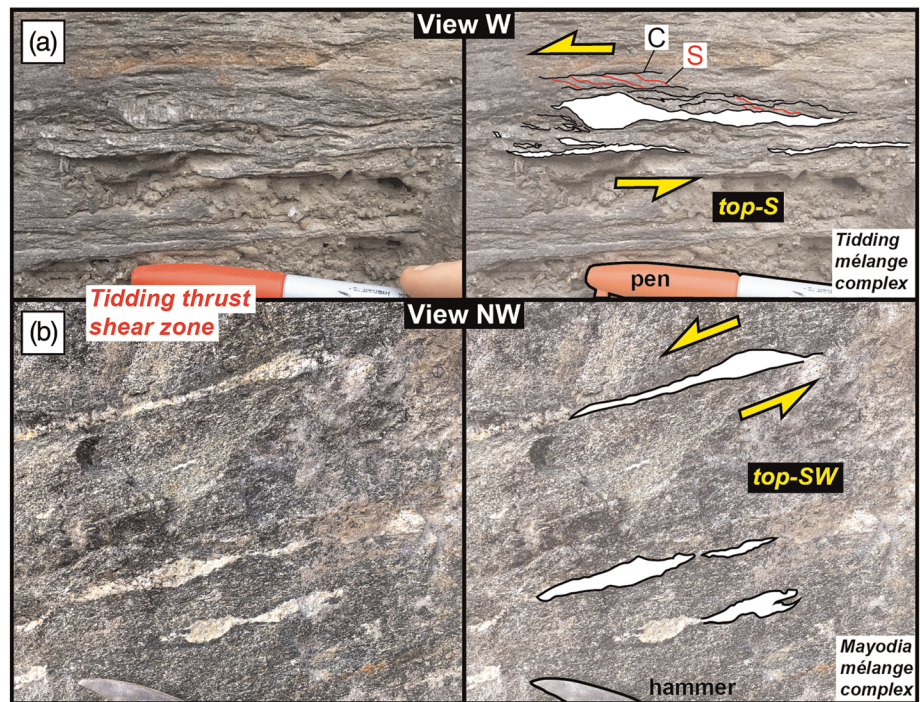


Figure 10. Field photographs of schist within the Tidding thrust shear zone exposed (a) at the base of the Tidding mélangé complex (i.e., root zone of the thrust) and (b) at the southern boundary of the Mayodia mélangé complex in Dibang Valley. Mylonitic fabrics including asymmetric clasts and S-C fabric indicate top-south to top-southwest sense of shear.

northern section of metaigneous rocks and the southern section of predominantly metasedimentary rocks (Figure 4). This interpretation is also supported by field and petrographic observations of the progression of quartz and feldspar recrystallization and ductile fabric development toward the fault.

We interpret the Lohit thrust to terminate at the northeast striking, left-slip Aniqiao shear zone (Ding et al., 2001) to the northwest of Dibang Valley (Haproff et al., 2018). South of Dibang Valley, the strike of the shear zone bends to a northerly strike and easterly dip in Lohit Valley (Haproff et al., 2018). The southern termination of the Lohit thrust remains unconstrained. However, the Lohit thrust may terminate at a younger thrust to the west, given the ~5-km width of the thrust belt south of Dibang Valley (Haproff et al., 2019), or merge with the right-slip Puqu fault in the hinterland.

In the hanging wall of the Lohit thrust, granitoids of the western Lohit Plutonic Complex belt are undeformed or display a weakly to moderately developed subsolidus foliation (Figure 4). One <1-km-wide, discrete zone of top-south deformation between the Lohit thrust and Walong thrust was mapped as a discrete north dipping thrust (Figure 4). Orthogneiss and migmatite of the eastern Lohit Plutonic Complex belt feature extensive subsolidus and magmatic foliation in various orientations that is extensively folded, which we interpret to possibly be pre-Cenozoic deformation.

The Walong thrust of Gururajan and Choudhuri (2003) is the northernmost-mapped thrust located in the hanging wall of the Lohit thrust (Figure 4). This structure is poorly exposed in Dibang Valley but was identified by a <1-km-wide zone of mylonitic deformation that separates Mesoproterozoic migmatitic orthogneiss (i.e., eastern Lohit Plutonic Complex belt) atop weakly foliated Mesozoic granitoids (i.e., western Lohit Plutonic Complex belt) (Haproff et al., 2019). Subsolidus foliations within the shear zone dip steeply (~60°) to the north in Dibang Valley and to the east in Lohit Valley (Haproff et al., 2018). Outcrop-scale kinematic indicators within the shear zone include top-south S-C fabrics, asymmetric folds, and asymmetric clasts.

4.2. Tidding Thrust and Its Hanging Wall Structures

The Tidding thrust of Gururajan and Choudhuri (2003) is expressed as a ~1-km-wide mylonitic shear zone that juxtaposes the Tidding-Mayodia mélangé complex atop mostly schist and paragneiss of the Mayodia

gneiss (Figure 4). Shear zone ductile fabrics observed in the field include sub-meter-scale quartz and feldspar boudins and rotated clasts, S-C fabrics, and asymmetric ribbons indicative of top-south to top-southwest sense of shear (Figure 10).

The northernmost exposure of the Tidding thrust in Dibang Valley is the root zone of the thrust located at the base of the Tidding mélangé complex (Figure 4). There, the shear zone places garnet mica schist atop paragneiss and leucogranite and displays well-developed, north dipping foliation ($\sim 30\text{--}60^\circ\text{N}$) and north trending stretching lineation (Figure 4). Extensive isoclinal and south vergent recumbent folds within schist and paragneiss have wavelengths of ~ 5 to <1 m. We interpret the root zone of the Tidding thrust to merge with a ramp in the Main Himalayan Detachment at ~ 6 -km depth (Figure 6b). Like the Lohit thrust shear zone to the north, the root zone of the Tidding thrust transitions to a nearly north-south orientation and easterly dip to the south of Dibang Valley (Haproff et al., 2019). The southern termination of the Tidding thrust is unclear. Both the thrust and overlying Tidding mélangé complex may be offset from lithologic equivalents of the Jade Mines Ophiolite Belt and Western Belt Ophiolites of the central Eastern Flanking Belt by series of north striking right-slip faults associated with the Sagaing fault (Searle et al., 2017) (Figure 2).

The southernmost exposures of the Tidding thrust in Dibang Valley are located along the northern and southern boundaries of the ~ 10 -km-wide, synformal Mayodia klippe, which contains the Mayodia mélangé complex in the hanging wall and the Mayodia gneiss in the footwall (Figure 4). Folding of the Tidding thrust likely occurred during the development of the Hunli duplex at depth, which generated the northwest trending synform of the Mayodia klippe and the broad, ~ 20 -km-wide, northwest trending Hunli antiform in the core of the thrust belt (Figures 4 and 6b). The Tidding thrust exposed along the northern boundary of the klippe is northwest striking and southwest dipping ($\sim 30^\circ\text{SW}$) and juxtaposes amphibolite and garnet mica schist atop paragneiss. The Tidding thrust exposed along the southern boundary of the klippe is northwest striking and northeast dipping ($\sim 36^\circ\text{NE}$) and juxtaposes a tectonic mélangé of dismembered serpentinitized ultramafic blocks, amphibolite, gabbro, and schist atop paragneiss. The Mayodia klippe is not laterally continuous to the south of Dibang Valley, as only the root zone of the thrust is exposed in Lohit Valley (Haproff et al., 2018). Similarly, we interpret that the two surface traces of the Tidding thrust that bound the klippe merge together to the northwest of Dibang Valley based on the exposure of only LHS rocks along the eastern flank of the Siang half-window (Kumar, 1997) and the Aniqiao shear zone (Ding et al., 2001).

Rocks in the hanging wall of the Tidding thrust display different styles of deformation based on their structural position. In the Tidding mélangé complex, amphibolite and schist display well-developed foliation that strikes east and dips north ($\sim 20\text{--}85^\circ\text{N}$) (Figure 4). Foliation commonly forms south vergent recumbent and isoclinal folds with wavelengths of ~ 10 to <1 m. Extensive isoclinal folding throughout the mélangé complex has resulted in axial cleavage replacing original bedding. Stretching lineation are generally north trending in Dibang Valley and northeast to east trending in Lohit Valley (Haproff et al., 2018). Metamorphic garnet porphyroblasts of >4 -mm diameter are common throughout the Tidding mélangé complex, which display “snowball” texture indicative of syngrowth rotation during top-south to top-southwest shear (Figure S9). Several discrete, meter-scale zones of ductile shear were observed throughout the Tidding mélangé complex but were excluded in the bulk shortening estimate across the thrust belt (Figure 7).

In contrast to the Tidding mélangé complex, the Mayodia mélangé complex resembles more of a classic tectonic mélangé containing fragmented blocks of variable lithologies entrained in a finer-grained, deformed matrix composed mostly of chlorite schist but also chert and carbonate (Haproff et al., 2018, 2019; Misra, 2009; Salvi et al., 2020; Sarma et al., 2012; Singh & Singh, 2011, 2013; Sinha Roy & Singh, 2002; Thakur & Jain, 1974). The schistose parts of the matrix displays moderately developed foliation that is generally southeast striking and northeast dipping ($\sim 30\text{--}80^\circ\text{N}$). Isoclinal folds and slaty cleavage are not as widespread compared to the Tidding mélangé complex to the north. Several <1 -m-wide discrete brittle faults and ductile shear zones were observed throughout the Mayodia mélangé complex (Haproff et al., 2018). Deformation increases toward the Tidding thrust from moderately developed foliation and stretching lineation to well-developed mylonitic textures and fabrics including complete recrystallization of quartz and feldspar and <1 -m-wide boudinage, S-C fabrics, and asymmetric clasts (Figure S10).

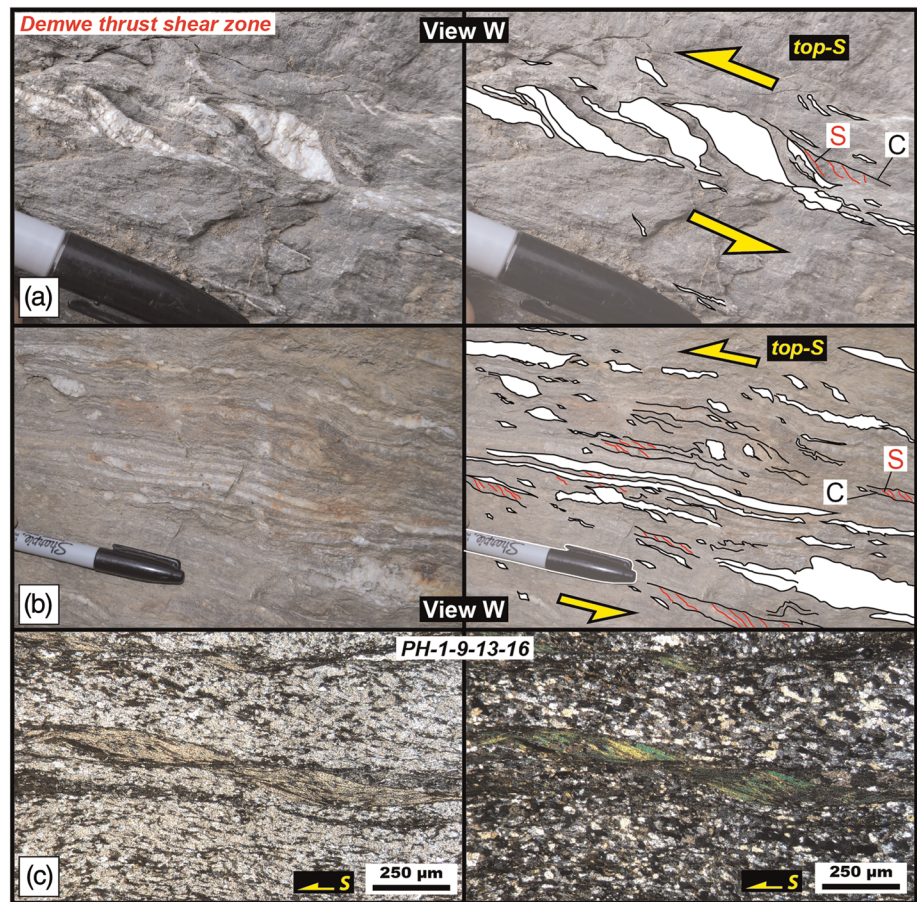


Figure 11. (a and b) Field photographs of paragneiss of the Mayodia gneiss within the Demwe thrust shear zone, Dibang Valley. Mylonitic fabrics including asymmetric clasts, S-C fabric, and asymmetric folds indicate top-south sense of shear. (c) Photomicrographs in plane-polarized light (left) and crossed-polarized light (right) of paragneiss within the Demwe thrust shear zone exhibiting mica fish and S-C fabric indicative of top-south sense of shear.

4.3. Demwe Thrust and Its Hanging Wall Structures

The Demwe thrust is expressed as a ~1-km-wide mylonite shear zone that places paragneiss and schist of the Mayodia gneiss atop metasedimentary rocks of the Lalpani schist (Figure 4). Field observations of mylonitic fabrics include sub-meter-scale boudins and σ and δ clasts defined by quartz and feldspar and S-C fabric indicative of top-south to top-southwest sense of shear (Figure 11). South vergent asymmetric and isoclinal folds have wavelengths of ~10 to <1 m. North plunging, meter-scale sheath folds are common throughout the shear zone. In thin section, schist and paragneiss samples display top-south to top-southwest mica fish, rotated garnet porphyroblasts, and asymmetric folds, σ and δ porphyroclasts, and S-C fabric defined by quartz, feldspar, and mica (Figure S11).

Like the structurally higher Tidding thrust, the Demwe thrust is folded into a ~15-km-wide, northwest trending synform in the foreland and a ~10-km-wide, northwest trending antiform in the core of the thrust belt (Figures 4 and 6). Subsequent erosion resulted in three surface exposures of the Demwe thrust along Dibang Valley: an east striking north dipping (~30°N) root zone of the thrust in the north, and two northwest striking and northeast and southwest dipping (~35°N and ~30°N, respectively) faults that are subparallel to the respective northern and southern boundaries of the Mayodia klippe (Figures 4 and 6). We interpret that the northern two surface traces of the Demwe thrust merge to the southeast and diverge to the northwest, forming the boundaries of the Hunli half-window (Figure 4). In cross section, we show the root zone of the Demwe thrust merging with the Main Himalayan Detachment at ~5-km depth (Figure 6b).

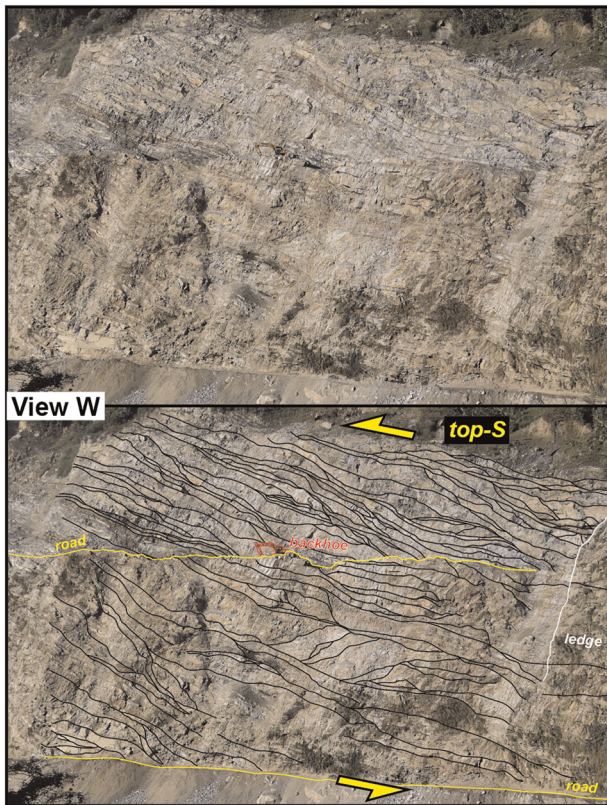


Figure 12. Field photograph of south directed thrust faults (black lines) within the Mayodia gneiss in the hanging wall of the Demwe thrust, Dibang Valley traverse. The locations of thrusts were identified based on truncations of foliation. A backhoe is in the center of the photograph for scale.

Previous studies have mapped the Demwe thrust as the MCT based on comparable lithologies in the footwall and hanging wall (e.g., Gururajan & Choudhuri, 2003; Misra, 2009). Previous studies in the northern Indo-Burma Ranges have considered the Demwe thrust to be the easternmost continuation of the MCT based on their interpretation of high-grade metamorphic rocks thrust atop medium-grade metasedimentary rocks (e.g., Gururajan & Choudhuri, 2003; Misra, 2009), which follows the classic definition of Heim and Gansser (1939). However, both Haproff et al. (2019) and Salvi et al. (2020) did not observe a significant change in metamorphic grade and lithologies across the structure. Furthermore, Haproff et al. (2019) showed that the Mayodia gneiss in the hanging wall and the Lalpani schist in the footwall both correlate with the LHS based on similar detrital zircon U-Pb ages and negative ϵ_{Nd} values. Thus, the Demwe thrust is not the lateral equivalent of the classically defined MCT separating the LHS from the overlying GHS (e.g., Heim & Gansser, 1939). Alternatively, the Demwe thrust may be the southeastern continuation of the MCT-I, which separates the underlying LHS from the overlying Lesser Himalayan Crystalline Complex and parallels the MBT around the Siang half-window (Ding et al., 2001; Kumar, 1997; Nandini & Thakur, 2011). However, more geological mapping is needed to elucidate this. The southernmost trace of the Demwe thrust is traceable to the southeast in Lohit Valley, where it was mapped by Haproff et al. (2018, 2019). The southern termination of the Demwe thrust remains unconstrained.

The northernmost Demwe thrust hanging wall features a ~5-km-wide zone that contains numerous ~1-5-m-thick, discrete ductile shear zones that bound >5-m-thick rock packages (Figure 12). These discrete shear zones feature top-south S-C fabrics and asymmetric clasts and form a larger hinterland-dipping thrust duplex system that has repeated the Mayodia gneiss (Figure S12). Between shear zones, foliation is generally northwest to northeast dipping (~25–60°) (Figure 4) and commonly forms south vergent isoclinal and asymmetric folds with wavelengths

of >1 to ~5 m (Figures S11 and 12). Stretching lineation is largely defined by quartz and feldspar and trends to the north and northwest in Dibang Valley (Figure 4). Deformed ~3- to <1-m-wide leucogranite sills and dikes were observed to crosscut and lie parallel to the foliation of host schist and paragneiss. On the Dibang Valley map, we depict the ~5-km-wide zone of intraunit duplexing as two north dipping thrusts located between the structurally lower Demwe thrust and overlying Tidding thrust (Figures 4 and 6b). Thicknesses of the Mayodia gneiss thrust sheets shown on the map are based on the observed thickness of the Mayodia gneiss in the foreland (Figures 4 and 6b). Together with the Demwe thrust, the three faults repeating the Mayodia gneiss are interpreted to be the structurally highest thrusts of the orogen-scale Hunli duplex and form opposite limbs of the Hunli antiform (Figure 6b). Slip along the Demwe thrust and two hanging wall thrusts were restored to calculate horizontal crustal shortening across the thrust belt (Figure 7). We emphasize that the simplification of the intraunit duplex as a layered thrust stack highlights the interpretation that our shortening estimate is an absolute minimum value.

4.4. Lalpani Thrust and Its Hanging Wall Structures

The north-northeast dipping Lalpani thrust of Misra (2009) is expressed as a ~1-km-wide mylonitic shear zone in the foreland of the thrust belt that places schist, phyllite, quartzite, metacarbonate, and paragneiss of the Lalpani schist atop low-grade to unmetamorphosed metasedimentary rocks of the Sewak unit (Figure 4). Well-developed shear zone foliation is generally west to northwest striking and north to northeast dipping (~30–60°). Mineral stretching lineation within the shear zone trend to the northeast in Dibang Valley. Mylonitic fabrics include sub-meter-scale boudins and top-south to top-southwest σ and δ clasts and S-C fabric defined by mica, quartz, and feldspar (Figures 13a and 13b). South vergent asymmetric and

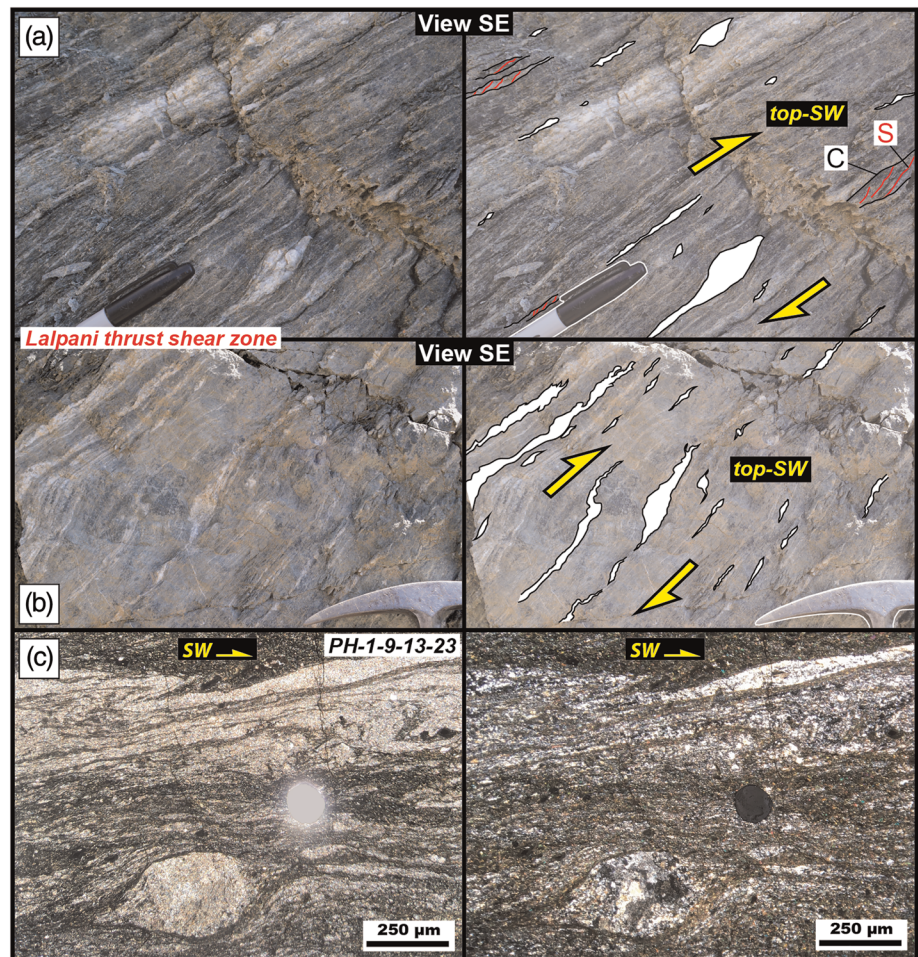


Figure 13. (a and b) Field photographs of paragneiss and schist of the Lalpani schist within the Lalpani thrust shear zone, Dibang Valley. Mylonitic fabrics including asymmetric clasts and S-C fabric indicate top-southwest sense of shear. (c) Photomicrographs in plane-polarized light (left) and cross-polarized light (right) of mylonitic schist containing top-southwest S-C fabric, asymmetric clasts, and asymmetric folds. The sample was collected within a ~1-km-wide mylonitic thrust shear zone that repeated the Lalpani schist in foreland region.

isoclinal folds are common within the shear zone and have wavelengths of ~1 to <1 m. In thin section, shear zone samples display top-south to top-southwest σ and δ porphyroclasts and asymmetric folds defined by quartz and feldspar, and S-C fabric (Figure 13c).

The Lalpani thrust may be the southeastern continuation of the MBT, which forms the boundary of the Siang half-window to the northwest and separates similar hanging wall and footwall lithologies (Ding et al., 2001; Kumar, 1997; Nandini & Thakur, 2011). South of Dibang Valley, the strike of the Lalpani thrust transitions to a northerly strike and easterly dip in Lohit Valley (Haproff et al., 2018). The southward termination of the Lalpani thrust is unknown, although the thrust may be cut by the active range-bounding Mishmi thrust. In the Dibang Valley cross section, we show the Lalpani thrust merging with the Main Himalayan Detachment at ~3-km depth (Figure 6b).

The hanging wall of the Lalpani thrust features three discrete <1-km-wide thrust shear zones that repeated the Lalpani schist (Figure 4). These thrust shear zones were mapped based on more intense ductile strain observed in the field and thin section compared to more rigid thrust sheets. Shear zone fabrics include well-developed foliation and stretching lineation, south vergent asymmetric folds, and top-southwest asymmetric porphyroclasts and S-C fabric defined by quartz, feldspar, mica, and amphibole (Figure S13). Within

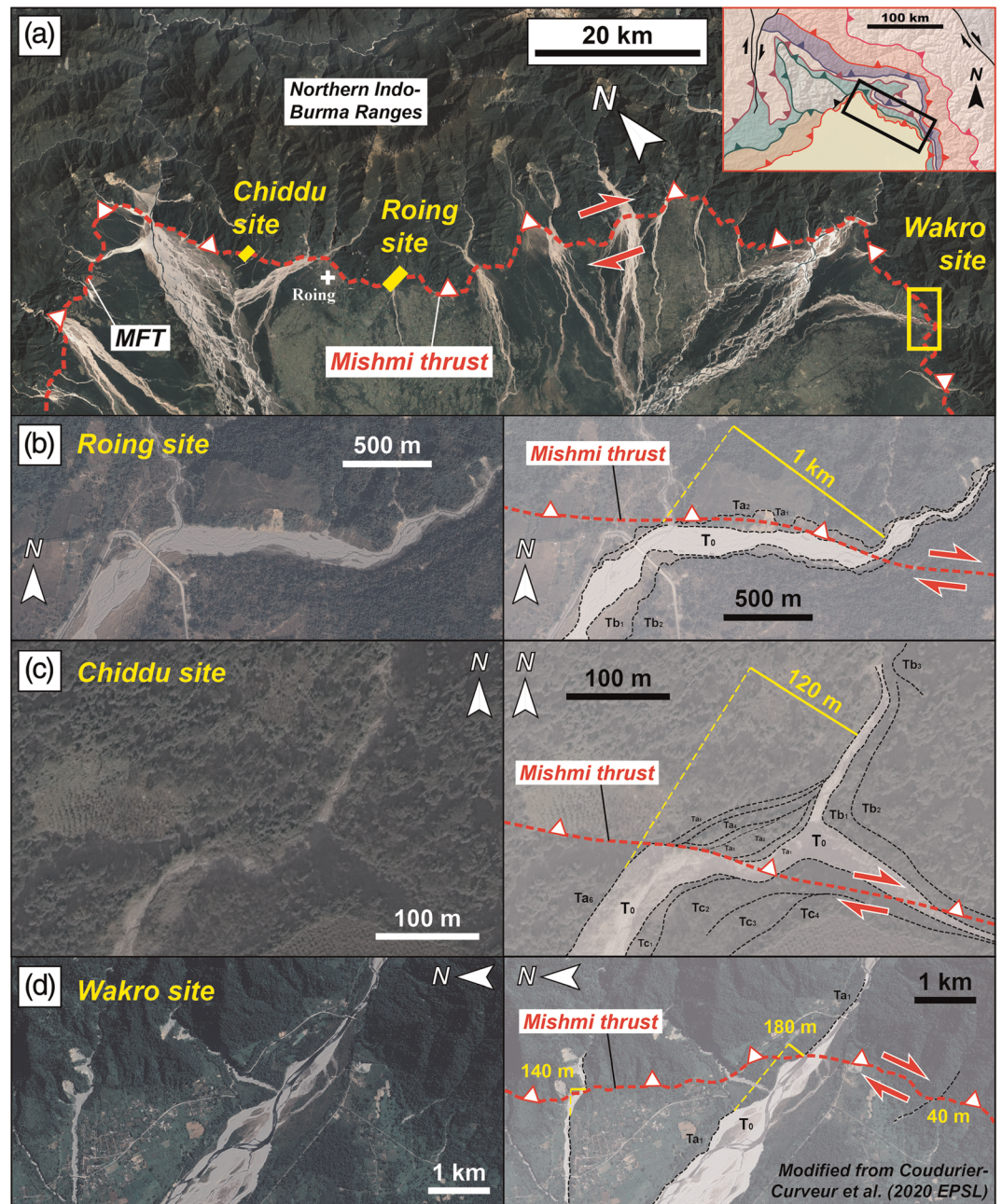


Figure 14. Google Earth-based maps of the range-bounding Mishmi thrust including (a) the surface trace of the fault along the southwest margin of the northern Indo-Burma Ranges and (b–d) three sites with geomorphic evidence of potential right-lateral slip (modified from Coudurier-Curveur et al., 2020; Haproff et al., 2018).

the shear zones, feldspar and quartz have undergone dynamic recrystallization via subgrain rotation and grain boundary migration (Figure S13). Thrust sheets contain moderately developed foliation and stretching lineation, and less recrystallized quartz and feldspar (Figure S14). Thrust sheets of ~1-km thickness were observed to comprise Mesoproterozoic-Mesozoic metasedimentary strata, whereas thrust sheets of <1-km thickness involve Mesoproterozoic-Cambrian metasedimentary strata (Haproff et al., 2019). In the core of the thrust belt, two exposed north dipping and southwest dipping (~30°), <1-km-wide mylonitic thrust shear zones have repeated the Lalpani schist and form opposite limbs of the Hunli antiform (Figures 4 and 6). These shear zones feature well-developed foliation and stretching

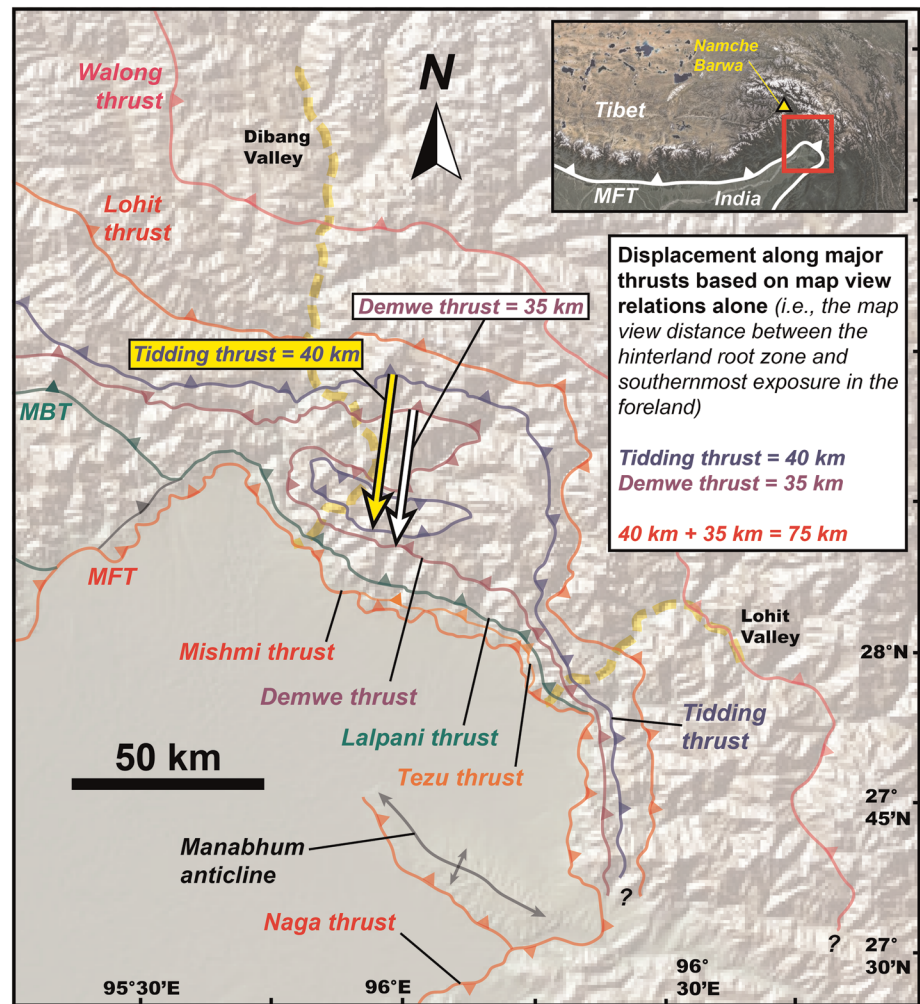


Figure 15. Map of the northern Indo-Burma showing the minimum displacements along the Tidding thrust (40 km) and Demwe thrust (35 km) based on the map view distances between their respective root zones in the hinterland and southernmost exposures the foreland (modified from Haproff et al., 2019). Horizontal crustal shortening accommodated by slip along both the Tidding thrust and Demwe thrust based on map view distance alone is 75 km. The slip vectors shown by the yellow and white arrows parallel the trend of mineral stretching lineation observed along Diband Valley (Figure 4). The yellow dashed lines show the locations of the Diband and Lohit river valleys.

lineation, top-southwest asymmetric porphyroclasts and S-C fabrics, and fully recrystallized quartz and feldspar (Figure S15). We interpret that the two thrusts are the structurally highest thrusts of the Hunli duplex out of a total of nine thrusts that have repeated the Lalpani schist (Figure 6B). The thicknesses of thrust sheets within the Hunli duplex are based on the observed thicknesses of Lalpani schist thrust sheets in the foreland (Figures 4 and 6).

4.5. Mishmi Thrust and Its Hanging Wall Structures

The northeast dipping Mishmi thrust is a brittle thrust that forms a sinuous trace along the southwestern front of the northern Indo-Burma Ranges (Figure 14a). At the opening of Diband Valley, the Mishmi thrust places metasedimentary rocks of the Sewak unit atop Quaternary alluvium deposits of the Brahmaputra foreland basin (Figure 4). At the opening of Lohit Valley, the Mishmi thrust places sandstone and conglomerate of the Tezu unit atop Quaternary alluvial deposits (Haproff et al., 2018). At Diband Valley, the range-bounding Mishmi thrust is part of a larger ~10-km-wide thrust zone also includes at least two northeast dipping imbricate brittle thrusts within the foreland basin (Figure 4). The two imbricate thrusts were identified by discrete fault surfaces that dip ~50°NE and cut Quaternary fluvial terraces (Figure S16). The

range-bounding Mishmi thrust is identified by series of northwest striking, ~5- to 10-km-long and ~20-m to <10-m-high escarpments (Coudurier-Curveur et al., 2020; Haproff et al., 2018). The irregular trace of the Mishmi thrust suggests that the fault is the surface expression of the active, low-angle Main Himalayan Detachment at depth (Figure 5). Geomorphic evidence suggests that coseismic slip along the Main Himalayan detachment and surface traces of the Mishmi thrust and the MFT triggered the M_W 8.7 1950 Assam earthquake, which remains the largest continental earthquake ever recorded (Ben-Menahem et al., 1974; Chen & Molnar, 1977; Coudurier-Curveur et al., 2020). The reinterpreted focal mechanism of Coudurier-Curveur et al. (2020) for coseismic slip along the Mishmi thrust shows southwest directed thrust kinematics with a minor strike-slip component. The geomorphic expression of the Mishmi thrust features evidence of potential right-slip displacement of Quaternary river terraces near the villages of Roing (Figure 14b), Chiddu (Figure 14c), and Wakro (Figure 14d) (Coudurier-Curveur et al., 2020). However, more detailed field investigations are needed to elucidate any right-slip component along the fault.

The Mishmi thrust links with the northeast striking MFT at the Eastern Himalayan syntaxis (Figure 14a). The southern continuation of the Mishmi thrust is unclear; the fault may merge with the northeast striking Naga thrust near the Manabhum anticline (Figure 15). On the Dibang Valley cross section, we show the Mishmi thrust dipping $\sim 15^\circ$ NE before merging with the Main Himalayan Detachment at ~ 2 -km depth (Figure 6b).

Deformation of the Sewak unit in the hanging wall of the Mishmi thrust is expressed as series of meter-scale brittle thrusts and south vergent asymmetric folds with wavelengths of ~ 5 to <1 m. Low-grade metasedimentary rocks of the Sewak unit display weakly to moderately developed foliation. One northeast dipping brittle thrust was mapped as repeating the Sewak unit (Figures 4 and 6b).

South of Dibang Valley, the hanging wall of the Mishmi thrust contains the northeast to east dipping, brittle Tezu thrust, which places metasedimentary rocks of the Sewak unit atop conglomerate and sandstone of the Tezu unit (Haproff et al., 2018) (Figure S17). The thrust is expressed by a ~ 2 -m-thick, brittle fault core within a ~ 10 -m-thick damage zone (Figure S17a). The fault core features cleavage-defined S-C fabric and a discrete thrust surface with northeast to east plunging striations, which indicate top-southwest to top-west sense of shear (Figures S17b and S17c).

5. Results of Thermochronology

In this section, we describe ZHe ages from each lithologic unit along the Dibang Valley traverse from south-east to northwest (Table 1 and Figures 4 and 6b). Quartzite PH-1-14-13-5 from the Sewak unit has a ZHe age of 5.8 ± 0.2 Ma. Structurally above the Sewak unit, samples of phyllite PH-1-12-13-5 and quartzo-feldspathic augen gneiss PH-1-9-13-27 of the Lalpani schist have ZHe ages of 5.9 ± 1.3 and 5.6 ± 0.8 Ma, respectively. Samples of a quartzo-feldspathic augen-gneiss PH-1-9-13-23 and a paragneiss PH-1-3-13-11B from the structural middle section of the Lalpani schist in the foreland yields ages of 7.8 ± 1.6 and 8.1 ± 1.4 Ma, respectively. In the uppermost structural section of the Lalpani schist in the foreland, samples of paragneiss PH-1-9-13-19A and biotite muscovite schist PH-1-3-13-9 have ZHe ages of 6.5 ± 1.3 and 9.1 ± 1.8 Ma, respectively. One augen gneiss sample PH-1-3-13-8 from the structurally uppermost section of the Mayodia gneiss in the foreland has a ZHe age of 8.1 ± 1.2 Ma. Garnet schist Sample PH-1-9-13-10 of the Mayodia mélange complex in the center of thrust belt has a ZHe age of 7.1 ± 0.8 Ma. Quartzo-feldspathic schist PH-1-9-13-2 of the Lalpani schist within the Hunli half-window has an average ZHe age of 7.8 ± 1.4 Ma. In the hinterland of the thrust belt, garnet biotite muscovite schist PH-1-8-13-26 of the Tidding mélange complex yields six ZHe ages from oldest to youngest of 32.6 ± 2.6 , 27.6 ± 2.2 , 18.1 ± 1.5 , 17.4 ± 1.4 , 16.3 ± 1.3 , and 12.4 ± 1 Ma. The northernmost three granitoid samples of this study from the western belt of the Lohit Plutonic Complex have average ZHe ages from southwest to northeast of 6 ± 0.8 Ma (PH-1-8-13-8), 7.9 ± 0.1 Ma (PH-1-8-13-7), and 10.5 ± 0.6 Ma (PH-1-8-13-1B). Sample ANI-7 collected from the Lohit Plutonic Complex and dated by Salvi et al. (2020) has single zircon grain ZHe ages of 11.6 ± 0.7 , 16.9 ± 1 , 14 ± 0.9 , and 26.7 ± 1.7 Ma. We report an average of 14.2 ± 2.7 Ma for the youngest three ages and exclude the oldest individual age of 26.7 Ma due to a low effective uranium concentration, which may indicate incomplete grain dissolution. The majority of the ZHe ages from this study and Salvi et al. (2020) are Middle to Late Miocene (Figure 6a), with no observed age-eU trends (i.e., the ages are uniform across the sample eU values) (Figure 6c), which we interpret to reflect a widespread pulse of relatively rapid cooling that occurred across the orogen.

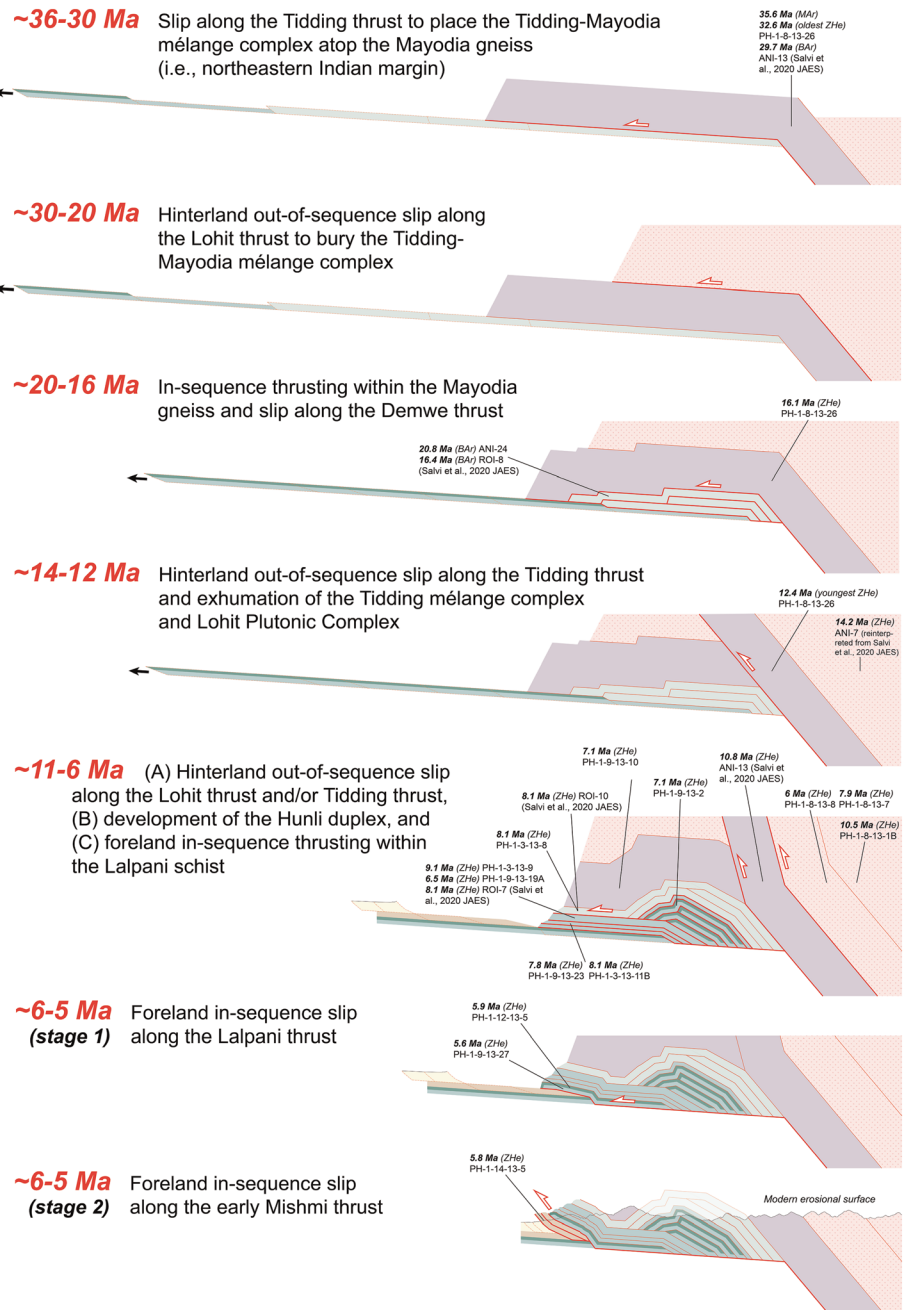


Figure 16. Palinspastic reconstruction of the Dibang Valley cross section since ~36–30 Ma based on $^{40}\text{Ar}/^{39}\text{Ar}$ and zircon (U-Th)/He ages from this study and Salvi et al. (2020). Abbreviations: BAR: biotite $^{40}\text{Ar}/^{39}\text{Ar}$, MAR: muscovite $^{40}\text{Ar}/^{39}\text{Ar}$, ZHe: zircon (U-Th)/He.

Muscovite $^{40}\text{Ar}/^{39}\text{Ar}$ thermochronology results of garnet schist PH-1-8-13-26 show that the sample probably contained excess argon, and its spectra shows older ages (>50 Ma) for the first two steps and a range of ages between ~30 and ~40 Ma for the remaining >90% of gas released (Figure S2 and Table S3). The weighted mean of eight steps in the $^{40}\text{Ar}/^{39}\text{Ar}$ age spectra is 35.6 ± 1.5 Ma (Figure S2). We interpret that the sample passed through an effective muscovite closure temperature of ~350–425°C at ~36 Ma. Quartz grains within the sample display interlobate grain boundaries indicative grain boundary migration dynamic recrystallization, which suggests deformation temperatures of ~500–550°C (Stipp et al., 2002) (Figure S18).

ZHe ages from sample PH-1-8-13-26 from the Tidding mélangé complex are characterized by a positive ZHe age-effective uranium ($eU = [U] + 0.235[Th]$) trend (shown as purple diamonds on Figure 6c), which is consistent with protracted residence in the ZHe partial retention zone based on the radiation damage-annealing model for He diffusion in zircon (Guenther et al., 2013). We explored possible thermal histories for this sample on the basis of representative ZHe ages over the eU range through inverse modeling using HeFTy v.1.9.1 (Ketchum, 2005) (see the supporting information for modeling details and results). Inverse modeling results of these ZHe ages and age- eU trends (Table 1) suggest two distinct phases of cooling separated by an intermittent isothermal or very slow cooling phases (Figures S3 and S4). Expected age- eU trends from forward models of selected “good” fit time-temperature paths (derived from the inverse models) are broadly consistent with the observed age- eU trend from the data (Figures S5 and S6). Both inverse and forward HeFTy models support our interpretation that Sample PH-1-8-13-26 records two distinct phases of cooling since ~36 Ma (Figures 4 and 6b), yielding the dispersed ages and age- eU trends, which is integrated in the palinspastic reconstruction of the Dibang Valley cross section (Figure 16).

6. Restored Cross Section

The horizontal length of the deformed Dibang Valley section (L_f), measured from the surface trace of the Mishmi thrust to the pin line at the ramp-to-flat kink in the basal décollement, is 44 km (Figure 7). Restoration of the section yields undeformed horizontal length (L_o) of 324 km and a minimum shortening estimate of 280 km, equivalent to a ~86% strain (Figure 7). Similar shortening strain values of ~83% and ~86% were constrained by Ningthoujam et al. (2015) and Salvi et al. (2020), respectively, despite different interpretations to the subsurface structural geometry along Dibang Valley.

We interpret that the Tidding and Mayodia mélangé complexes originate from the same tectonic mélangé in the hanging wall of the Tidding thrust, which was telescoped along a thrust flat and subsequently folded during the development of the Hunli duplex (Figure 7). Therefore, the minimum displacement of the Tidding thrust based on the horizontal map view distance between the root zone of the thrust in the hinterland to the southernmost exposure in the foreland is 40 km (Figure 15). Similarly, the Demwe thrust has displaced the Mayodia gneiss 35 km to the southwest based solely on the map view geometry of the thrust (Figure 15). The combined map view displacements along the Demwe thrust and Tidding is 75 km, which represents a significant portion of the >280 km shortening estimate.

We emphasize that our crustal shortening estimate is a minimum value based on several assumptions and simplifications regarding the construction and restoration of the Dibang Valley cross section. These assumptions and simplifications include (1) the exclusion of intraunit shortening, (2) the exclusion of slip along the Tidding thrust at crustal levels deeper than 6 km, (3) the exclusion of slip along the Lohit thrust and Walong thrust, (4) minimization of projected hanging wall cutoffs, (5) the exclusion of potential pre-Cenozoic deformation, and (6) the observation of meter-scale thrust duplex systems within the Mayodia gneiss that have been simplified in the cross section (Figure 12).

7. Discussion

The structural framework of the northern Indo-Burma Ranges is comparable to that of Himalaya to the west based on the exposure of a Cenozoic southwest to west directed, imbricate thrust belt featuring a hinterland-dipping duplex system that involves mostly rocks of the LHS (i.e., Lalpani schist and Mayodia gneiss) (Figure 6b). North dipping thrusts branch from a single low-angle, northeast to east dipping décollement, which is exposed on the surface as the southernmost Mishmi thrust (=easternmost MFT) (Figure 6b). However, the northern Indo-Burma thrust belt is distinct from the Himalayan orogen based on evidence of potential right-slip motion along the active Mishmi thrust (Figure 5) and the absence of faults with top-to-Lhasa terrane kinematics such as the STD or Great Counter thrust. Furthermore, the northern Indo-Burma thrust belt exposes part of the India-Asia suture as an isolated klippe in the foreland (i.e., the Mayodia klippe) (Figures 4 and 6b), which is a seldom identified feature in the Himalayan orogen (e.g., Corfield et al., 2001; Hodges, 2000; Searle et al., 1988, 1997). Lastly, the map view horizontal width across the thrust belt measured from the southernmost range-bounding thrust to the India-Asia suture zone decreases dramatically from ~33 km along Dibang Valley in the north to ~5 km along Lohit Valley in the south (Haproff et al., 2019). This southward narrowing of the thrust belt starkly contrasts the ~200-km

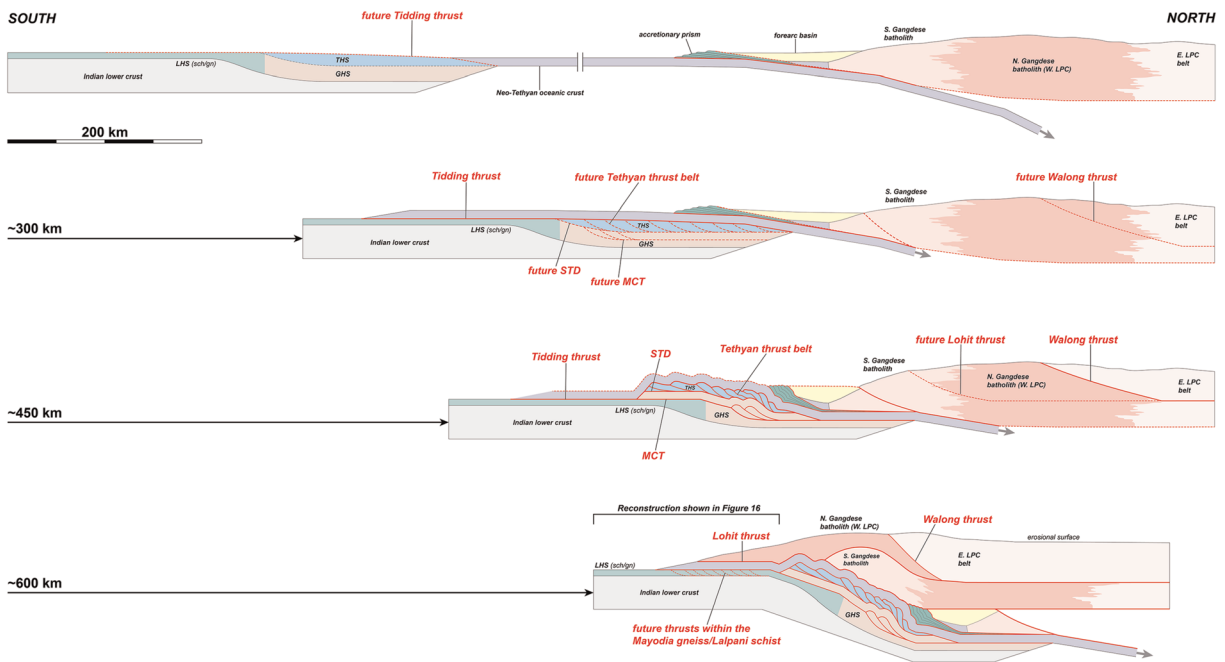


Figure 17. Possible scenario for the kinematic history of the northern Indo-Burma Ranges since the latest Jurassic depicted as series of schematic cross sections oriented along $\sim E95^\circ$ longitude.

distance across the central Himalayan orogen to the west (Figure 1). These elements of the structural framework of the northern Indo-Burma Ranges imply a unique Cenozoic geological evolution for the Eastern Flanking Belt, which is described in the following sections.

7.1. Cenozoic Shortening and Development of the Northernmost Eastern Flanking Belt

Restoration of the Dibang Valley cross section produces a minimum horizontal shortening estimate of 280 km ($\sim 86\%$ strain) (Figure 7). This shortening magnitude is less compared to estimates across the western Arunachal Himalaya directly to the west (e.g., 515–775 km (Yin, Dubey, Kelty, et al., 2010) and other segments of the orogen (see Long, McQuarrie, Tobgay, & Grujic, 2011, for a compilation). Percent shortening strain across the northern Indo-Burma Ranges exceeds estimates for the western Arunachal Himalaya south of the Indus-Yarlung suture zone ($\sim 70\text{--}75\%$) (Yin, Dubey, Kelty, et al., 2010). The $\sim 86\%$ strain in the study area only compares to estimates for the central Himalaya of Western Nepal and Sikkim that exclude the Tethyan Himalayan thrust belt ($\sim 80\text{--}85\%$ and 80% , respectively) (Bhattacharyya & Mitra, 2009; Long, McQuarrie, Tobgay, & Grujic, 2011; Mitra et al., 2010; Robinson et al., 2006).

We interpret that in the northern Indo-Burma Ranges, the combination of (1) $\sim 86\%$ shortening strain, (2) southward narrowing of the thrust belt, and (3) absence of the GHS, THS, and Cenozoic Gangdese magmatic arc complex are related to a greater magnitude of crustal shortening and erosion and/or continental underthrusting along the margin of the present-day eastern Himalayan syntaxis and northern Indo-Burma Ranges compared to Himalayan orogen to the west. In this model, entire tectonostratigraphic divisions of the Himalayan orogen and southern Lhasa terrane that were potentially shortened by hundreds of kilometers have completely eroded or been underthrust along the easternmost collisional boundary. This spatial gradient in shortening strain from the Himalayan orogen to the northern Indo-Burma thrust belt supports tectonic models that involve Cenozoic clockwise rotation of the Eastern Flanking Belt during viscous crustal flow around the eastern Himalayan syntaxis (Figure 3c) (e.g., Cobbold & Davy, 1988; England & Houseman, 1986; Haproff et al., 2018; Kreemer et al., 2014; Li et al., 2013; Royden et al., 1997). Figure 17 depicts the one scenario for the kinematic history of the northern Indo-Burma Ranges as series of orogen-scale schematic cross sections from precollision to the present day. In this model, the progressive development the orogen involved (1) the Tidding thrust placing the Tidding-Mayodia mélangé complex atop the Greater Indian margin (i.e., THS, GHS, and LHS), (2) initial shortening within the THS, GHS, and

overlying Tidding-Mayodia mélangé complex and within the forearc basin and Gangdese batholith of the Lhasa terrane, and (3) underthrusting of the shortened margins of Greater India (i.e., THS, GHS, and LHS) and the Lhasa terrane beneath the Lohit Plutonic Complex (i.e., northern Gangdese batholith) along the Lohit thrust. Although the kinematic evolution is nonunique, given alternatives for the precollisional lithostratigraphic configurations to the Greater Indian margin and progression of postcollisional shortening and erosion and/or underthrusting, we emphasize that it provides a viable model to explain the present-day exposures in the context of the known structural architecture.

7.2. Timing of Cenozoic Thrusting

The application of ZHe and $^{40}\text{Ar}/^{39}\text{Ar}$ thermochronology along Dibang Valley of the northern Indo-Burma Ranges allows for the palinspastic reconstruction of the thrust belt since late Eocene to Oligocene time (~36–30 Ma) (Figure 16). We exclude major Himalayan-Tibetan lithologic units located between the LHS and Indus-Yarlung suture zone that are not exposed at the present day (i.e., GHS, THS, and Cenozoic Gangdese magmatic arc complex).

At ~36–30 Ma, the Tidding-Mayodia mélangé complex cooled through the temperatures of $^{40}\text{Ar}/^{39}\text{Ar}$ muscovite and ZHe closure (i.e., ~425°C and ~180°C, respectively) (Figures S3 and S4). Given the implied fast rate of cooling (i.e., >30°C/Myr) and the spatial position of the samples within the Tidding thrust hanging wall, we interpret that this cooling was related to motion up a ramp along the Tidding thrust that placed the mélangé complex atop the northeastern Greater Indian margin (i.e., the Mayodia gneiss). The potential for spatially or temporally varying thermal structure in this region can complicate this interpretation, but ramp-related cooling of the hanging wall remains the simplest explanation. From ~30–20 Ma, the out-of-sequence Lohit thrust placed the Lohit Plutonic Complex atop the Tidding-Mayodia mélangé complex, which may have reburied the mélangé complex to within or beneath the zircon He partial retention zone. From ~20–16 Ma, the Mayodia gneiss and the Tidding-Mayodia mélangé complex were exhumed as the Demwe thrust and thrusts within the Demwe thrust hanging wall propagated toward the foreland (Figure 16).

Beginning in the Middle to Late Miocene, a widespread pulse of cooling occurred across the orogen from the Lohit Plutonic Complex to the Sewak unit, which we relate to coeval foreland thrust propagation and hinterland out-of-sequence thrusting. From ~14–12 Ma, out-of-sequence motion up a ramp of the Tidding thrust exhumed the hinterland section of the Tidding-Mayodia mélangé complex and the Lohit Plutonic Complex. From ~11–6 Ma, continued out-of-sequence slip along ramps of the Tidding thrust and possibly the Lohit thrust exhumed the mélangé complex and the Lohit Plutonic Complex. Continued out-of-sequence slip along the Tidding thrust in the hinterland may have generated the more well-developed ductile strain observed in the Tidding mélangé complex in contrast to the Mayodia mélangé complex in the foreland. During the same period, the Lalpani schist was exhumed in the core of the thrust belt as the Hunli duplex was developing. From ~6–5 Ma, the Lalpani thrust exhumed the southernmost-exposed section of the Lalpani schist in the foreland. Sometime after this, the Mishmi thrust placed the Sewak unit atop alluvium of the active foreland basin.

We calculated long-term shortening and strain rates across the northern Indo-Burma thrust belt based on initiation ages of thrusting at 36–30 and 21–16 Ma. The 36-Ma age corresponds to the oldest $^{40}\text{Ar}/^{39}\text{Ar}$ ages from the Tidding-Mayodia mélangé complex in the hinterland, and the 21- to 16-Ma age corresponds to the oldest $^{40}\text{Ar}/^{39}\text{Ar}$ ages from the Mayodia gneiss (Figure 16). All shortening rates are minimums. Assuming thrusting initiated at 36–30 Ma, our total shortening of >280 km equates to a minimum long-term bulk shortening rate of 7.8–9.3 mm/yr. This range of shortening rates is comparable to those determined for the Bhutan Himalaya from ~10 Ma to the present (3–10 mm/yr) but much slower than the shortening rates estimated prior to 10 Ma (e.g., 28–35 and 10–23 mm/yr) (Long et al., 2012; McQuarrie et al., 2014). The long-term shortening rates of 7.8–9.3 mm/yr are also less than the Holocene shortening rate across the MFT zone of the western Arunachal Himalaya (~23 mm/yr) and the GPS velocities across the Arunachal Himalaya, southeastern Tibet, and Shillong plateau (17–29 mm/yr) (Banerjee et al., 2008; Burgess et al., 2012; Devachandra et al., 2014; Gupta et al., 2015; Stevens & Avouac, 2015). Alternatively, the 21- to 16-Ma onset of thrusting south of the Tidding mélangé complex corresponds to >242-km shortening, which equates to shortening rates of 11.5–15.1 mm/yr. These shortening rates since 21–16 Ma are comparable to some of

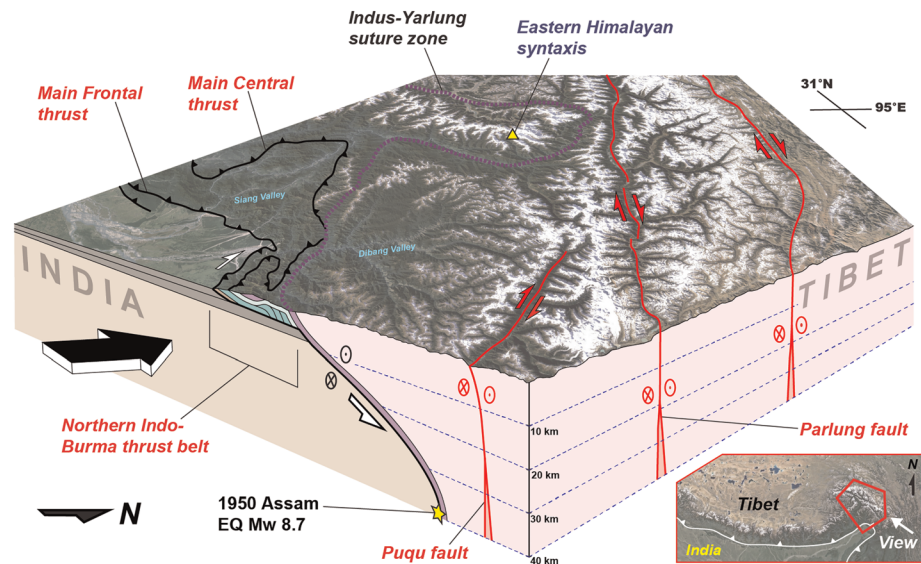


Figure 18. Oblique-view block diagram depicting strain partitioning around the eastern Himalayan syntaxis. Base satellite imagery is from Google Earth. The magnitude of the 1950 Assam earthquake (M_W 8.7) is from Ben-Menahem et al. (1974), Chen and Molnar (1977), and Coudurier-Curveur et al. (2020).

the >10 -Ma rates across Bhutan and the GPS velocities in the region but slightly slower than the Holocene MFT shortening rate in the western Arunachal Himalaya.

We calculated bulk, one-dimensional strain rates for the northern Indo-Burma Ranges by dividing strain values by the duration of deformation. Shortening of 86% beginning in the Tidding-Mayodia mélange complex since 36–30 Ma yields strain rates of $7.6\text{--}9.1 \times 10^{-16} \text{ s}^{-1}$, whereas shortening of 85% beginning in the Lalpani schist at 21–16 Ma yields strain rates of $1.3\text{--}1.7 \times 10^{-15} \text{ s}^{-1}$. The strain rates of $7.6\text{--}9.1 \times 10^{-16} \text{ s}^{-1}$ are comparable to average strain rates calculated for the entire Himalayan-Tibetan orogen at the present day and throughout the Cenozoic (Clark, 2012; Zusa et al., 2019). The faster strain rates of $1.3\text{--}1.7 \times 10^{-15} \text{ s}^{-1}$ since 21–16 Ma are similar to the long-term rate across the western Arunachal Himalaya of $1.1 \times 10^{-15} \text{ s}^{-1}$ since 20 Ma (70% strain) (Yin, Dubey, Kelty, et al., 2010) and the averaged rate from GPS velocities across the same region of $\sim 2\text{--}6 \times 10^{-15} \text{ s}^{-1}$ (23 mm/yr across the ~ 300 -km-wide Himalayan orogen) (Banerjee et al., 2008; Burgess et al., 2012; Kreemer et al., 2014; Stevens & Avouac, 2015).

We prefer the shortening rate and strain rate calculated since 21–16 Ma (i.e., 11.5–15.1 mm/yr and $1.3\text{--}1.7 \times 10^{-15} \text{ s}^{-1}$, respectively) as most of the shortening in the study area was accommodated since that time within the Mayodia gneiss, the Lalpani schist, and the Sewak unit (Figure 16). Comparable long-term and short-term rates for the northern Indo-Burma Ranges and western Arunachal Himalaya to the west may suggest that shortening strain since the middle Miocene has remained relatively constant. However, shortening strain across the easternmost Himalaya and northern Indo-Burma Ranges may vary at shorter time-scales as observed for the Bhutan Himalaya (Long et al., 2012; McQuarrie et al., 2014). Furthermore, our interpretation that strain markers in the study area have been erased due to increased shortening and erosion and/or underthrusting implies that long-term rates may be significantly faster.

7.3. Active Strain Partitioning

Active deformation in the northern Indo-Burma Ranges is expressed by two fault systems: the oblique-slip Mishmi thrust along the range front in the southwest and right-slip Puqu and Parlung faults of southeast Tibet in the northeast (Figure 5). The Mishmi thrust is thought to be the surface trace of the Main Himalayan detachment at depth and responsible for the M_W 8.6 1950 Assam earthquake that occurred at ~ 37 -km depth (Coudurier-Curveur et al., 2020). In southeast Tibet, the active right-slip Puqu and Parlung faults are the southeastern extensions of the Jiali fault zone, located directly north of the eastern Himalayan syntaxis (Figure 1). Based on this structural framework, we suggest that active deformation surrounding the eastern Himalayan syntaxis is partitioned between right-lateral thrust motion along the Main

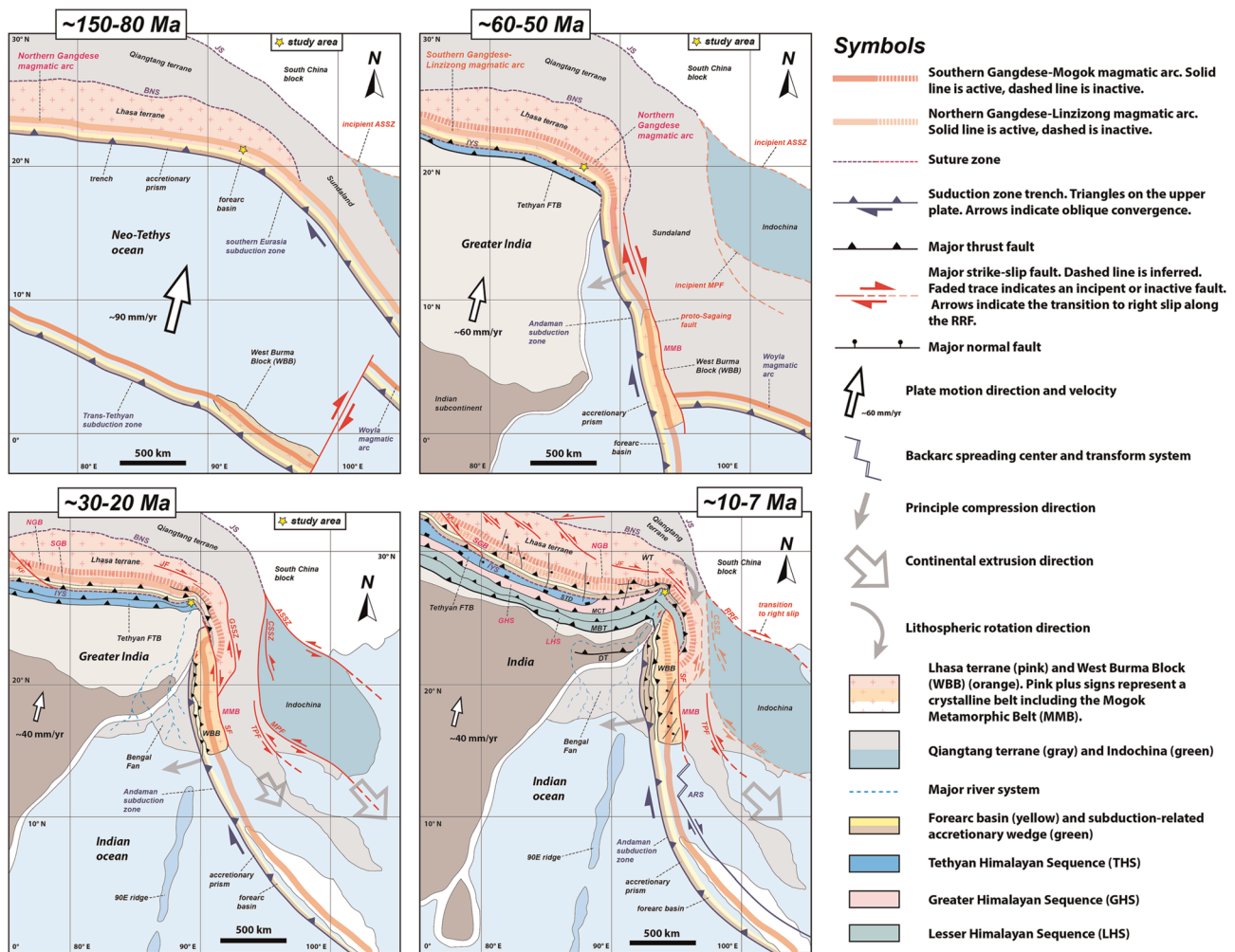


Figure 19. Tectonic evolution of the eastern Himalayan orogen, southeastern Tibetan Plateau, and Southeast Asia since the Late Cretaceous, depicted at ~80, ~50, ~20, and ~10 Ma. References are listed on the bottom of the figure. The paleogeographic configuration is adapted from Lee and Lawver (1995), Hall (2012), van Hinsbergen et al. (2011), Metcalfe (2013), Morley and Searle et al. (2017), van Hinsbergen et al. (2019), and Westerweel et al. (2019). Abbreviations: ARS: Andaman rift system, ASSZ: Ailao Shan shear zone, BNS: Bangong-Nujiang suture, CSSZ: Chongshan shear zone, DT: Dauki thrust, FTB: fold and thrust belt, GHS: Greater Himalayan Sequence, GSSZ: Gaoligong Shan shear zone, IYS: Indus-Yarlung suture, JF: Jiali fault, JS: Jinsha suture, KF: Karakorum fault, LHS: Lesser Himalayan Sequence, MBT: Main Boundary thrust, MCT: Main Central thrust, MMB: Mogok Metamorphic Belt, MPF: Mae Ping fault, NIBR: northern Indo-Burma Ranges, NGB: northern Gangdese belt, PF: Puqu-Parlung fault, pSF: proto-Sagaing fault, RRF: Red River fault, SF: Sagaing fault, SGB: southern Gangdese belt, STD: South Tibetan detachment, TPF: Three Pagodas fault, WBB: West Burma block, WT: Walong thrust.

Himalayan detachment (i.e., the Mishmi thrust) and right-slip motion along the Puqu and Parlung faults. In the hinterland of the thrust belt, the Main Himalayan detachment may merge at depth with the Puqu fault, forming a crustal-scale right-slip flower structure (Figure 18). Slip along this structure likely accommodates oblique India-Asia convergence along the western boundary of the northernmost Eastern Flanking Belt and continued southward crustal flow of overriding plate lithosphere around the eastern Himalayan syntaxis.

7.4. Mesozoic-Cenozoic Tectonic Evolution of the Easternmost India-Asia Collisional System

We present a model for the Mesozoic-Cenozoic evolution of the easternmost India-Asia collisional system including the easternmost Himalayan orogen, Eastern Flanking Belt, southeast Tibetan Plateau, and part of southeast Asia, compiled from the findings of this study and published knowledge of the geological framework and paleogeography of the region. The Mesozoic-Cenozoic evolution is shown in map view in four time stages (~150–80, ~60–50, ~30–20, and ~10–7 Ma) (Figure 19). Important elements of the reconstruction are the locations and migrations of major lithospheric blocks and terranes, the lifespans, kinematics, and

displacements of major faults, and the petrogenesis, deformation, and erosion of major lithologic units. Deformation to the north of the Bangong-Nujiang suture is not included in the reconstruction. The longitudinal size of northeast Greater India is based on that of van Hinsbergen et al. (2011).

7.4.1. Stage 1: Circa 150–80 Ma

Continuous northward subduction of Neo-Tethys oceanic lithosphere occurred along a northwest trending southern Asian margin comprising the Lhasa terrane and Sibumasu block (Li et al., 2020; Lin et al., 2013; Westerweel et al., 2019). Latest Jurassic-Cretaceous arc magmatism and forearc sedimentation occurred along a continuous belt that included the northern Gangdese batholith belt, western Lohit Plutonic Complex belt, and Mogok-Mandalay-Mergui belt. At the present-day E95° longitude of the northern Indo-Burma Ranges and southeastern Tibet, Mesozoic granitoids intruded preexisting basement rocks including Mesoproterozoic orthogneiss of the eastern Lohit Plutonic Complex belt and Bomi-Chayu Complex of the southern Lhasa terrane (Xu et al., 2013). The Tidding-Mayodia mélange complex developed as part of a subduction-related accretionary prism to the south of a forearc basin sequence. By ~80 Ma, the Greater India was located >4,000 km south of the southern Lhasa terrane at latitude S20° (Torsvik et al., 2012). The West Burma block was located just north of the equator as part of a Trans-Tethyan island arc system (Westerweel et al., 2019).

7.4.2. Stage 2: Circa 60–50 Ma

By Eocene time, the Western Belt Ophiolites, Naga ophiolite, and Andaman ophiolite of the southern Indo-Burma Ranges were emplaced between the West Burma block and India (Westerweel et al., 2019). Subsequent collision of the West Burma block and India with Asia (i.e., southern Lhasa terrane and Sibumasu block) resulted in the emplacement of ophiolitic rocks of the Indus-Yarlung suture zone, Tidding-Mayodia mélange complex, and the Mogok-Mandalay-Mergui Belt. Cenozoic magmatism continued throughout the southern Lhasa terrane (Coulon et al., 1986; Ding et al., 2003; Guan et al., 2012; Lee et al., 2009), including the present-day northern Indo-Burma Ranges, and the central and southern zones of the Eastern Flanking Belt (Mitchell, 1993; Mitchell et al., 2012).

In the eastern Himalayan orogen and the northern Indo-Burma thrust belt, initial shortening across the Tethyan thrust belt occurred following emplacement of the ophiolitic rocks atop Greater India (e.g., Murphy & Yin, 2003; Ratschbacher et al., 1994). Collision between the northeastern margin of Greater India and the newly accreted West Burma block occurred at a highly oblique angle, resulting in right-slip shear along the plate boundary (Westerweel et al., 2019).

7.4.3. Stage 3: Circa 30–20 Ma

By Oligo-Miocene time, the Linzizong volcanic sequence was emplaced and arc magmatism continued throughout the southern Lhasa terrane (Coulon et al., 1986; Ding et al., 2003; Guan et al., 2012; Lee et al., 2009). In the eastern Himalayan orogen, the Gangdese thrust placed the southern Gangdese batholith atop Xigaze forearc sediments and ophiolitic mélange rocks of the Indus-Yarlung suture zone (Yin et al., 1994, 1999). The Greater Counter thrust (=Renbu-Zedong thrust) placed the ophiolitic mélange rocks atop the Xigaze forearc basin (Yin et al., 1999). In the eastern Himalayan orogen, shortening within the Tethyan Himalayan thrust belt was coeval with slip along the MCT and STD to the south (DeCelles et al., 2016; Yin, Dubey, Kelty, et al., 2010).

In the northern Indo-Burma thrust belt, slip along the Walong thrust, Lohit thrust, Tidding thrust, and Demwe thrust shortened the Lohit Plutonic Complex, the Tidding-Mayodia mélange complex, and the Mayodia gneiss (i.e., LHS). Erosion of the thrust belt results in deposition of the Sewak and Tezu units in a foreland basin. Slip along the east to southeast striking Jiali and Parlung faults accommodated southeastward extrusion of Asian lithosphere (Lee et al., 2003).

In the central and southern segments of the Eastern Flanking Belt, magmatism continued due to northward oblique subduction of relict Neo-Tethys oceanic lithosphere attached to the Indian continent (Lee et al., 2016). In the southern Indo-Burma Ranges, southwest to west directed thrust belts developed within continental shelf deposits to the west of the Central Burma basin as the Indian continent was underthrust below (Maurin & Rangin, 2009a; Rangin et al., 2013). Slip along the north-south striking Sagaing fault between the West Burma block and Sibumasu block resulted in transpressional deformation and basin inversion in the eastern sections of the Central Burma basin (Morley, 2004; Morley & Searle, 2017). At the southern termination of the Sagaing fault, the Andaman ridge and transform system initiated in the

backarc region of the Andaman subduction zone (Raju et al., 2004). In southeastern Tibet, slip along major north-south and northeast-southwest striking strike-slip faults including the Ailao Shan fault, Mae Ping fault, Three Pagodas fault, Gaoligong fault, and Chong Shan fault accommodated southeastward extrusion and clockwise rotation of the Sibumasu block and Indochina block (Akciz et al., 2008; Eroglu et al., 2013; Harrison et al., 1996; Leloup et al., 1995; Tapponnier et al., 1990; Wang et al., 2000; Wang & Burchfiel, 1997).

7.4.4. Stage 4: Circa 10–7 Ma

In the eastern Himalayan orogen and northern Indo-Burma thrust belt, shortening propagated southward as the MBT and Lalpani thrusts involved the LHS (i.e., the Lalpani schist) (DeCelles et al., 2016; Yin, Dubey, Kelty, et al., 2010). Rocks equivalent to the northern Gangdese batholith, forearc basin sequence, GHS, and THS were eroded and/or underthrust beneath the Lohit Plutonic Complex at the E95° longitude of the study area.

By the late Miocene, the Chong Shan fault and Gaoligong fault became inactive in southeastern Tibet (Akciz et al., 2008) and left-slip motion along the Ailao-Shan fault transitioned to right-slip motion (Leloup et al., 1995). Continued clockwise rotation of the Eastern Flanking Belt resulted in a north-south oriented configuration. In the northern Indo-Burma thrust belt and southeastern Tibetan Plateau, oblique-slip motion along the Mishmi thrust and right-slip motion along the Puqu fault accommodated both northward oblique India-Asia convergence and southward crustal flow. In the southern Indo-Burma Ranges, shortening propagated westward to involve Miocene sedimentary rocks of the Bengal Basin (Maurin & Rangin, 2009a). In the central and eastern parts of the southern Indo-Burma thrust belt, right-slip transpression was accommodated by the Kaladan fault, Lelon fault, Churachandpur Mao fault, and Kabaw fault (Morley & Searle, 2017). Alkaline and calc-alkaline magmatism continued throughout the central zone of the Eastern Flanking Belt, likely due to dehydration of the steeply dipping Neo-Tethys lithosphere still attached to the eastern margin of India (Maury et al., 2004). South of the Himalayan orogen, the Dauki and Oldham thrusts accommodated uplift of the Shillong plateau (Clark & Bilham, 2008).

8. Conclusions

In this paper, we presented an investigation of the structural framework, magnitude of Cenozoic shortening strain, and cooling and exhumation history, based on new (U-Th)/He and ⁴⁰Ar/³⁹Ar data, of the northern Indo-Burma Ranges, the northernmost segment of the Eastern Flanking Belt that bounds the eastern margin of the Indian subcontinent. The study area is dominated by southwest to west directed thrust faults that accommodated >280 km (~86%) of horizontal shortening since the Cenozoic India-Asia collision. ZHe and ⁴⁰Ar/³⁹Ar thermochronology tracks activity of this thrust belt since ~36 Ma and show a widespread Late Miocene cooling episode, which we relate to coeval in-sequence and out-of-sequence thrusting. Our shortening estimate, combined with the absence of several Himalayan-Tibetan lithologic units and the southward decrease in the width of the thrust belt, suggests that the magnitude of Cenozoic crustal shortening and/or continental underthrusting along the collisional boundary increases across the eastern Himalayan syntaxis to the Eastern Flanking Belt, potentially due to syncollisional clockwise rotation during viscous flow around the syntaxis. The mode of active deformation in the region is expressed by right-slip transpression partitioned between the oblique-slip Mishmi thrust and the right-slip Jiali fault zone.

Acknowledgments

This work was supported by a grant from the Tectonics Program of the U.S. National Science Foundation awarded to An Yin (EAR Award 1145038). We thank Chief Editor Laurent Jolivet, Associate Editor Stephane Guillot, reviewer Djordje Grujic, and three anonymous reviewers for their constructive comments that have led to a significant improvement of the original draft of this paper. We also thank Dr. Kathleen Zanetti at UNLV for performing the ⁴⁰Ar/³⁹Ar thermochronologic analyses and Rudra Chatterjee and Des Patterson for assistance with the ZHe data acquisition.

Data Availability Statement

Data presented in this paper are available online in the Earthchem Geochron data repository (at <https://www.geochron.org/results.php?pkey=30143>).

References

- Acharyya, S. K. (1980). Stratigraphy and tectonics of Arunachal Lesser Himalaya. In *Stratigraphy and correlations of Lesser Himalayan formations* (pp. 231-241).
- Acharyya, S. K. (1987). Cenozoic plate motions creating the Eastern Himalayan and Indo Burmese range around the northeast corner of India: Ophiolites and Indian plate margins (pp. 143-160).
- Acharyya, S. K. (1994). The Cenozoic foreland basin and tectonics of the eastern sub-Himalaya: Problems and prospects. *Himalayan Geology*, 15, 3–21.
- Acharyya, S. K., & Ray, K. K. (1977). Geology of the Darjeeling-Sikkim Himalaya. *Guide to Excursion*, 4.
- Acharyya, S. K., Ray, K. K., & Sengupta, S. (1990). Tectonics of the ophiolite belt from Naga Hills and Andaman Islands, India. *Journal of Earth System Science*, 99(2), 187–199.

- Aikman, A. B., Harrison, T. M., & Lin, D. (2008). Evidence for early (>44 Ma) Himalayan crustal thickening, Tethyan Himalaya, south-eastern Tibet. *Earth and Planetary Science Letters*, *274*(1), 14–23.
- Aitchison, J. C., Ao, A., Bhowmik, S., Clarke, G. L., Ireland, T. R., Kachovich, S., et al. (2019). Tectonic evolution of the western margin of the Burma microplate based on new fossil and radiometric age constraints. *Tectonics*, *38*(5), 1718–1741.
- Akciz, S., Burchfiel, B. C., Crowley, J. L., Jiyun, Y., & Liangzhong, C. (2008). Geometry, kinematics, and regional significance of the Chong Shan shear zone, Eastern Himalayan Syntaxis, Yunnan, China. *Geosphere*, *4*(1), 292–314.
- Allégre, C. J., et al. (1984). Structure and evolution of the Himalaya-Tibet orogenic belt. *Nature*, *307*, 17–22.
- Allmendinger, R. W., Cardozo, N., & Fisher, D. M. (2012). *Structural geology algorithms: Vectors and tensors in structural geology*. Cambridge, UK: Cambridge University Press.
- Ao, A., & Bhowmik, S. K. (2014). Cold subduction of the Neotethys: The metamorphic record from finely banded lawsonite and epidote blueschists and associated metabasalts of the Nagaland Ophiolite Complex, India. *Journal of Metamorphic Geology*, *32*(8), 829–860.
- Armijo, R., Tapponnier, P., & Han, T. (1989). Late Cenozoic right-lateral strike-slip faulting in southern Tibet. *Journal of Geophysical Research*, *94*(B3), 2787–2838.
- Armijo, R., Tapponnier, P., Mercier, J. L., & Han, T. L. (1986). Quaternary extension in southern Tibet: Field observations and tectonic implications. *Journal of Geophysical Research*, *91*(B14), 13803–13872.
- Avouac, J. P. (2003). Mountain building, erosion, and the seismic cycle in the Nepal Himalaya. *Advances in Geophysics*, *46*, 1–80.
- Banerjee, P., Bürgmann, R., Nagarajan, B., & Apel, E. (2008). Intraplate deformation of the Indian subcontinent. *Geophysical Research Letters*, *35*(18).
- Barley, M. E., Pickard, A. L., Zaw, K., Rak, P., & Doyle, M. G. (2003). Jurassic to Miocene magmatism and metamorphism in the Mogok metamorphic belt and the India-Eurasia collision in Myanmar. *Tectonics*, *22*(3), 1019.
- Barley, M. E., & Zaw, K. (2009). SHRIMP U-Pb in zircon geochronology of granitoids from Myanmar: Temporal constraints on the tectonic evolution of Southeast Asia. *EGU General Assembly Conference Abstracts*, *11*, 3842.
- Ben-Menahem, A., Aboodi, E., & Schild, R. (1974). The source of the great Assam earthquake—An interplate wedge motion. *Physics of the Earth and Planetary Interiors*, *9*(4), 265–289.
- Bertrand, G., & Rangin, C. (2003). Tectonics of the western margin of the Shan plateau (central Myanmar): Implication for the India-Indochina oblique convergence since the Oligocene. *Journal of Asian Earth Sciences*, *21*(10), 1139–1157.
- Bhattacharyya, K., & Mitra, G. (2009). A new kinematic evolutionary model for the growth of a duplex—An example from the Rangit duplex, Sikkim Himalaya, India. *Gondwana Research*, *16*(3–4), 697–715.
- Bikramaditya, R. K., Chung, S. L., Singh, A. K., Lee, H. Y., Lin, T. H., & Iizuka, Y. (2019). Age and isotope geochemistry of magmatic rocks of the Lohit plutonic complex, eastern Himalaya: Implications for the evolution of Transhimalayan arc magmatism. *Journal of the Geological Society*.
- Bilham, R., & England, P. (2001). Plateau ‘pop-up’ in the great 1897 Assam earthquake. *Nature*, *410*(6830), 806–809.
- Boyer, S. E., & Elliott, D. (1982). Thrust systems. *AAPG Bulletin*, *66*(9), 1196–1230.
- Brunel, M., Chayé d’Albissin, M., & Locquin, M. (1985). The Cambrian age of magnesites from E. Nepal as determined through the discovery of paleobasidiospores. *Journal of the Geological Society of India*, *26*(4), 255–260.
- Brunnswheiler, R. O. (1966). On the geology of the Indoburman ranges: (Arakan Coast and Yoma, Chin Hills, Naga Hills). *Journal of the Geological Society of Australia*, *13*(1), 137–194.
- Burchfiel, B. C., Zhiliang, C., Hodges, K. V., Yuping, L., Royden, L. H., Changrong, D., & Jiene, X. (1992). The South Tibetan detachment system, Himalayan orogen: Extension contemporaneous with and parallel to shortening in a collisional mountain belt. *Geological Society of America Special Papers*, *269*, 1–41.
- Burg, J. P., Brunel, M., Gapais, D., Chen, G. M., & Liu, G. H. (1984). Deformation of leucogranites of the crystalline Main Central Sheet in southern Tibet (China). *Journal of Structural Geology*, *6*(5), 535–542.
- Burgess, W. P., Yin, A., Dubey, C. S., Shen, Z. K., & Kelty, T. K. (2012). Holocene shortening across the Main Frontal Thrust zone in the eastern Himalaya. *Earth and Planetary Science Letters*, *357*, 152–167.
- Butler, R. W. H. (1987). Thrust sequences. *Journal of the Geological Society*, *144*(4), 619–634.
- Caby, R., Pêcher, A., & LeFort, P. (1983). Le grand chevauchement central himalayen. Nouvelles données sur le métamorphisme inverse à la base de la Dalle du Tibet. (The Himalayan Main Central Thrust: New data about the reverse metamorphism at the bottom of the Tibetan Slab). *Revue de géologie dynamique et de géographie physique Paris*, *24*(2), 89–100.
- Cardozo, N., & Allmendinger, R. W. (2013). Spherical projections with OSXStereonet. *Computers & Geosciences*, *51*, 193–205.
- Carosi, R., Lombardo, B., Mollí, G., Musumeci, G., & Pertusati, P. C. (1998). The South Tibetan detachment system in the Rongbuk valley, Everest region. Deformation features and geological implications. *Journal of Asian Earth Sciences*, *16*(2–3), 299–311.
- Carosi, R., Montomoli, C., & Iaccarino, S. (2018). 20 years of geological mapping of the metamorphic core across Central and Eastern Himalayas. *Earth-Science Reviews*, *177*, 124–138.
- Carosi, R., Montomoli, C., Iaccarino, S., & Visonà, D. (2019). Structural evolution, metamorphism and melting in the Greater Himalayan Sequence in central-western Nepal. *Geological Society, London, Special Publications*, *483*(1), 305–323.
- Catlos, E. J., Harrison, T. M., Manning, C. E., Grove, M., Rai, S. M., Hubbard, M. S., & Upreti, B. N. (2002). Records of the evolution of the Himalayan orogen from in situ Th-Pb ion microprobe dating of monazite: Eastern Nepal and western Garhwal. *Journal of Asian Earth Sciences*, *20*(5), 459–479.
- Chatterjee, N., & Ghose, N. C. (2010). Metamorphic evolution of the Naga Hills eclogite and blueschist, Northeast India: Implications for early subduction of the Indian plate under the Burma microplate. *Journal of Metamorphic Geology*, *28*(2), 209–225.
- Chen, W. P., & Molnar, P. (1977). Seismic moments of major earthquakes and the average rate of slip in central Asia. *Journal of Geophysical Research*, *82*(20), 2945–2969.
- Clark, M. K. (2012). Continental collision slowing due to viscous mantle lithosphere rather than topography. *Nature*, *483*(7387), 74.
- Clark, M. K., & Bilham, R. (2008). Miocene rise of the Shillong Plateau and the beginning of the end for the Eastern Himalaya. *Earth and Planetary Science Letters*, *269*(3), 337–351.
- Cobbold, P. R., & Davy, P. H. (1988). Indentation tectonics in nature and experiment. 2. Central Asia. *Bull. Geol. Inst. Univ. Uppsala*, *14*, 143–162.
- Copeland, P., Harrison, T. M., Yun, P., Kidd, W. S. F., Roden, M., & Zhang, Y. (1995). Thermal evolution of the Gangdese batholith, southern Tibet: A history of episodic unroofing. *Tectonics*, *14*(2), 223–236.
- Corfield, R. I., Searle, M. P., & Pedersen, R. B. (2001). Tectonic setting, origin, and obduction history of the Spontang Ophiolite, Ladakh Himalaya, NW India. *The Journal of Geology*, *109*(6), 715–736.

- Coudurier-Curveur, A., Taponnier, P., Okal, E., Van der Woerd, J., Kali, E., Choudhury, S., et al. (2020). A composite rupture model for the great 1950 Assam earthquake across the cusp of the East Himalayan Syntaxis. *Earth and Planetary Science Letters*, *531*, 115928.
- Coulon, C., Maluski, H., Bollinger, C., & Wang, S. (1986). Mesozoic and Cenozoic volcanic rocks from central and southern Tibet: ³⁹Ar-⁴⁰Ar dating, petrological characteristics and geodynamical significance. *Earth and Planetary Science Letters*, *79*(3), 281–302.
- Coward, M. P., Kidd, W. S. F., Yun, P., Shackleton, R. M., & Hu, Z. (1988). The structure of the 1985 Tibet geotraverse, Lhasa to Golmud. *Philosophical Transactions of the Royal Society of London A: Mathematical, Physical and Engineering Sciences*, *327*(1594), 307–333.
- Curry, J. R., Moore, D. G., Lawver, L. A., Emmel, F. J., Raitt, R. W., Henry, M., & Kieckhefer, R. (1979). Tectonics of the Andaman Sea and Burma: Convergent margins. *Geological and Geophysical Investigations of Continental Margins*, 189–198.
- Dahlstrom, C. D. (1969). Balanced cross sections. *Canadian Journal of Earth Sciences*, *6*(4), 743–757.
- Dahlstrom, C. D. (1970). Structural geology in the eastern margin of the Canadian Rocky Mountains. *Bulletin of Canadian Petroleum Geology*, *18*(3), 332–406.
- Davy, P., & Cobbold, P. R. (1988). Indentation tectonics in nature and experiment. 1. Experiments scaled for gravity. *Bull. Geol. Inst. Univ. Uppsala*, *14*, 129–141.
- DeCelles, P. G., Carrapa, B., Gehrels, G. E., Chakraborty, T., & Ghosh, P. (2016). Along-strike continuity of structure, stratigraphy, and kinematic history in the Himalayan thrust belt: The view from Northeastern India. *Tectonics*, *35*(12), 2995–3027.
- DeCelles, P. G., Robinson, D. M., Quade, J., Ojha, T. P., Garzzone, C. N., Copeland, P., & Upreti, B. N. (2001). Stratigraphy, structure, and tectonic evolution of the Himalayan fold-thrust belt in western Nepal. *Tectonics*, *20*(4), 487–509.
- Devachandra, M., Kundu, B., Catherine, J., Kumar, A., & Gahalaut, V. K. (2014). Global positioning system (GPS) measurements of crustal deformation across the frontal eastern Himalayan syntaxis and seismic-hazard assessment. *Bulletin of the Seismological Society of America*, *104*(3), 1518–1524.
- Dewey, J. F., & Burke, K. C. (1973). Tibetan, Variscan, and Precambrian basement reactivation: Products of continental collision. *The Journal of Geology*, *81*(6), 683–692.
- Dewey, J. F., Cande, S., & Pitman, W. C. (1989). Tectonic evolution of the India/Eurasia collision zone. *Eclogae Geologicae Helveticae*, *82*(3), 717–734.
- Dewey, J. F., Shackleton, R. M., Chengfa, C., & Yiyin, S. (1988). The tectonic evolution of the Tibetan Plateau. *Philosophical Transactions of the Royal Society of London A: Mathematical, Physical and Engineering Sciences*, *327*(1594), 379–413.
- Ding, L., Kapp, P., Zhong, D., & Deng, W. (2003). Cenozoic volcanism in Tibet: Evidence for a transition from oceanic to continental subduction. *Journal of Petrology*, *44*(10), 1833–1865.
- Ding, L., Zhong, D., Yin, A., Kapp, P., & Harrison, T. M. (2001). Cenozoic structural and metamorphic evolution of the eastern Himalayan syntaxis (Namche Barwa). *Earth and Planetary Science Letters*, *192*(3), 423–438.
- Dong, X., Zhang, Z., Liu, F., Wang, W., Yu, F., & Shen, K. (2011). Zircon U-Pb geochronology of the Nyainqentanglha Group from the Lhasa terrane: New constraints on the Triassic orogeny of the south Tibet. *Journal of Asian Earth Sciences*, *42*(4), 732–739.
- Edwards, M. A., & Harrison, T. M. (1997). When did the roof collapse? Late Miocene north-south extension in the high Himalaya revealed by Th-Pb monazite dating of the Khula Kangri granite. *Geology*, *25*(6), 543–546.
- Edwards, M. A., Kidd, W. S., Li, J., Yue, Y., & Clark, M. (1996). Multi-stage development of the southern Tibet detachment system near Khula Kangri. New data from Gonto La. *Tectonophysics*, *260*(1–3), 1–19.
- Edwards, M. A., Pécher, A., Kidd, W. S. F., Burchfiel, B. C., & Royden, L. H. (1999). Southern Tibet Detachment System at Khula Kangri, Eastern Himalaya: A large-area, shallow detachment stretching into Bhutan? *The Journal of Geology*, *107*(5), 623–631.
- Elliott, D. (1976). The motion of thrust sheets. *Journal of Geophysical Research*, *81*, 949–963.
- England, P., & Houseman, G. (1986). Finite strain calculations of continental deformation 2. Comparison with the India-Asia collision zone. *Journal of Geophysical Research*, *91*, 3664–3676.
- England, P., & Molnar, P. (1990). Right-lateral shear and rotation as the explanation for strike-slip faulting in eastern Tibet. *Nature*, *344*(6262), 140–142.
- Enos, P. (2017). Sedimentary structures preserved in Greater Himalayan Gneiss: Phenomenon or fantasy? *The Journal of Geology*, *125*(2), 125–139.
- Eroglu, S., Siebel, W., Danišik, M., Pfänder, J. A., & Chen, F. (2013). Multi-system geochronological and isotopic constraints on age and evolution of the Gaoligongshan metamorphic belt and shear zone system in western Yunnan, China. *Journal of Asian Earth Sciences*, *73*, 218–239.
- Flowers, R. M., Farley, K. A., & Ketchum, R. A. (2015). A reporting protocol for thermochronologic modeling illustrated with data from the Grand Canyon. *Earth and Planetary Science Letters*, *432*, 425–435.
- Fossen, H., Cavalcante, G. C. G., Pinheiro, R. V. L., & Archanjo, C. J. (2019). Deformation-progressive or multiphase? *Journal of Structural Geology*, *125*, 82–99.
- Gansser, A. (1964). Geology of the Himalayas. *New York. Wiley Interscience*, 289.
- Gansser, A. (1983). Geology of the Bhutan Himalaya. *Birkhauser, Basel*, 181.
- Gehrels, G. E., DeCelles, P. G., Ojha, T. P., & Upreti, B. N. (2006). Geologic and U-Th-Pb geochronologic evidence for early Paleozoic tectonism in the Kathmandu thrust sheet, central Nepal Himalaya. *Geological Society of America Bulletin*, *118*(1–2), 185–198.
- Girardeau, J., et al. (1984). Tectonic environment and geodynamic significance of the Neo-Cimmerian Donqiao ophiolite, Bangong-Nujiang suture zone, Tibet. *Nature*, *307*, 27–31.
- Goswami, T. K. (2008). Implications of geochemical signatures in the Trans-Himalayan Lohit batholith, Arunachal Pradesh, India. *Himalayan Journal of Sciences*, *5*(7), 53.
- Goswami, T. K. (2011). Collision induces deformation of the Trans Himalayan Lohit Batholith, Arunachal Pradesh, India. *Memoir Geological Society of India*, *77*, 19–31.
- Goswami, T. K. (2013a). Geodynamic significance of leucogranite intrusions in the Lohit batholith near Walong, eastern Arunachal Pradesh, India. *Current Science*, *104*(2), 229.
- Goswami, T. K. (2013b). Subduction related magmatism: Constrains from the REE pattern in the Lohit Batholith, Arunachal Pradesh, India. *Geosciences*, *3*(4), 128–141.
- Grujic, D., Hollister, L. S., & Parrish, R. R. (2002). Himalayan metamorphic sequence as an orogenic channel: Insight from Bhutan. *Earth and Planetary Science Letters*, *198*(1), 177–191.
- Guan, Q., et al. (2012). Crustal thickening prior to 38 Ma in southern Tibet: Evidence from lower crust-derived adakitic magmatism in the Gangdese Batholith. *Gondwana Research*, *21*(1), 88–99.

- Guenther, W. R., Reiners, P. W., Ketcham, R. A., Nasdala, L., & Giester, G. (2013). Helium diffusion in natural zircon: Radiation damage, anisotropy, and the interpretation of zircon (U-Th)/He thermochronology. *American Journal of Science*, 313(3), 145–198.
- Guillot, S., Cosca, M., Allemand, P., & Le Fort, P. (1999). Contrasting metamorphic and geochronologic evolution along the Himalayan belt. *Special Papers-Geological Society of America*, 117–128.
- Guo, L., Zhang, H. F., Harris, N., Pan, F. B., & Xu, W. C. (2013). Late Cretaceous (~81 Ma) high-temperature metamorphism in the southeastern Lhasa terrane: Implication for the Neo-Tethys ocean ridge subduction. *Tectonophysics*, 608, 112–126.
- Guo, L., Zhang, H. F., Harris, N., Parrish, R., Xu, W. C., & Shi, Z. L. (2012). Paleogene crustal anatexis and metamorphism in Lhasa terrane, eastern Himalayan syntaxis: Evidence from U-Pb zircon ages and Hf isotopic compositions of the Nyingchi Complex. *Gondwana Research*, 21(1), 100–111.
- Gupta, T. D., Riguzzi, F., Dasgupta, S., Mukhopadhyay, B., Roy, S., & Sharma, S. (2015). Kinematics and strain rates of the Eastern Himalayan Syntaxis from new GPS campaigns in Northeast India. *Tectonophysics*, 655, 15–26.
- Gururajan, N. S., & Choudhuri, B. K. (2003). Geology and tectonic history of the Lohit valley, Eastern Arunachal Pradesh, India. *Journal of Asian Earth Sciences*, 21(7), 731–741.
- Hall, R. (2012). Late Jurassic-Cenozoic reconstructions of the Indonesian region and the Indian Ocean. *Tectonophysics*, 570, 1–41.
- Hames, W. E., & Bowring, S. A. (1994). An empirical evaluation of the argon diffusion geometry in muscovite. *Earth and Planetary Science Letters*, 124(1–4), 161–169.
- Haproff, P. J., Zuza, A. V., & Yin, A. (2018). West-directed thrusting south of the eastern Himalayan syntaxis indicates clockwise crustal flow at the indenter corner during the India-Asia collision. *Tectonophysics*, 722, 277–285.
- Haproff, P. J., Zuza, A. V., Yin, A., Harrison, T. M., Manning, C. M., Ding, L., et al. (2019). Geologic framework of the northern Indo-Burma Ranges: Lateral correlation of Himalayan-Tibetan lithologic units across the eastern Himalayan syntaxis. *Geosphere*, 15(3), 856–881.
- Harrison, T. M., Célérier, J., Aikman, A. B., Hermann, J., & Heizler, M. T. (2009). Diffusion of ⁴⁰Ar in muscovite. *Geochimica et Cosmochimica Acta*, 73(4), 1039–1051.
- Harrison, T. M., Copeland, P., Kidd, W. S. F., & Yin, A. (1992). Raising Tibet. *Science*, 255(5052), 1663–1670.
- Harrison, T. M., Leloup, P. H., Ryerson, F. J., Tapponnier, P., Lacassin, R., & Chen, W. (1996). Diachronous initiation of transtension along the Ailao Shan-Red River shear zone, Yunnan and Vietnam. In *The Tectonic Evolution of Asia, World and Regional Geology* (pp. 208–226). Cambridge, UK: Cambridge University Press.
- Harrison, T. M., Yin, A., Grove, M., Lovera, O. M., Ryerson, F. J., & Zhou, X. (2000). The Zedong Window: A record of superposed Tertiary convergence in southeastern Tibet. *Journal of Geophysical Research*, 105(B8), 19211–19230.
- Heim, A., & Gansser, A. (1939). *Central Himalaya*. Delhi: Hindustan Publishing.
- Hodges, K. V. (2000). Tectonics of the Himalaya and southern Tibet from two perspectives. *Geological Society of America Bulletin*, 112(3), 324–350.
- Hsü, K., et al. (1995). Tectonic evolution of the Tibetan Plateau: A working hypothesis. *International Geology Review*, 37, 473–508.
- Ji, W. Q., Wu, F. Y., Chung, S. L., Li, J. X., & Liu, C. Z. (2009). Zircon U-Pb geochronology and Hf isotopic constraints on petrogenesis of the Gangdese batholith, southern Tibet. *Chemical Geology*, 262(3), 229–245.
- Kapp, P., & DeCelles, P. G. (2019). Mesozoic-Cenozoic geological evolution of the Himalayan-Tibetan orogen and working tectonic hypotheses. *American Journal of Science*, 319(3), 159–254.
- Kapp, P., Murphy, M. A., Yin, A., Harrison, T. M., Ding, L., & Guo, J. (2003). Mesozoic and Cenozoic tectonic evolution of the Shiquanhe area of western Tibet. *Tectonics*, 22(4).
- Kayastha, N. B. (1992). Stratigraphy of the lower Tertiary rocks of Nepal Himalaya. *Journal of Nepal Geological Society*, 8, 21–30.
- Ketcham, R. A. (2005). Forward and inverse modeling of low-temperature thermochronometry data. *Reviews in Mineralogy and Geochemistry*, 58(1), 275–314.
- Kreemer, C., Blewitt, G., & Klein, E. C. (2014). A geodetic plate motion and Global Strain Rate Model. *Geochemistry, Geophysics, Geosystems*, 15(10), 3849–3889.
- Kumar, G. (1997). *Geology of Arunachal Pradesh* (Vol. 217). Bangalore: Geological Society of India.
- Kundu, A., Hazarika, D., Hajra, S., Singh, A. K., & Ghosh, P. (2020). Crustal thickness and Poisson's ratio variations in the northeast India-Asia collision zone: Insight into the Tuting-Tidding Suture zone, eastern Himalaya. *Journal of Asian Earth Sciences*, 188, 104099.
- Laskowski, A. K., Kapp, P., Vervoort, J. D., & Ding, L. (2016). High-pressure Tethyan Himalaya rocks along the India-Asia suture zone in southern Tibet. *Lithosphere*, 8(5), 574–582.
- Law, R. D., Searle, M. P., & Simpson, R. L. (2004). Strain, deformation temperatures and vorticity of flow at the top of the Greater Himalayan Slab, Everest Massif, Tibet. *Journal of the Geological Society*, 161(2), 305–320.
- Leary, R. J., DeCelles, P. G., Quade, J., Gehrels, G. E., & Waanders, G. (2016). The Liugu Conglomerate, southern Tibet: Early Miocene basin development related to deformation within the Great Counter Thrust system. *Lithosphere*, 8(5), 427–450.
- Le Fort, P. (1975). Himalayas, the collided range: Present knowledge of the continental arc. *American Journal of Science*, 275, 1–44.
- Lee, H. Y., Chung, S. L., Lo, C. H., Ji, J., Lee, T. Y., Qian, Q., & Zhang, Q. (2009). Eocene Neotethyan slab breakoff in southern Tibet inferred from the Linzizong volcanic record. *Tectonophysics*, 477(1), 20–35.
- Lee, H. Y., Chung, S. L., & Yang, H. M. (2016). Late Cenozoic volcanism in central Myanmar: Geochemical characteristics and geodynamic significance. *Lithos*, 245, 174–190.
- Lee, H. Y., et al. (2003). Miocene Jiali faulting and its implications for Tibetan tectonic evolution. *Earth and Planetary Science Letters*, 205(3), 185–194.
- Lee, T. Y., & Lawver, L. A. (1995). Cenozoic plate reconstruction of Southeast Asia. *Tectonophysics*, 251(1–4), 85–138.
- Leloup, P. H., et al. (1995). The Ailao Shan-Red River shear zone (Yunnan, China), Tertiary transform boundary of Indochina. *Tectonophysics*, 251(1), 3–84.
- Li, Z., Ding, L., Zaw, T., Wang, H., Cai, F., Yao, W., et al. (2020). Kinematic evolution of the West Burma block during and after India-Asia collision revealed by paleomagnetism. *Journal of Geodynamics*, 134, 101690.
- Li, Z. H., Xu, Z., Gerya, T., & Burg, J. P. (2013). Collision of continental corner from 3-D numerical modeling. *Earth and Planetary Science Letters*, 380, 98–111.
- Lin, T. H., Chung, S. L., Kumar, A., Wu, F. Y., Chiu, H. Y., & Lin, I. (2013). Linking a prolonged Neo-Tethyan magmatic arc in South Asia: Zircon U-Pb and Hf isotopic constraints from the Lohit Batholith, NE India. *Terra Nova*, 25(6), 453–458.
- Long, S., & McQuarrie, N. (2010). Placing limits on channel flow: Insights from the Bhutan Himalaya. *Earth and Planetary Science Letters*, 290(3–4), 375–390.
- Long, S., McQuarrie, N., Tobgay, T., & Grujic, D. (2011). Geometry and crustal shortening of the Himalayan fold-thrust belt, eastern and central Bhutan. *Geological Society of America Bulletin*, B30203–B30201.

- Long, S., McQuarrie, N., Tobgay, T., & Hawthorne, J. (2011). Quantifying internal strain and deformation temperature in the eastern Himalaya, Bhutan: Implications for the evolution of strain in thrust sheets. *Journal of Structural Geology*, 33(4), 579–608.
- Long, S., McQuarrie, N., Tobgay, T., Rose, C., Gehrels, G., & Grujic, D. (2011). Tectonostratigraphy of the Lesser Himalaya of Bhutan: Implications for the along-strike stratigraphic continuity of the northern Indian margin. *Geological Society of America Bulletin*, 123(7–8), 1406–1426.
- Long, S. P., McQuarrie, N., Tobgay, T., Coutand, I., Cooper, F. J., Reiners, P. W., et al. (2012). Variable shortening rates in the eastern Himalayan thrust belt, Bhutan: Insights from multiple thermochronologic and geochronologic data sets tied to kinematic reconstructions. *Tectonics*, 31(5).
- Maung, H. (1987). Transcurrent movements in the Burma-Andaman Sea region. *Geology*, 15(10), 911–912.
- Maurin, T., Masson, F., Rangin, C., Min, U. T., & Collard, P. (2010). First global positioning system results in northern Myanmar: Constant and localized slip rate along the Sagaing fault. *Geology*, 38(7), 591–594.
- Maurin, T., & Rangin, C. (2009a). Structure and kinematics of the Indo-Burmese Wedge: Recent and fast growth of the outer wedge. *Tectonics*, 28(2).
- Maurin, T., & Rangin, C. (2009b). Impact of the 90°E ridge at the Indo-Burmese subduction zone imaged from deep seismic reflection data. *Marine Geology*, 266(1), 143–155.
- Maury, R. C., et al. (2004). Quaternary calc-alkaline and alkaline volcanism in a hyper-oblique convergence setting, central Myanmar and western Yunnan. *Bulletin de la Société Géologique de France*, 175(5), 461–472.
- McQuarrie, N., Robinson, D., Long, S., Tobgay, T., Grujic, D., Gehrels, G., & Ducea, M. (2008). Preliminary stratigraphic and structural architecture of Bhutan: Implications for the along strike architecture of the Himalayan system. *Earth and Planetary Science Letters*, 272(1), 105–117.
- McQuarrie, N., Tobgay, T., Long, S. P., Reiners, P. W., & Cosca, M. A. (2014). Variable exhumation rates and variable displacement rates: Documenting recent slowing of Himalayan shortening in western Bhutan. *Earth and Planetary Science Letters*, 386, 161–174.
- Metcalfe, I. (2013). Gondwana dispersion and Asian accretion: Tectonic and palaeogeographic evolution of eastern Tethys. *Journal of Asian Earth Sciences*, 66, 1–33.
- Misra, D. K. (2009). Litho-tectonic sequence and their regional correlation along the Lohit and Dibang valleys, eastern Arunachal Pradesh. *Journal of the Geological Society of India*, 73(2), 213–219.
- Misra, D. K., & Singh, T. (2002). Tectonic setting and neotectonic features along the Eastern Syntaxial Bend (Lohit and Dibang). *Arunachal Himalaya. Aspects of Geology and Environment of the Himalaya*, 19–40.
- Mitchell, A. H. G. (1993). Cretaceous-Cenozoic tectonic events in the western Myanmar (Burma)-Assam region. *Journal of the Geological Society*, 150(6), 1089–1102.
- Mitchell, A. H. G., Chung, S. L., Oo, T., Lin, T. H., & Hung, C. H. (2012). Zircon U-Pb ages in Myanmar: Magmatic-metamorphic events and the closure of a neo-Tethys ocean? *Journal of Asian Earth Sciences*, 56, 1–23.
- Mitchell, A. H. G., Htay, M. T., Htun, K. M., Win, M. N., Oo, T., & Hlaing, T. (2007). Rock relationships in the Mogok metamorphic belt, Tatkon to Mandalay, central Myanmar. *Journal of Asian Earth Sciences*, 29(5), 891–910.
- Mitra, G., Bhattacharyya, K., & Mukul, M. (2010). The Lesser Himalayan duplex in Sikkim: Implications for variations in Himalayan shortening. *Journal of the Geological Society of India*, 75(1), 289–301.
- Mitra, S., Priestley, K., Bhattacharyya, A. K., & Gaur, V. K. (2005). Crustal structure and earthquake focal depths beneath northeastern India and southern Tibet. *Geophysical Journal International*, 160(1), 227–248.
- Molnar, P., & Tapponnier, P. (1975). Cenozoic tectonics of Asia: Effects of a continental collision. *Science*, 189(4201), 419–426.
- Montomoli, C., Carosi, R., & Iaccarino, S. (2015). Tectonometamorphic discontinuities in the Greater Himalayan Sequence: A local or a regional feature? *Geological Society, London, Special Publications*, 412(1), 25–41.
- Morley, C. K. (2004). Nested strike-slip duplexes, and other evidence for Late Cretaceous-Palaeogene transpressional tectonics before and during India-Eurasia collision, in Thailand, Myanmar and Malaysia. *Journal of the Geological Society*, 16(5), 799–812.
- Morley, C. K., Naing, T. T., Searle, M., & Robinson, S. A. (2020). Structural and tectonic development of the Indo-Burma ranges. *Earth-Science Reviews*, 200, 102992.
- Morley, C. K., & Searle, M. (2017). Regional tectonics, structure and evolution of the Andaman-Nicobar Islands from ophiolite formation and obduction to collision and back-arc spreading. *Geological Society, London, Memoirs*, 47(1), 51–74.
- Mukhopadhyay, B., & Dasgupta, S. (2015). Earthquake swarms near eastern Himalayan Syntaxis along Jiali Fault in Tibet: A seismotectonic appraisal. *Geoscience Frontiers*, 6(5), 715–722.
- Murphy, M. A., & Yin, A. (2003). Structural evolution and sequence of thrusting in the Tethyan fold-thrust belt and Indus-Yalu suture zone, southwest Tibet. *Geological Society of America Bulletin*, 115(1), 21–34.
- Murphy, M. A., et al. (1997). Did the Indo-Asian collision alone create the Tibetan Plateau? *Geology*, 25(8), 719–722.
- Nandini, P., & Thakur, S. S. (2011). Metamorphic evolution of the Lesser Himalayan Crystalline Sequence, Siyom Valley, NE Himalaya, India. *Journal of Asian Earth Sciences*, 40(5), 1089–1100.
- Nandy, D.R., 1973, Geology and structural lineaments of the Lohit Himalaya (Arunachal Pradesh) and adjoining area: Seminar on geodynamics of the Himalayan region, NGRI, Hyderabad, 167-172.
- Nandy, D. R. (1980). Tectonic patterns in northeastern India. *Indian Journal of Earth Science*, 7, 103–107.
- Nandy, D. R., Mullick, B. B., Basu Chowdhury, S., & Murthy, M. V. N. (1975). Geology of the NEFA Himalaya. *Geological Survey of India Miscellaneous Publication*, 24(1), 91–144.
- Nelson, K. D., Zhao, W., Brown, L. D., & Kuo, J. (1996). Partially molten middle crust beneath southern Tibet: Synthesis of project INDEPTH results. *Science*, 274(5293), 1684.
- Ni, J., & York, J. E. (1978). Late Cenozoic tectonics of the Tibetan Plateau. *Journal of Geophysical Research: Solid Earth*, 83(B11), 5377–5384.
- Ningthoujam, P. S., Dubey, C. S., Lolee, L. K., Shukla, D. P., Naorem, S. S., & Singh, S. K. (2015). Tectonic studies and crustal shortening across Easternmost Arunachal Himalaya. *Journal of Asian Earth Sciences*, 111, 339–349.
- Patriat, P., & Achahe, J. (1984). India-Eurasia collision chronology has implications for crustal shortening and driving mechanism of plates. *Nature*, 311(5987), 615–621.
- Pebam, J., & Kamalakannan, D. (2019). Petrogenesis and emplacement of magmatic rocks of Lohit Plutonic Complex, Arunachal Trans-Himalaya, Northeast India. *Indian Journal of Geosciences*, 73(3), 213–230.
- Pellegrino, A. G., Zhang, B., Speranza, F., Maniscalco, R., Yin, C., Hernandez-Moreno, C., & Winkler, A. (2018). Tectonics and paleomagnetic rotation pattern of Yunnan (24°N–25°N, China): Gaoligong fault shear versus megablock drift. *Tectonics*, 37(5), 1524–1551.
- Peltzer, G., & Tapponnier, P. (1988). Formation and evolution of strike-slip faults, rifts, and basins during the India-Asia collision: An experimental approach. *Journal of Geophysical Research*, 93(B12), 15085–15117.

- Rajkakat, M., Bhowmik, S. K., Ao, A., Ireland, T. R., Avila, J., Clarke, G. L., et al. (2019). Thermal history of Early Jurassic eclogite facies metamorphism in the Nagaland Ophiolite Complex, NE India: New insights into pre-Cretaceous subduction channel tectonics within the Neo-Tethys. *Lithos*, *346*, 105166.
- Raju, K. K., Ramprasad, T., Rao, P. S., Rao, B. R., & Varghese, J. (2004). New insights into the tectonic evolution of the Andaman basin, northeast Indian Ocean. *Earth and Planetary Science Letters*, *221*(1), 145–162.
- Rangin, C., Maurin, T., & Masson, F. (2013). Combined effects of Eurasia/Sunda oblique convergence and East-Tibetan crustal flow on the active tectonics of Burma. *Journal of Asian Earth Sciences*, *76*, 185–194.
- Rangin, C., Spakman, W., Pubellier, M., & Bijwaard, H. (1999). Tomographic and geological constraints on subduction along the eastern Sundaland continental margin (South-East Asia). *Bulletin de la Société géologique de France*, *170*(6), 775–788.
- Ratschbacher, L., Frisch, W., Liu, G., & Chen, C. (1994). Distributed deformation in southern and western Tibet during and after the India-Asia collision. *Journal of Geophysical Research*, *99*(B10), 19917–19945.
- Reiners, P. W. (2005). Zircon (U-Th)/He thermochronometry. *Reviews in Mineralogy and Geochemistry*, *58*(1), 151–179.
- Ridd, M. F., & Watkinson, I. (2013). The Phuket-Slate Belt terrane: Tectonic evolution and strike-slip emplacement of a major terrane on the Sundaland margin of Thailand and Myanmar. *Proceedings of the Geologists' Association*, *124*(6), 994–1010.
- Robinson, D. M., DeCelles, P. G., & Copeland, P. (2006). Tectonic evolution of the Himalayan thrust belt in western Nepal: Implications for channel flow models. *Geological Society of America Bulletin*, *118*(7–8), 865–885.
- Royden, L. H., Burchfiel, B. C., & van der Hilst, R. D. (2008). The geological evolution of the Tibetan Plateau. *Science*, *321*, 1054–1058.
- Royden, L. H., et al. (1997). Surface deformation and lower crustal flow in eastern Tibet. *Science*, *276*, 788–790.
- Ryan, W. B., et al. (2009). Global multi-resolution topography synthesis. *Geochemistry, Geophysics, Geosystems*, *10*(3).
- Sakai, H. (1983). Geology of the Tansen group of the Lesser Himalaya in Nepal. Mem. Faculty of Sci., Kyushu Univ., Ser. D *Geology*, *25*, 27–74.
- Salvi, D., Mathew, G., Kohn, B., Pande, K., & Borgohain, B. (2020). Thermochronological insights into the morphotectonic evolution of Mishmi hills across the Dibang Valley, NE Himalayan Syntaxis. *Journal of Asian Earth Sciences*, 104158.
- Sarma, K. P., Nandy, S., Devi, N. R., & Konwar, P. (2009). *Is Mishmi Block a tectonic roof? Some observations. Magmatism, Tectonism and Mineralization* (pp. 167–178). New Delhi, India: Macmillan Publishers India Ltd.
- Sarma, K. P., Nandy, S., & Mazumdar, N. (2012). Structural studies of the Mishmi block in parts of Dibang Valley of Arunachal Himalaya, Northeast India. *International Journal of Geology, Earth and Environmental Sciences*, *2*(3), 43–56.
- Schärer, U., Xu, R. H., & Allègre, C. J. (1984). U-Pb geochronology of Gangdese (Transhimalaya) plutonism in the Lhasa-Xigaze region, Tibet. *Earth and Planetary Science Letters*, *69*(2), 311–320.
- Schelling, D. (1992). The tectonostratigraphy and structure of the eastern Nepal Himalaya. *Tectonics*, *11*(5), 925–943.
- Searle, M. P., Cooper, D. J. W., Rex, A. J., & Colchen, M. (1988). Collision tectonics of the Ladakh-Zaskar Himalaya. *Phil Trans. R. Soc. Lond. A*, *326*(1589), 117–150.
- Searle, M. P., Corfield, R. I., Stephenson, B. E. N., & McCarron, J. O. E. (1997). Structure of the North Indian continental margin in the Ladakh-Zaskar Himalayas: Implications for the timing of obduction of the Spontang ophiolite, India-Asia collision and deformation events in the Himalaya. *Geological Magazine*, *134*(3), 297–316.
- Searle, M. P., Law, R. D., Godin, L., Larson, K. P., Streule, M. J., Cottle, J. M., & Jessup, M. J. (2008). Defining the Himalayan main central thrust in Nepal. *Journal of the Geological Society*, *165*(2), 523–534.
- Searle, M. P., & Morley, C. K. (2011). Tectonic and thermal evolution of Thailand in the regional context of SE Asia. *The Geology of Thailand, Chapter 20*, 539–571.
- Searle, M. P., Morley, C. K., Waters, D. J., Gardiner, N. J., Htun, U. K., Nu, T. T., & Robb, L. J. (2017). Tectonic and metamorphic evolution of the Mogok Metamorphic and Jade Mines belts and ophiolitic terranes of Burma (Myanmar). *Geological Society, London, Memoirs*, *48*(1), 261–293.
- Searle, M. P., Noble, S. R., Cottle, J. M., Waters, D. J., Mitchell, A. H. G., Hlaing, T., & Horstwood, M. S. A. (2007). Tectonic evolution of the Mogok metamorphic belt, Burma (Myanmar) constrained by U-Th-Pb dating of metamorphic and magmatic rocks. *Tectonics*, *26*(3).
- Sharma, K. K., Choubey, V. M., & Chatti, H. R. (1991). Geological setting of the ophiolites and magmatic arc of the Lohit Himalaya (Arunachal Pradesh) India with special reference to their petrochemistry. *Physics and Chemistry of the Earth*, *18*, 277–292.
- Sharma, R., & Sarma, K. P. (2013). Microstructural study and strain history of Mesoproterozoic augen gneiss of Lohit District, Arunachal Himalaya, India: International Journal of Geology. *Earth and Environment Sciences*, *3*(2), 68–76.
- Singh, A. K., & Singh, R. B. (2011). Zn- and Mn-rich chrome-spinels in serpentinite of Tidding Suture Zone, Eastern Himalaya and their metamorphism and genetic significance. *Current Science*, 743–749.
- Singh, A. K., & Singh, R. B. (2013). Genetic implications of Zn- and Mn-rich Cr-spinels in serpentinites of the Tidding Suture Zone, eastern Himalaya, NE India. *Geological Journal*, *48*(1), 22–38.
- Sinha Roy, S., & Singh, T. (2002). Tectonic belts and some problems in the Geology of Arunachal Himalaya. In R. C. Sundriyal, T. Singh, & G. N. Sinha (Eds.), *Arunachal Pradesh: Environmental planning and sustainable development—Opportunities and challenges* (Vol. 16, pp. 399–418). Uttaranchal, India: Himavikas Occasional Publication.
- Socquet, A., Goffe, B., Pubellier, M., & Rangin, C. (2002). Late Cretaceous to Eocene metamorphism of the internal zone of the Indo-Burma range (western Myanmar): Geodynamic implications. *Comptes Rendus Geoscience*, *334*(8), 573–580.
- Staudacher, T. H., Jessberger, E. K., Dorflinger, D., & Kiko, J. (1978). A refined ultrahigh-vacuum furnace for rare gas analysis. *J. Phys. E: Sci. Instrum.*, *11*, 781–784.
- Stevens, V. L., & Avouac, J. P. (2015). Interseismic coupling on the main Himalayan thrust. *Geophysical Research Letters*, *42*(14), 5828–5837.
- Stipp, M., Stünitz, H., Heilbronner, R., & Schmid, S. M. (2002). Dynamic recrystallization of quartz: Correlation between natural and experimental conditions. *Geological Society, London, Special Publications*, *200*(1), 171–190.
- Suppe, J. (1983). Geometry and kinematics of fault-bend folding. *American Journal of science*, *283*(7), 684–721.
- Tapponnier, P., Peltzer, G., & Armijo, R. (1986). On the mechanics of the collision between India and Asia. *Geological Society, London, Special Publications*, *19*(1), 113–157.
- Tapponnier, P., Peltzer, G., Le Dain, A. Y., Armijo, R., & Cobbold, P. (1982). Propagating extrusion tectonics in Asia: New insights from simple experiments with plasticine. *Geology*, *10*, 611–616.
- Tapponnier, P., Zhiqin, X., Roger, F., Meyer, B., Arnaud, N., Wittlinger, G., & Jingsui, Y. (2001). Oblique stepwise rise and growth of the Tibet Plateau. *Science*, *294*(5547), 1671–1677.
- Tapponnier, P., et al. (1990). The Ailao Shan/Red River metamorphic belt: Tertiary left-lateral shear between Indochina and South China. *Nature*, *343*(6257), 431.

- Taylor, M., & Yin, A. (2009). Active structures of the Himalayan-Tibetan orogen and their relationships to earthquake distribution, contemporary strain field, and Cenozoic volcanism. *Geosphere*, 5(3), 199–214.
- Thakur, V. C., & Jain, A. K. (1974). Tectonics of the region of Eastern Himalayan syntaxis. *Current Science*, 43(24), 783–785.
- Thakur, V. C., & Jain, A. K. (1975). Some observations of deformation and metamorphism in the rocks of some parts of Mishmi Hills, Lohit district, (NEFA), Arunachal Pradesh. *Himalayan Geology*, 5, 339–364.
- Thingbaijam, K. K. S., Nath, S. K., Yadav, A., Raj, A., Walling, M. Y., & Mohanty, W. K. (2008). Recent seismicity in Northeast India and its adjoining region. *Journal of Seismology*, 12(1), 107–123.
- Torsvik, T. H., et al. (2012). Phanerozoic polar wander, palaeogeography and dynamics. *Earth-Science Reviews*, 114(3), 325–368.
- Tun, S. T., Thein, M., Htay, N., & Sein, K. (2014). *Geological map of Myanmar (1:2,250,000)*. Yangon, Myanmar: Myanmar Geosciences Society.
- van Hinsbergen, D. J., Kapp, P., Dupont-Nivet, G., Lippert, P. C., DeCelles, P. G., & Torsvik, T. H. (2011). Restoration of Cenozoic deformation in Asia and the size of Greater India. *Tectonics*, 30(5).
- van Hinsbergen, D. J., Lippert, P. C., Li, S., Huang, W., Advokaat, E. L., & Spakman, W. (2019). Reconstructing Greater India: Paleogeographic, kinematic, and geodynamic perspectives. *Tectonophysics*, 760, 69–94.
- Vigny, C., et al. (2003). Present-day crustal deformation around Sagaing fault, Myanmar. *Journal of Geophysical Research*, 108(B11).
- Wadia, D. N. (1931). The syntaxis of the northwest Himalaya: Its rocks, tectonics and orogeny. *Records of the Geological Survey of India*, 65(2), 189–220.
- Wang, C., Ding, L., Zhang, L. Y., Kapp, P., Pullen, A., & Yue, Y. H. (2016). Petrogenesis of Middle-Late Triassic volcanic rocks from the Gangdese belt, southern Lhasa terrane: Implications for early subduction of Neo-Tethyan oceanic lithosphere. *Lithos*, 262, 320–333.
- Wang, E., & Burchfiel, B. C. (1997). Interpretation of Cenozoic tectonics in the right-lateral accommodation zone between the Ailao Shan shear zone and the eastern Himalayan syntaxis. *International Geology Review*, 39(3), 191–219.
- Wang, J. H., Yin, A., Harrison, T. M., Grove, M., Zhang, Y. Q., & Xie, G. H. (2001). A tectonic model for Cenozoic igneous activities in the eastern Indo-Asian collision zone. *Earth and Planetary Science Letters*, 188(1), 123–133.
- Wang, P. L., Lo, C. H., Chung, S. L., Lee, T. Y., Lan, C. Y., & Van Thang, T. (2000). Onset timing of left-lateral movement along the Ailao Shan-Red River shear zone: ⁴⁰Ar/³⁹Ar dating constraint from the Nam Dinh area, northeastern Vietnam. *Journal of Asian Earth Sciences*, 18(3), 281–292.
- Wang, Y., Sieh, K., Aung, T., Min, S., Khaing, S. N., & Tun, S. T. (2011). Earthquakes and slip rate of the southern Sagaing fault: Insights from an offset ancient fort wall, lower Burma (Myanmar). *Geophysical Journal International*, 185(1), 49–64.
- Wang, Y., Zhang, L., Cawood, P. A., Ma, L., Fan, W., Zhang, A., et al. (2014). Eocene supra-subduction zone mafic magmatism in the Sibumasu Block of SW Yunnan: Implications for Neotethyan subduction and India-Asia collision. *Lithos*, 206, 384–399.
- Watkinson, I. (2011). Structural geology of Thailand during the Cenozoic. *The Geology of Thailand*, 273.
- Watkinson, I., Elders, C., Batt, G., Jourdan, F., Hall, R., & McNaughton, N. J. (2011). The timing of strike-slip shear along the Ranong and Khlong Marui faults, Thailand. *Journal of Geophysical Research*, 116(B9).
- Webb, A. A. G., Guo, H., Clift, P. D., Hussou, L., Müller, T., Costantino, D., et al. (2017). The Himalaya in 3D: Slab dynamics controlled mountain building and monsoon intensification. *Lithosphere*, 9(4), 637–651.
- Webb, A. A. G., Yin, A., & Dubey, C. S. (2013). U-Pb zircon geochronology of major lithologic units in the eastern Himalaya: Implications for the origin and assembly of Himalayan rocks. *Geological Society of America Bulletin*, 125(3–4), 499–522.
- Wen, D. R., et al. (2008). Zircon SHRIMP U-Pb ages of the Gangdese Batholith and implications for Neotethyan subduction in southern Tibet. *Chemical Geology*, 252(3), 191–201.
- Westerweel, J., et al. (2019). Burma Terrane part of the Trans-Tethyan arc during collision with India according to palaeomagnetic data. *Nature Geoscience*, 12, 863–868.
- Wolfe, M. R., & Stockli, D. F. (2010). Zircon (U-Th)/He thermochronometry in the KTB drill hole, Germany, and its implications for bulk He diffusion kinetics in zircon. *Earth and Planetary Science Letters*, 295(1–2), 69–82.
- Wu, C., et al. (1998). Yadong cross structure and South Tibetan Detachment in the east central Himalaya (89–90). *Tectonics*, 17(1), 28–45.
- Xu, W. C., Zhang, H. F., Harris, N., Guo, L., Pan, F. B., & Wang, S. (2013). Geochronology and geochemistry of Mesoproterozoic granitoids in the Lhasa terrane, south Tibet: Implications for the early evolution of Lhasa terrane. *Precambrian Research*, 236, 46–58.
- Yang, L., Xiao, W., Rahman, M. J. J., Windley, B. F., Schulmann, K., Ao, S., et al. (2020). Indo-Burma passive amalgamation along the Kaladan Fault: Insights from zircon provenance in the Chittagong-Tripura Fold Belt (Bangladesh). *Geological Society of America Bulletin*.
- Yin, A. (2006). Cenozoic tectonic evolution of the Himalayan orogen as constrained by along-strike variation of structural geometry, exhumation history, and foreland sedimentation. *Earth-Science Reviews*, 76(1), 1–131.
- Yin, A. (2010). Cenozoic tectonic evolution of Asia: A preliminary synthesis. *Tectonophysics*, 488(1), 293–325.
- Yin, A., Dubey, C. S., Kelty, T. K., Gehrels, G. E., Chou, C. Y., Grove, M., & Lovera, O. (2006). Structural evolution of the Arunachal Himalaya and implications for asymmetric development of the Himalayan orogen. *Current Science*, 195–206.
- Yin, A., Dubey, C. S., Kelty, T. K., Webb, A. A. G., Harrison, T. M., Chou, C. Y., & Célérier, J. (2010). Geologic correlation of the Himalayan orogen and Indian craton: Part 2. Structural geology, geochronology, and tectonic evolution of the Eastern Himalaya. *Geological Society of America Bulletin*, B26461-1.
- Yin, A., Dubey, C. S., Webb, A. A. G., Kelty, T. K., Grove, M., Gehrels, G. E., & Burgess, W. P. (2010). Geologic correlation of the Himalayan orogen and Indian craton: Part 1. Structural geology, U-Pb zircon geochronology, and tectonic evolution of the Shillong Plateau and its neighboring regions in NE India. *Geological Society of America Bulletin*, 122(3–4), 336–359.
- Yin, A., & Harrison, T. M. (2000). Geologic evolution of the Himalayan-Tibetan orogen. *Annual Review of Earth and Planetary Sciences*, 28, 211–280.
- Yin, A., Harrison, T. M., Ryerson, F. J., Wenji, C., Kidd, W. S. F., & Copeland, P. (1994). Tertiary structural evolution of the Gangdese thrust system, southeastern Tibet. *Journal of Geophysical Research*, 99(B9), 18175–18201.
- Yin, A., & Taylor, M. H. (2011). Mechanics of V-shaped conjugate strike-slip faults and the corresponding continuum mode of continental deformation. *Geological Society of America Bulletin*, 123(9–10), 1798–1821.
- Yin, A., et al. (1999). Tertiary deformation history of southeastern and southwestern Tibet during the Indo-Asian collision. *Geological Society of America Bulletin*, 111(11), 1644–1664.
- Zhang, X., et al. (2014). Early Jurassic high-pressure metamorphism of the Amdo terrane, Tibet: Constraints from zircon U-Pb geochronology of mafic granulites. *Gondwana Research*, 26(3), 975–985.
- Zhu, D. C., Chung, S. L., Mo, X. X., Zhao, Z. D., Niu, Y., Song, B., & Yang, Y. H. (2009). The 132 Ma Comei-Bunbury large igneous province: Remnants identified in present-day southeastern Tibet and southwestern Australia. *Geology*, 37(7), 583–586.

- Zhu, D. C., Mo, X., Niu, Y., Zhao, Z., Wang, L., Liu, Y., & Wu, F. (2009). Geochemical investigation of Early Cretaceous igneous rocks along an east-west traverse throughout the central Lhasa Terrane, Tibet. *Chemical Geology*, *268*(3), 298–312.
- Zhu, D. C., Pan, G. T., Chung, S. L., Liao, Z. L., Wang, L. Q., & Li, G. M. (2008). SHRIMP zircon age and geochemical constraints on the origin of Lower Jurassic volcanic rocks from the Yeba Formation, southern Gangdese, South Tibet. *International Geology Review*, *50*(5), 442–471.
- Zhu, D. C., Zhao, Z. D., Niu, Y., Dilek, Y., Hou, Z. Q., & Mo, X. X. (2013). The origin and pre-Cenozoic evolution of the Tibetan Plateau. *Gondwana Research*, *23*(4), 1429–1454.
- Zhu, D. C., Zhao, Z.-D., Pan, G.-T., Lee, H.-Y., Kang, Z.-Q., Liao, Z.-L., et al. (2009). Early Cretaceous subduction-related adakite-like rocks of the Gangdese Belt, southern Tibet: Products of slab melting and subsequent melt-peridotite interaction? *Journal of Asian Earth Sciences*, *34*(3), 298–309.
- Zhu, D. C., et al. (2012). Cambrian bimodal volcanism in the Lhasa Terrane, southern Tibet: Record of an early Paleozoic Andean-type magmatic arc in the Australian proto-Tethyan margin. *Chemical Geology*, *328*, 290–308.
- Zuza, A. V., Cheng, X., & Yin, A. (2016). Testing models of Tibetan Plateau formation with Cenozoic shortening estimates across the Qilian Shan-Nan Shan thrust belt. *Geosphere*, *12*(2), 501–532.
- Zuza, A. V., Wu, C., Wang, Z., Levy, D. A., Li, B., Xiong, X., & Chen, X. (2019). Underthrusting and duplexing beneath the northern Tibetan Plateau and the evolution of the Himalayan-Tibetan orogen. *Lithosphere*, *11*(2), 209–231.